

# Review of performance metrics of spin qubits in gated semiconducting nanostructures

Peter Stano<sup>1</sup> and Daniel Loss<sup>1,2</sup>

<sup>1</sup>RIKEN Center for Emergent Matter Science (CEMS), Wako, Saitama 351-0198, Japan

<sup>2</sup>Department of Physics, University of Basel, Klingelbergstrasse 82, CH-4056 Basel, Switzerland

(Dated: November 18, 2021)

We collect values of selected performance characteristics of semiconductor spin qubits defined in electrically controlled nanostructures. The characteristics are envisioned to serve as a community source for the values of figures of merit with agreed-on definitions allowing comparison of different qubit platforms. We include characteristics on the qubit coherence, speed, fidelity, and the qubit-size of multi-qubit devices. The review focuses on collecting the values of these characteristics as reported in the literature, rather than on the details of their definitions or significance. The core of the review are thus tables and figures.

## I. SCOPE, FORMAT, AND AIM OF THIS REVIEW

Spin qubits are among platforms pursued to serve as quantum computing hardware. We focus on spin qubits hosted in semiconducting nanostructures controlled and probed electrically. Their perspective for scalability stems from compatibility with modern silicon industrial fabrication. Even with the restriction on gated nanostructures, the field of spin qubits is vast. There is a host of variants on the sample material and structure, device design, or qubit encoding. While this versatility in the qubit types is beneficial for overcoming possible roadblocks, it also makes comparison of different spin qubits difficult. The main motivation for this work is to provide a basis for such a comparison and for a judgement of the progress of various spin-qubit types over time. We believe that for such tasks, a reliable database of figures of merit normalized to common definitions is of primary importance.

The restriction also implies what is not covered in this review. We do not include other than solid-state qubits; within the solid-state, we do not include superconducting qubits and qubits based on optically accessed impurities and self-assembled dots. We also skip qubits based on the spin of atomic nuclei, that is, hyperfine-spin qubits. Even though spin-related, we sacrifice these possible extensions to keep the review manageable in length and in time of preparation. On the other hand, we include charge qubits, that is qubits with states encoded into the charge degree of freedom of a confined particle. One reason is that often the experimental devices are identical for both spin and charge qubit experiments. Another is that there are configurations where the spin and charge degrees of freedom are hybridized and tunable. With the character continuously tunable from fully spin- to fully charge-like, it would be difficult to decide objectively which cases to include and which ones not. Finally, we point out that this document is not a review on the physics of spin qubits, such as principles of their operation and measurements, the decoherence channels, and so on. The reader interested in these aspects can consult, for example, Refs. [37, 80, 84, 131, 140, 204, 206, 232, 238, 239, 254, 267, 273].

The core of the review are tables and plots of selected qubit characteristics on qubit coherence, operation speed, operation fidelity, quality factors, and the size of multi-qubit arrays. The related quantities are defined, and their values collected from the literature given, in Sections II-VI, respectively.

We hope that this review becomes useful and used as a database for spin-qubit characteristics. To this end, it is crucial that the database is up-to-date, error-free, and contains relevant quantities. These goals can hardly be met without an active participation of the spin-qubit community. We encourage the community members to provide us with feedback on any errors, omissions, or suggestions for changes.

### A. We present a database of values

Though not necessarily of a concern for the reader, we note that the presented collection reflects a formally defined database. This fact might be useful to understand certain nomenclature, details of the presentation, and requirements on the included values and possible extensions. Let us briefly explain these aspects.

Every *value* given in this review belongs to a certain *attribute*. These two categories are the basic elements defining the database and constitute keywords with precise meaning. The *attributes* are used as headers in tables and axes labels in plots. For example, the first line of Tab. I contains the value  $LD/e$  under the attribute *Qubit*. It means that the corresponding experiment used a qubit encoded into a spin of an electron. While most of the attributes are self-explanatory, they are additionally listed alphabetically, together with their definitions, in Appendix D. The attributes defined therein are typographically distinguished using *Italics* font. The typographic distinction is done only in this section and App. D.

### B. Spin-qubit types, device geometries, material choices

Before we discuss specific characteristics, we comment on their common aspects. They stem from the fact that each *value* inherits a set of characteristics from the publication it was reported in and the experimental device it was measured with. We describe these common aspects in the following two paragraphs.

Every value given in this review (such as a coherence time of 10 ns) is a result of a measurement with a specific device

and qubit type, reported in a published reference.<sup>1</sup> This means, first of all, that we include only numbers explicitly stated and directly measured. We do not include extrapolations to other conditions or materials. Also, we do not usually derive the values ourselves even if it would be possible. For example, if the reference gives the operation time and the dephasing time, but does not state the quality factor, we do not evaluate the latter ourselves. However, if a quantity is discussed and presented as a figure (for example, the operation time implied from oscillations displayed by a resonantly driven qubit), we might include a value read-off from the figure. In such cases, the table entry contains a *Note* with keywords (*derived*) or (*estimated*), which are explained in Appendix D. With this requirement, every value given in this review should be easy to find using the reference, given under the attribute *Reference*, and within the reference as described by the attribute *Source*. An example for the latter is “page 4 and Fig. 1b”. One possible difference between the value given here and in the original work is normalization. In that case, a *Note* explains how the value was converted. Any additional information, for example, alerting on an unusual configuration or a specific method used in the experiment, is also given as a *Note*.

The second group of common characteristics concerns the details of the qubit. We found useful to categorize the following: the sample material, the geometry of the host, and the qubit type. They belong to the attributes *Material*, *Host*, and *Qubit*, respectively. While the value for material, for example, *Si/SiGe*, is self-explanatory,<sup>2</sup> in some figures we group several different materials under a common tag, such as *Si*. Concerning the host geometry, we discriminate qubits based on gating the structures which are (quasi-)*2D*, for example, a 2DEG, (quasi-)*1D*, for example a nanowire, and quasi-zero-dimensional, denoted by *imp*, an example being an implanted impurity. Some of these are not clear-cut cases, for example the hut-wires with a flat cross-section [287], or some variants of CMOS devices [278]; nevertheless, we assign both to *1D*. Finally, perhaps the largest variation exists among the qubit types. We distinguish the charge carrier: conduction electron, valence hole, and atomic impurity; and the spin-encoding: spin-one-half (*LD*), singlet-triplet (*ST*), and hybrid

(*HY*) qubits. We have not found beneficial to subdivide further the hybrid qubits: everything which is not a spin-one-half or a singlet-triplet is assigned the value hybrid here. A note might give additional information on the qubit type. The reader would benefit from a short look at Appendix D now, to understand the database organization through attributes and values.

### C. Choosing which values to collect is subjective

A disclaimer is in order here: Assigning a single specific value for each characteristic is necessary for a meta-analysis such as done here. However, converting an experimental investigation into a single number is inevitably a drastic compression. The choice of the value to quote requires subjective judgement: in a typical experiment, the value of a given figure of merit is seldom a unique value, but rather spans a range, sometimes a very large range, such as several orders of magnitude. We tend to take the most beneficial values, but it does not mean we simply take the largest one. Especially when an experiment presents a set of values for different characteristics, we try to choose a representative set measured at a common setting. For example, in an experiment with three qubits, where each is measured for relaxation, dephasing, and the echo coherence time, we do not simply take the largest value seen among all experiments. We choose a qubit and quote the three numbers for this particular qubit. We proceed similarly when several characteristics are measured under various conditions. Our overall approach is to adopt values which are mutually consistent (such as the coherence time and the operation speed) as much as possible. Nevertheless, we warn the reader that all such choices are largely subjective. The final authority to judge the value meaning and importance is the original reference itself.

---

After these preliminaries, we now present the spin-qubit figures of merit published until around October 2021.

---

## II. COHERENCE TIMES

By far the largest amount of published data on spin qubits exist on their coherence times. Qualitatively, a coherence time extracted in an experiment has the meaning of a time during which state oscillations stemming from quantum mechanical superpositions can be observed.

### A. The definition and meaning of experimentally extracted coherence times

Additional specifications of the conditions under which such a superposition decay is observed lead to several variants of the coherence time. The inhomogeneous dephasing

---

<sup>1</sup> While we count arxiv preprints as “published references”, the absolute majority of the entries are from journal publications. The current bibliography contains 17 arxiv preprints, only two of which were uploaded before year 2020: Refs. [32, 92].

<sup>2</sup> Qubits based on silicon-oxide structures is one case which needs a comment. A unique identification in this review for such structures is the value *Si/SiO<sub>2</sub>* of the attribute *Material*. The attribute *Host* is typically also straightforward to assign, being either *2D*, for example for an epilayer, or *1D* for finFETs or structures denoted as nanowires by their authors. One can often find further specifications for such devices, such as: [complementary-]metal-oxide-semiconductor([C]MOS), silicon-on-insulator(SOI), field-effect-transistor(FET), foundry-compatible, and similar, including their combinations. These specifications hint on fabrication details and the degree of compatibility with the industrial silicon technology. However, they are sometimes used interchangeably, even within one laboratory. Therefore, and since the fabrication details are not our focus, we do not include such additional specifications even if given in the original work.

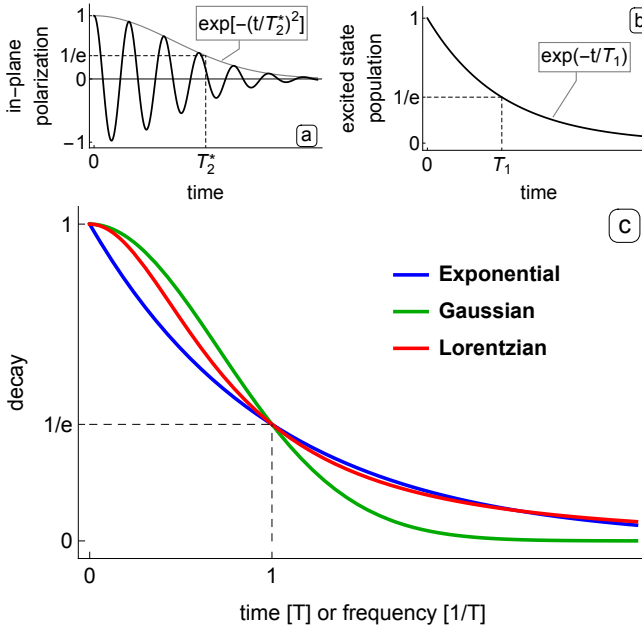


FIG. 1. Typical decay-curve envelopes. (a) Oscillations with a Gaussian decay envelope, typical in Ramsey experiments measuring the inhomogeneous dephasing time  $T_2^*$  in the time domain. (b) Exponential decay typical for relaxation processes, reflecting the relaxation time  $T_1$ . (c) Three curves are plotted for comparison. They are normalized to a common value at their parameter equal 0 and 1. The Gaussian and Lorentzian, the Fourier transforms of the two envelopes given in (a) and (b), arise in probing the decay in the frequency domain.

time  $T_2^*$  implies a Ramsey experiment, meaning the following sequence. The qubit initialized to a state polarized within the equatorial plane of the Bloch sphere, for example along the  $x$  axis, and is let to precess freely for time  $t$  after which the in-plane polarization is measured. The evolution time  $t$  is varied, and for each value of  $t$  the sequence is repeated to gather enough statistics. A typical time-trace of the averaged signal fits a cosine with a Gaussian decay envelope  $f(t)$ ,

$$P_x(t) = f(t) \frac{1 + \cos \omega t}{2} = \exp \left[ -(t/T_2^*)^2 \right] \frac{1 + \cos \omega t}{2}. \quad (1)$$

This curve is plotted in Fig. 1(a).

The decay of a spin qubit in a Ramsey experiment described by Eq. (1) is often due to fluctuating nuclear spins. The strong effect of nuclei on the spin coherence was predicted in Refs. [126, 178] and confirmed experimentally in Ref. [218]. Because the dynamics of nuclear spins is slow, one can protect the spin-qubit coherence using the spin-echo techniques developed in the field of Nuclear Magnetic Resonance [250]. The simplest protecting protocol is the Hahn echo[83]. It means that the spin is flipped (rotated around an in-plane axis by angle  $\pi$ ) in the middle of the free evolution, at time  $t/2$ , of the described Ramsey sequence. The coherence time measured under a Hahn echo is denoted in this review as  $T_2^H$ . Already in Ref. [218], Hahn echo prolonged the spin qubit coherence by a factor of hundred. There are more elaborate protocols, applying more echo pulses, which prolong the coherence further.

While there are several different variants [1], here we assign any sequence containing more than a single echo under a common category, denoting the coherence time as  $T_2^D$ . A typical member of this family is the CPMG protocol, with which the coherence of a singlet-triplet spin-qubit was prolonged to almost a millisecond in Ref. [168].

All these protocols aim at prolonging the coherence of an idling spin qubit. The decay of a driven spin, meaning the decay of coherent Rabi oscillations, is another important time scale which is often reported. It is denoted here as  $T_2^R$ . The understanding that the decay of coherence of a driven and idling spins can strongly differ goes back to Redfield [224] and has been demonstrated with a spin qubit [149]. Finally, we include also the time  $T_1$ , called the relaxation time, to denote the decay of qubit energy. That it is a different type of process is denoted by its subscript “1” as opposed to “2” for the times describing the decay of phase. These subscripts refers to the notation usual in Bloch equations, where these two processes with distinct physical origin are called the “longitudinal” and “transverse” relaxation, respectively [13]. See App. A for the notation of various decay times.

For simplicity, in the preceding paragraphs we exemplified several of the coherence times with experiments measuring them under the dominant influence of nuclear spins. However, the nomenclature works the same for other noise sources, such as the charge or phonon noise, influencing the spins through spin-orbit interaction. More importantly, the functional form of the envelope  $f(t)$  in Eq. (1) is often different from the Gaussian. Another typical case is an exponential,

$$f(t) = \exp(-t/T_1). \quad (2)$$

We have suggestively used  $T_1$  for the time scale, as the energy relaxation is often described by such an envelope. The function is plotted in Fig. 1(b). Because of the superimposed oscillations in Eq. (1), it is not easy to discriminate exponential and Gaussian decay envelopes. While the functions differ strongly in their exponential tails, these tails are basically never resolvable, due to measurement errors and statistical fluctuations. If the discrimination is possible, it is based on the different shape of the two functions at small times: linear versus quadratic.

The discrimination gets even more difficult in experiments where the qubit is probed in the frequency domain. A typical example is recording the amplitude and phase response of a resonant electrical circuit which the qubit is a part of. Both of these quantities are parametrized by the circuit reflection coefficient, a complex number. A standard result for it reads<sup>3</sup>

$$r(\omega_p) = \frac{\omega_r - \omega_p + i\kappa/2 + \chi(\omega_p)}{\omega_r - \omega_p - i\kappa/2 + \chi(\omega_p)}. \quad (3)$$

Here,  $\omega_p$  is the frequency of the signal probing the circuit,  $\omega_r$  is the circuit resonant frequency,  $\kappa$  is the circuit-field decay

<sup>3</sup> We copy Eq. (A15) from Ref. [63]. Ref. [43] gives an analogous result in its Eq. (57).

rate, and  $\chi$  is the qubit response function, the Fourier transform of the decay envelope  $f(t)$ . For a qubit described by an exponential decay, the latter is[43, 63]

$$\chi(\omega_p) = -\frac{g^2}{\omega_q - \omega_p - i\Gamma_2} D, \quad (4)$$

with  $\hbar\omega_q$  the energy difference of the qubit excited and ground states,  $g$  the qubit–circuit coupling,  $D$  the difference of the population probability of the qubit ground and excited state, and  $\Gamma_2 = \Gamma_1/2 + \Gamma_\varphi$  is defined in App. A. These formulas are valid also when the qubit itself is driven, so called two-tone spectroscopy[236]. In that case, all parameters on the right hand side of Eq. (4) should be replaced by the corresponding quantities in the rotating reference frame [105]. From Eq. (3) one can see that the departure of the response amplitude from one is solely due to the imaginary part of the qubit response function,

$$|r(\omega_p)|^2 - 1 = \frac{2\kappa \text{Im}\{\chi\}}{(\kappa/2 - \text{Im}\{\chi\})^2 + (\text{Re}\{\chi\} - \omega_p + \omega_r)^2}. \quad (5)$$

Scanning the probe frequency  $\omega_p$  in a steady-state experiment, the resonance with the qubit frequency is signaled by a dip in the circuit response<sup>4</sup>, and the width of the dip gives  $\Gamma_2$ . Most often, the articles give the dip linewidth, meaning its full width at half maximum (FWHM) in frequency (and not angular frequency) units,  $\Delta f_{\text{FWHM}}$ . In this case, we transform the linewidth to the inhomogeneous dephasing time using

$$T_2^* = \left( \frac{2\pi\Delta f_{\text{FWHM}}}{2} \right)^{-1}. \quad (6)$$

Here, the factor  $2\pi$  in the numerator converts the frequency to angular frequency entering Eq. (4) and the factor 2 in the denominator converts the dip full width to its half width.

Coming back to the possibility of discrimination of the decay envelopes, we now consider the Fourier transforms  $\chi(\omega)$  for the above two examples. While the Fourier transform of a Gaussian is a Gaussian, the exponential transforms into a complex function with both the real and imaginary parts Lorentzian,

$$\text{Gaussian } f(t) \xrightarrow{\text{F.T.}} \chi(\omega) = \exp(-\omega^2 T^2 / 4), \quad (7a)$$

$$\text{Exponential } f(t) \xrightarrow{\text{F.T.}} \chi(\omega) = \frac{i\omega T - 1}{\omega^2 T^2 + 1}, \quad (7b)$$

In these equations, we Fourier transformed (F.T.) Eqs. (1) and (2), normalized the results to the same value at zero frequency, and dropped the time-scale subscripts. To discriminate the two cases given in Eq. (7) in the frequency domain is even

more difficult than in the time domain, since both Gaussian and Lorentzian are quadratic at small frequencies. Compared to the time domain, now the two functions differ more strongly at their tails (that is, for large  $\omega$ ), with algebraic and exponential decay, respectively. However, as already stated, these tails are seldom accessible with the required precision. The three envelope functions discussed so far are plotted in Fig. 1(c) for comparison.

The reason for discussing the discrimination between different functional forms of the decay envelopes is that it hints to the origin of the noise causing the decay. A minimal description of noise is to give its autocorrelation function, either in time or frequency domain. If it is the latter, the function is called the noise spectrum. The form of the noise spectrum decides what will be the decay envelope. Noises with different physical origins, for example nuclear spins versus charge impurities, will have different spectra. The functional form of the decay envelope then can serve as an alternative to obtaining the noise spectrum, in hinting on the possible origin of the dominant noise affecting the qubit. Finally, we note that the above three possibilities, Gaussian, exponential, and Lorentzian, are not the only ones. For example, going to the next order in the calculation reveals that algebraic tails in the decay exist [105]. Algebraic tails were also obtained in calculations considering the backaction of the qubit on its environment giving rise to non-Markovian behavior [66].

To conclude, the coherence times are typically extracted from fits to simple functional forms. Some are given above, and there are more, such as the “stretched exponential” used to fit data from dynamical-decoupling sequences [49, 177]. The true decay envelope is a complicated function, which can hardly be parameterized by a single number. A typical fit returns the time scale over which the envelope decays to a fraction of its initial value, for example, 1/e. This operational definition should be the first guess on the meaning of a coherence time in the tables we give. Not much is implied about the functional form itself, let alone the decay long-time tails.

---

The data on coherence times are listed in Tab. I. We additionally present it here in figures, discussing them shortly. We split the figures to two groups, separating the charge qubits, the states of which do not rely on the spin degree of freedom in any way, from qubits which rely on spin at least to some degree. We start with the latter group.

---

## B. Measured coherence times of spin qubits

The coherence times of spin qubits are given in Fig. 2. The values had started at around 10 ns inhomogeneous dephasing time in early experiments with qubits in GaAs. Echo techniques can extend the coherence by orders of magnitudes, as can a different material choice. The coherence times published during the year 2020 span six orders of magnitude, depending

---

<sup>4</sup> Since normally  $D > 0$ . However, the population inversion,  $D < 0$ , is also possible, see Ref. [90]. It would give a peak in  $|r(\omega_p)|$ , instead of a dip.

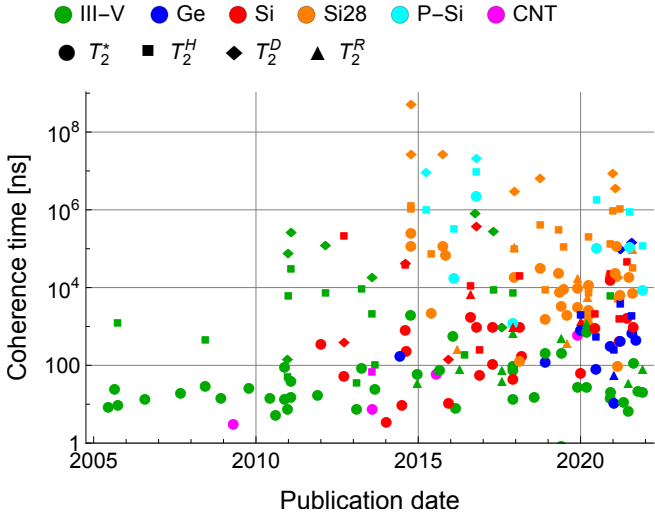


FIG. 2. Spin coherence times according to the publication date. The point color shows the device material and the point symbol shows the coherence type as given in the legend. The plotted data are values from Tab. I excluding the data on the relaxation time  $T_1$ . The value  $T_2^* = 0.12$  ns from Ref. [19] falls out of the vertical-axis range displayed.

on the qubit type, material, and protection measures.

To examine the influence of some of these factors, we plot separately each type of coherence in Fig. 3. The separation allows us to group additionally the values according to the qubit type, being the discrete category on the horizontal axis. To reflect the publication date for an easier comparison, we displace the data within each category horizontally. For example, Fig. 3(a) shows that the most recent electron spin-one-half ( $LD/e$ ) qubits implemented in purified silicon reach longer coherence times than singlet-triplet qubits, in turn longer than hole qubits. Impurity spins hold record coherence times in each category where data for them exist.

We next turn to the energy relaxation time. For a spin qubit, this time can be made very long by: isolating the qubit from reservoirs, so that the electron does not escape the dot; minimizing its dipole moment, so that the qubit couples weakly to phonons; and decreasing the transition energy, typically using a lower magnetic field, so that the available phase space for the process is reduced. Under these conditions, relaxation times have reached seconds and can be considered not of concern for quantum computing. On the other hand, the relaxation times remain of concern if these conditions are not met: for example, a finite relaxation time of a two-electron singlet and triplet states is the main limitation for the spin measurement fidelities [11, 25, 193]. Because of this crucial role, there are numerous values on the relaxation time for (mostly the triplet states of) singlet-triplet qubits, either explicitly reported or implicitly implied in many experiments using Pauli spin blockade for the spin measurement. As the relaxation time in this setting is a by-product of the maximization of the measurement fidelity, rather than a figure of merit maximized itself, we normally do not include singlet-triplet relaxation rates in this review. We do

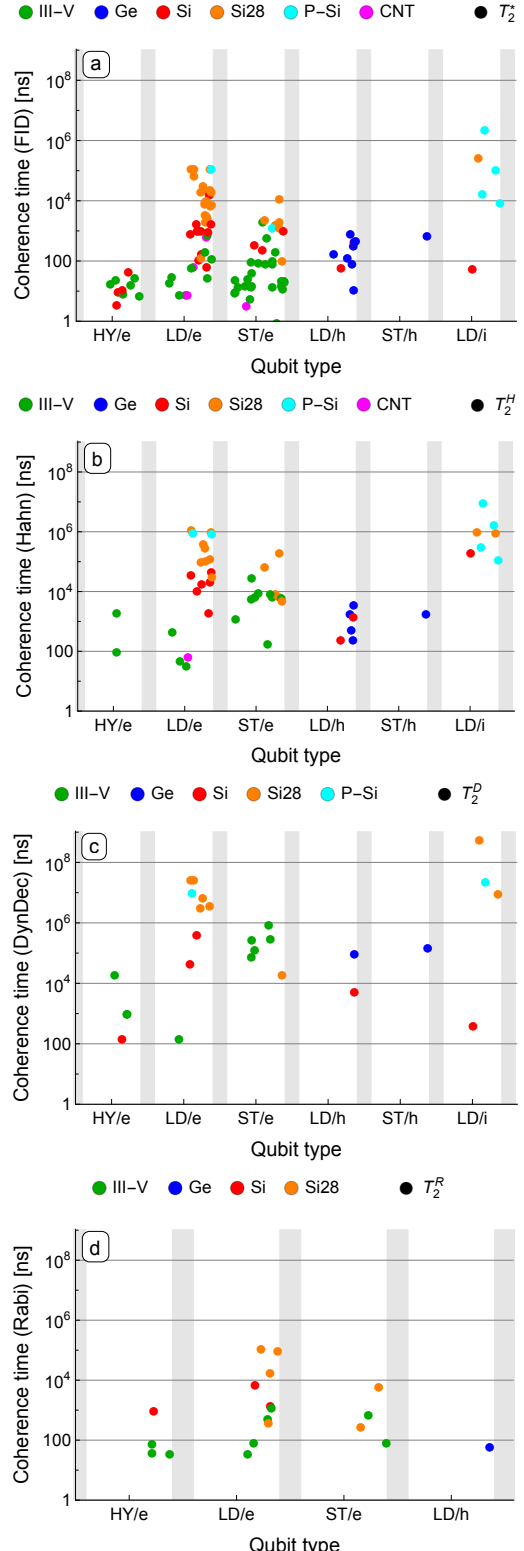


FIG. 3. Spin coherence times, showing the data of Fig. 2 split to the four panels according to the coherence type, denoted in the legend, from the set: inhomogeneous dephasing  $T_2^*$ , Hahn echo  $T_2^H$ , dynamical decoupling  $T_2^D$ , and Rabi decay  $T_2^R$ . In each panel, the horizontal axis uses the qubit type as a discrete category, displacing the points according to their publication date: more recent data are shifted to the right within the shaded area which is normalized to the year span 2003–2021. All vertical-axes ranges are the same and the point colors show the material.

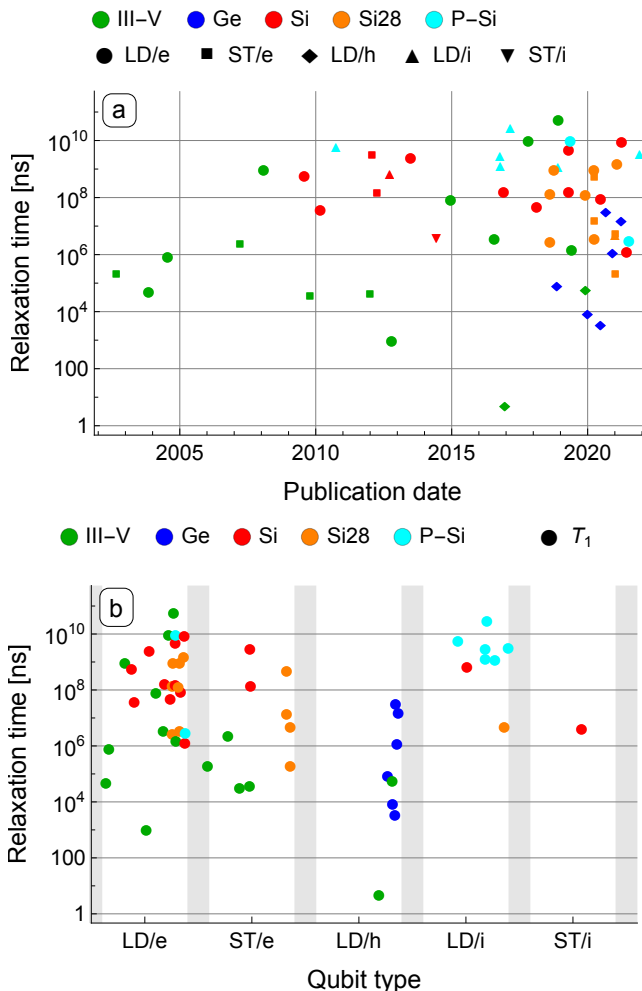


FIG. 4. Relaxation times of spin qubits. Both panels show the same data, the relaxation times from Tab. I. The point color shows the material. In (a), the horizontal axis shows the publication date and the point symbol shows the qubit type. In (b), the qubit type is on the horizontal axis as a discrete category, while the publication date is reflected by shifting the points laterally, similarly as in Fig. 3.

include a few values, from either early experiments, or when they are the article main topic.

We show the reported relaxation times in Fig. 4, plotting the same set of data in two different ways. Figure 4(a) gives them according to the publication date. One can see how the longest-reached times developed: In the first decade, electron one-half spin-qubits were in the lead. Since 2010, impurities took over. Currently, the record is back with a single electron in GaAs, with the relaxation time of one minute [29]. As already noted, while reaching such long times is not directly improving other figures of merit of the qubit, the increase of the record time illustrates the experimental progress with the given qubit platform. Figure 4(b) groups the times according to qubit types, making it easier to judge the progress over the years within each group.

### C. Measured coherence times of charge qubits

We finish the overview of the coherence times by looking at charge qubits. As already said, we include them even though they implement qubits which do not rely on spin. The reason is a close relation of the devices where the two type of experiments are typically done and of used techniques: for example, the measurement of spin is done indirectly, converting different spin states to different charge states, which are then detected.

All types of coherence times, including the relaxation time, of charge qubits are gathered in Fig. 5. In the three panels of the figure, the same data are shown according to the publication date, the device material, and the coherence type, respectively. One can see several differences compared to spin qubits. First, with the exception of a single experiment<sup>5</sup>, the relaxation times are not the longest scale. Therefore, the relaxation is a bigger issue for charge qubits even in single-qubit experiments. Second, unlike for spin qubits, the echo techniques do not result a substantial increase of coherence. Third, there is much less variation among the data: With some exceptions, coherence times of any type were limited from above by roughly ten nanoseconds until 2015, and hundred nanoseconds since then. Finally, as one would expect, there is no apparent difference between devices made in Si and III-V materials concerning charge-qubit coherence.

<sup>5</sup> Ref. [283]; the value plotted is the maximal observed relaxation time, from a set spanning four orders of magnitude.

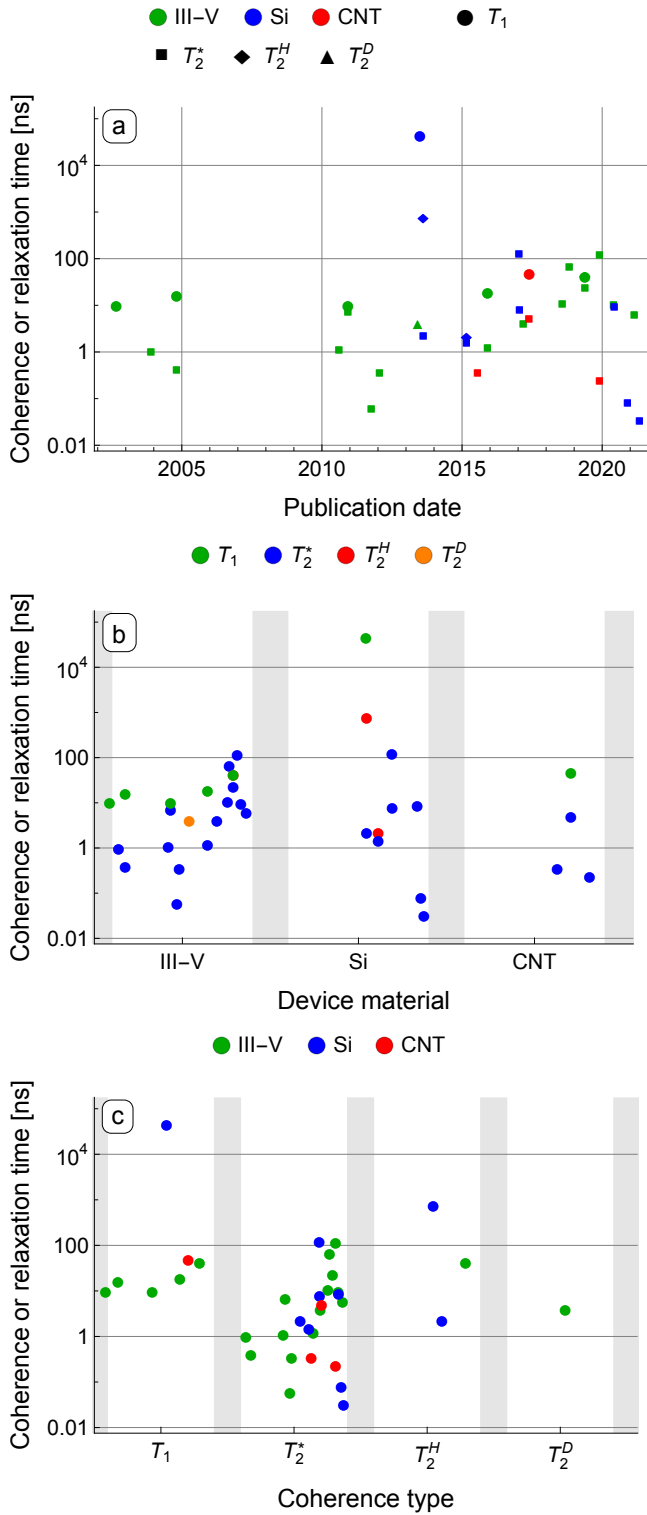


FIG. 5. Charge coherence. Every panel plots the same data, being the values from Tab. II. The panels differ by their horizontal axis, plotting the data according to the quantity given as the horizontal-axis label. Concerning the point symbols and colors, (a) is analogous to Fig. 2. In (b) and (c), the role of the point colors and the horizontal axis is swapped.

### III. OPERATION TIMES

The second most abundant data exist on characteristics of spin-qubit operations. We understand the qubit gates, measurements, and initializations as three operation types, treated on equal footing. We are motivated by their actual physical implementations which are similar: All three types of operations are typically implemented by pulsing the system to a specific configuration, or driving it resonantly, for a fixed time. Another reason is that while the algorithms considering logical qubits might assign initializations to the beginning and measurements to the end of the algorithm only, the physical qubits will need error correction. There, the initializations and measurements are used heavily, interspersing the application of gates.

There is an additional attribute introduced in this section, the number of qubits that a given operation involves, *Qubit#*. The most typical cases are one-qubit and two-qubit gates. However, the initialization and measurements can also be done in larger multi-qubit bases, and some such data exist.

Finally, let us list the operation characteristics. In the next three sections, we discuss, respectively, operation times, a quantitative measure, and operation fidelities and quality factors, two related qualitative measures.

#### A. The definition of experimentally extracted gate times

We begin with the gate times. Their advantage is that they reveal the natural time-scale for working with a given qubit and that they can be compared to the coherence times. The disadvantage arises if they are not compared to any coherence time: a fast qubit does not mean automatically a good qubit, since the judgement largely depends also on the coherence time. Conversely, a qubit with extremely long coherence becomes less appealing if the corresponding gates are also extremely slow. The disadvantage, namely a dimensionful quantity having a limited meaning without comparison to other dimensionful quantities, applies also for the coherence times presented in the previous section.

Let us specify the normalization for the operation times. For the measurements and initialization, the definition is straightforward, even though one should count also the preparation if it is a necessary part of the measurement or initialization sequence. On the other hand, more ambiguity exists for gates, since gates are realized as unitary evolutions induced by certain Hamiltonians. A typical signal which is interpreted as a gate being induced looks as in Fig. 1(a). Neglecting for now the decay and taking a single-qubit case, the oscillating signal is due to a unitary evolution such as

$$U(t) = \exp(-i\omega t s_z) \equiv \exp(-i2\pi f t s_z). \quad (8)$$

Here, we used  $s_z = \sigma_z/2$  for the rotation generator and  $f = \omega/2\pi$  for the signal frequency. At various times, various gates are carried out on the qubit: for  $ft = 1/2$ , one gets a  $Z$  gate, for  $ft = 1$  an identity, while  $ft = 1/4$  can act as a Hadamard gate in a certain basis. If such a continuous signal is presented,

we define the operation time to be one half of the signal period,

$$T_{op} = \frac{1}{2f}. \quad (9)$$

In the case of Eq. (8), the value  $t = 1/2f$  would be taken as the operation time, and it would correspond to the  $Z$  gate, that is a spin rotation by  $\pi$ . Note that this definition is different to the one adopted for the quality factor (see below).

### B. Measured values of gate times

Let us now look at the reported values plotted in Fig. 6(a). Since the set of operations is diverse, we present the data with the qubit type as the primary category on the horizontal axis. The data are additionally tagged according to the device material and the number of qubits. The shortest in the set are the times of single-qubit gates on charge qubits, being below 0.1 ns. One can deduce more instances of such short times in the literature than those shown on the figure. The reason is that these speeds are perhaps not claimed explicitly in the experiments: for charge qubits, the gate speed is limited by the experiment electronics, rather than the qubit itself.<sup>6</sup>. The hybrid qubits can reach similar speeds, since they can be tuned into a configuration where they resemble a charge qubit. Arguably, this tunability is their biggest advantage. When they are tuned into a spin-like configuration, their gate (and coherence) times go up. Similarly, a strong direct coupling to the electric field can be exploited also for holes, with gate speeds in hundreds of mega Hertz seen. Such driving, either by electric (EDSR) or magnetic (ESR) oscillating field is less efficient for spin qubits, either in quantum dots or impurities. For these types of qubits, the highest gate speeds were reached using the spin-spin exchange interaction. As seen from the times in the singlet-triplet column of the figure, the singlet-triplet oscillations can reach giga-Hertz frequencies. Fast exchange-based gates were demonstrated for both one and two-qubit operations of spin-one-half qubits and singlet-triplet qubits, and for two-qubit operations of hole and impurity qubits. Finally, we would like to note that the exchange-based gate for, first, a pair of one-half spins and, second, the singlet and triplet two-electron states, is an identical process. Whether such a process should be interpreted as a one-qubit gate or two-qubit gate depends on additional functionalities implemented, or implementable, in the given experiment. The boundary between the two cases is blurry.

### C. The definition and values of measurement times

We begin this part by a comment that we do not review the measurement times of charge qubits. The reason is that the

<sup>6</sup> Instead of quoting the gate speed, they are often judged by how strongly they couple to a microwave cavity field, using the charge-photon coupling strength. However, at the moment that figure of merit is not included in this review.

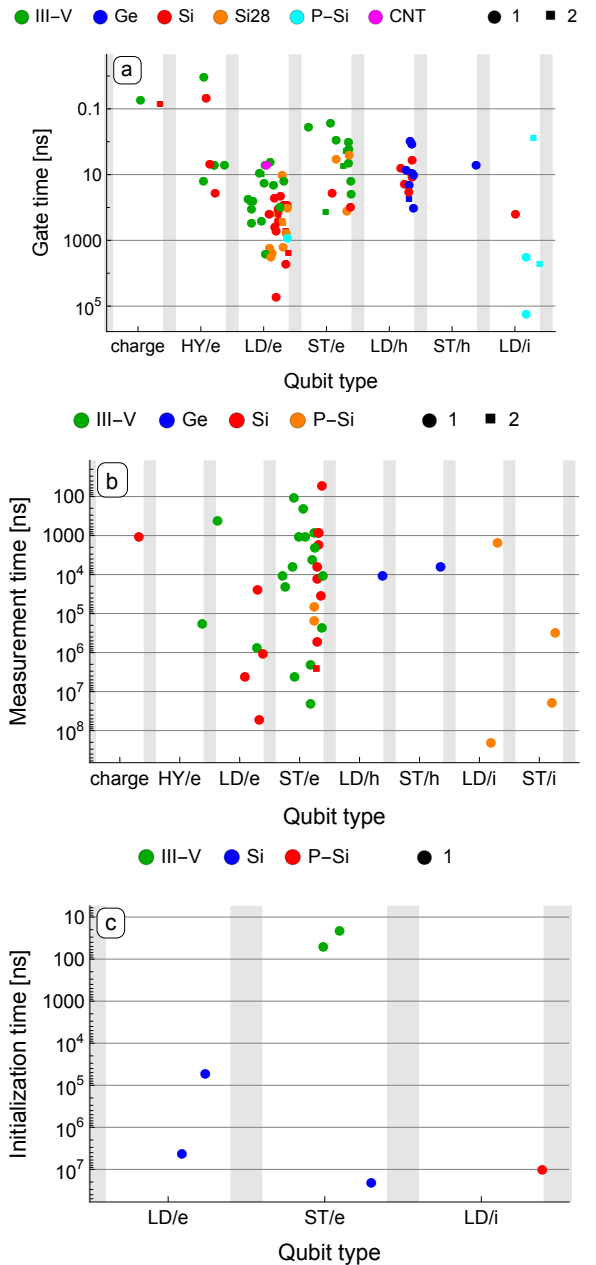


FIG. 6. Operation times: (a) gates, (b) measurements, and (c) initializations. In all panels the horizontal axis shows the qubit type, restricting to those for which values exist. Within each type, the publication date is reflected by shifting the points laterally, similarly as in Fig. 3. The vertical axis shows the operation time in nanoseconds. The point color indicates the material and its symbol the number of qubits involved in the operation, according to the panel legend.

task of the measurement of a charge qubit is the task of the detection of a charge—typically an elementary charge—in a nanodevice. First, this task is separable from and not exclusive to spin qubits, and thus not our focus. Second, the analysis of methods and results of this task is a topic rich enough for a review of its own. For our purposes, it will be enough to give the following minimum. The charge detection is typically

characterized through the detection sensitivity  $s$  with a typical number being<sup>7</sup>

$$s = \text{a few} \times 10^{-4} e \text{ Hz}^{-1/2}. \quad (10)$$

This parameter quantifies the reliability of the output of a charge-meter signal if integrated for time  $T_M$  as

$$\text{var}[q] = s^2/T_M. \quad (11)$$

Assuming that one aims to distinguish a signal of one elementary charge,  $q_1 = e$ , from the signal of zero charge,  $q_2 = 0$ , where "to distinguish" means to make the signal error,  $\sqrt{\text{var}[q]}$ , as small as the signal magnitude,  $|q_1 - q_2| = e$ , would give the required time

$$T_M = s^2/e^2 \sim 100 \text{ ns}. \quad (12)$$

While higher sensitivity[237] and shorter times[124] for elementary charge detection were reported, let us take this value for the measurement time  $T_M$  as a lower limit realistic for many experimental configurations.

With 100 ns for the time required to detect an event employing elementary charge, we now look at the spin qubit measurements times shown in Fig. 6(b). We see that while the times start at about the elementary charge-detection limit of Eq. (12), they might become orders of magnitude longer. The variance reflects the fact that the spin is detected indirectly, by first converting it to a charge event, which is in turn resolved by a charge sensor. The time required for the spin to charge conversion can vary a lot, depending on the process details. One example for a spin to charge conversion is spin-dependent tunneling: An electron with spin down can tunnel out a quantum dot, while the one with spin up can not, the difference originating in their Zeeman energies [85]. Since the quantum dot has to be well isolated for the qubit to keep its coherence, the tunneling out of the dot is slow. As a second example, the spin singlet and triplet can be discriminated according to being allowed or not allowed to traverse a double dot (the Pauli Spin Blockade invented by Ono et al. [205]). While here the charge reconfiguration can be very fast, following the gate-voltage pulses on a nanosecond scale, the two charge configurations being discriminated differ only by a dot-size shift of an elementary charge. The discrimination of such states requires a longer time compared to those differing by the presence, rather than the displacement, of an elementary charge.

#### D. The values of initialization times

The initialization times are shown in Fig. 6(c). Only a few values are present. The reason might be that the most typical experimental scenario is to repeat a cycle: initialization –

operation – measurement, where the measurement part plays the role of the initialization, and, therefore, the latter is not reported separately and explicitly. There are more values published on the initialization fidelities, see below.

## IV. OPERATION FIDELITY

The operation fidelity is a dimensionless figure of merit allowing a comparison of diverse qubits. Using randomized benchmarking [61], one can extract the gate errors independently of the measurement errors, even if the former are orders of magnitude smaller than the latter. Though it is not strictly correct, the fidelity is used to judge the progress towards error-correction thresholds required for fault-tolerant quantum computing.<sup>8</sup> For all these reasons, evaluating the gate fidelities is popular and impressive values have been reached.

### A. The definition and meaning of experimentally extracted fidelities

The fidelity characterizes how close the actual operation is to the desired one. While the fidelity of one means that the two operations are the same, quantification of a measure when they are not the same is less straightforward. The usual definitions derive from the fidelity  $\mathcal{F}$ , in the sense of distance, of two quantum states described by their respective density matrices  $\rho$  and  $\rho'$ ,

$$\mathcal{F} = \left( \text{tr} \sqrt{\sqrt{\rho} \rho' \sqrt{\rho}} \right)^2. \quad (13)$$

If one of the two states is pure, say  $\rho' = |\Psi\rangle\langle\Psi|$ , the formula simplifies to

$$\mathcal{F} = \text{tr}(\rho|\Psi\rangle\langle\Psi|). \quad (14)$$

If the second state  $\rho$  is also pure,  $\mathcal{F}^{1/2}$  is closely related to an unambiguous discrimination of the two pure states [94], while  $\arccos \mathcal{F}^{1/2}$  is a measure of their statistical distinguishability [291].<sup>9</sup>

We use the definition of Eq. (13) leading to Eq. (14) because of its connection to the randomized benchmarking. Namely, the essence of the latter is to prepare a pure state  $|\Psi\rangle\langle\Psi|$ , act on it by a sequence of gates, and then evaluate the overlap of the resulting density matrix  $\rho$  with the original state  $|\Psi\rangle$  using Eq. 14. In the sequence, the gates are chosen from a discrete set, the Clifford group [81], at random except for the last gate

---

<sup>7</sup> Here a few numbers that one can find in the literature: 10 in Ref. [226], 63 in Ref. [40], 0.37 in Ref. [79], 8.2 in Ref. [305], 4.1 in Ref. [309], 21 in Ref. [36], 0.60 in Ref. [240]; all in  $10^{-4} \times e/\sqrt{\text{Hz}}$ .

<sup>8</sup> The problem is that the fidelity, as defined below, is not the error parameter entering the threshold theorem. The two parameters can differ by orders of magnitude, in the unfavorable way: while the fidelity extracted by the randomized benchmarking can be low, the error rate can remain much larger [17, 231].

<sup>9</sup> What is the best measure to quantify distance of two operations is discussed at length in Ref. [78]. We thank Andrea Morello for pointing this reference to us.

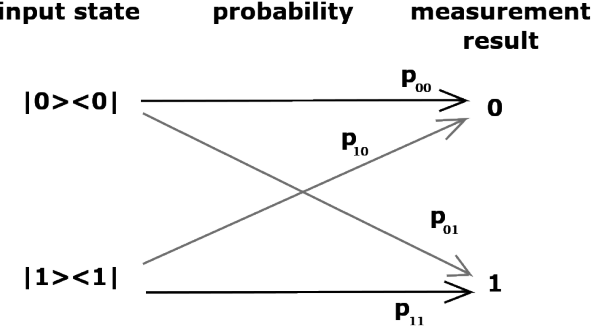


FIG. 7. Probabilities describing a two-outcome qubit measurement. The two mutually orthogonal pure states are on the left, the two measurement outcomes on the right. A perfect measurement would have unit probabilities  $p_{ii}$  denoted by horizontal lines. Due to imperfections, diagonal lines appear with non-zero probabilities. The infidelity defined by Eq. (19) gives for this diagram  $1 - \mathcal{F} = \frac{1}{2}(p_{01} + p_{10})$ .

which is such that the whole sequence reduces to the identity if all gates are perfect. The resulting fidelity, called also the probability of the survival of the initial state, falls off exponentially with the sequence length  $m$ ,

$$\mathcal{F}(m) \approx Ap^m + B. \quad (15)$$

Experimentally, the three coefficients  $A$ ,  $B$ , and  $p$  are fitted.<sup>10</sup> The first two absorb the errors of the state preparation and measurement, so that the infidelity  $1 - \mathcal{F}$  can be found from the parameter  $p$  using the formula<sup>1112</sup>

$$1 - \mathcal{F} = (1 - p)\frac{d - 1}{d}. \quad (16)$$

Here,  $d = 2^n$  with  $n$  the number qubits;  $d = 2$  for a single-qubit gate benchmarking. While the exponential decay form displayed by Eq. (15) relies on the discrete set being the Clifford group, many articles convert  $\mathcal{F}$  to fidelities of experiment-specific “elementary” or “primitive” gates, such as  $\pi/2$  and  $\pi$  rotations around various axes. Even though such a conversion is questionable [165], we follow the prevailing practice and in

<sup>10</sup> Even though Ref. [165] stresses that one should always use a more refined decay model, adding a term proportional to  $(m - 1)p^m$  to the right hand side of Eq. (15), this advice does not seem to be followed in practice.

<sup>11</sup> Some comments are in order: The exponential decay reflected by Eq. (15) happens under broad conditions investigated in detail in Refs. [61, 165]. The fidelity extracted in this way is the average of  $\mathcal{F}$  in Eq. (14) over all pure input states  $|\Psi\rangle\langle\Psi|$  and also the average over the gates in the Clifford group. There is an extension procedure, called interleaved randomized benchmarking [166] which can assign a fidelity—still averaged over all pure states—to a single specific gate from the Clifford group.

<sup>12</sup> Ref. [78] presents further arguments against using the average fidelity  $\mathcal{F}$ , as extracted from randomized benchmarking, Eq. (16), and advocates entanglement fidelity  $\mathcal{F}_e$  instead. The two measures are related by  $(d + 1)\mathcal{F} = d\mathcal{F}_e + 1$ . Since the majority of the spin-qubit publications give  $\mathcal{F}$ , we stick to  $\mathcal{F}$  as the reported figure of merit.

figures and tables we give the infidelity for the elementary-gate set (and not for the Clifford-gate set). For one-qubit or two-qubit gates, one Clifford gate requires typically a few elementary gates. Therefore, the infidelity of a Clifford gate would be around a factor of 2–3 larger than the infidelity of an elementary gate<sup>13</sup>, the value quoted in this review.

The fidelities of initialization and measurement are less ambiguous to define as they can be based on Eq. (14) which is more intuitive than Eq. (13). Let us start with the measurement. The probability to get an outcome  $j$  in measuring the state described by a density matrix  $\rho$  is given by Eq. (14) upon replacing the pure state  $|\Psi\rangle\langle\Psi|$  by a positive semi-definite operator  $A$ . The most general measurement with possible outcomes labeled by index  $i$  is specified by a set  $\{A_i\}_i$  of such operators summing to identity,  $\sum_i A_i = 1$ . In experiments, these operators are approximations of a set of mutually orthogonal projectors spanning the qubit basis  $A_i \approx |\Psi_i\rangle\langle\Psi_i|$ . Due to experimental imperfections, these approximations are not exact. The probability of the measurement outcome  $j$  upon measuring the pure state  $\rho = |\Psi_j\rangle\langle\Psi_j|$  follows as

$$p_{ij} = \text{tr}(|\Psi_j\rangle\langle\Psi_j|A_j). \quad (17)$$

Due to the normalization of  $A_i$ , the probabilities fulfill

$$\sum_j p_{ij} = 1. \quad (18)$$

Were the measurement perfect, all non-diagonal probabilities would be zero. The infidelity of the measurement can be quantified through the off-diagonal probabilities. For example,

$$1 - \mathcal{F} = 1 - \frac{1}{d} \sum_i p_{ii} = \frac{1}{d} \sum_i \sum_{j \neq i} p_{ij}. \quad (19)$$

Here, the first equality sign is a definition, the second one follows from the sum rule, Eq. (18). Also,  $d$  is the number of outcomes, assumed to be the size of the Hilbert space: For example,  $d = 2$  for a two-outcome measurement of a two-level system (a qubit). In this most usual case, the measurement probabilities are quantified by two error probabilities,  $p_{01}$  and  $p_{10}$ , as depicted in Fig. 7. The resulting measurement infidelity according to the definition in Eq. (19) is  $(p_{01} + p_{10})/2$ .

Finally, let us consider the fidelity of the initialization. Typically, one is interested in an initialization into a single pure state  $|\Psi\rangle$ . In this case, we can use Eq. (14) to define the initialization fidelity with  $\rho$  the actual, perhaps imperfectly prepared, state.

## B. Measured values of fidelities

The three panels of Fig. 8 show the published fidelities of the gates, measurements, and initializations, respectively. For

<sup>13</sup> Ref. [61] gives one list of elementary gates for a single-qubit case, resulting in the ratio of 1.875. For the two-qubit case, Refs. [103, 216] used elementary-gate sets with the ratio of 2.57. However, larger ratios also appear: for example, 9.75 in Ref. [297].

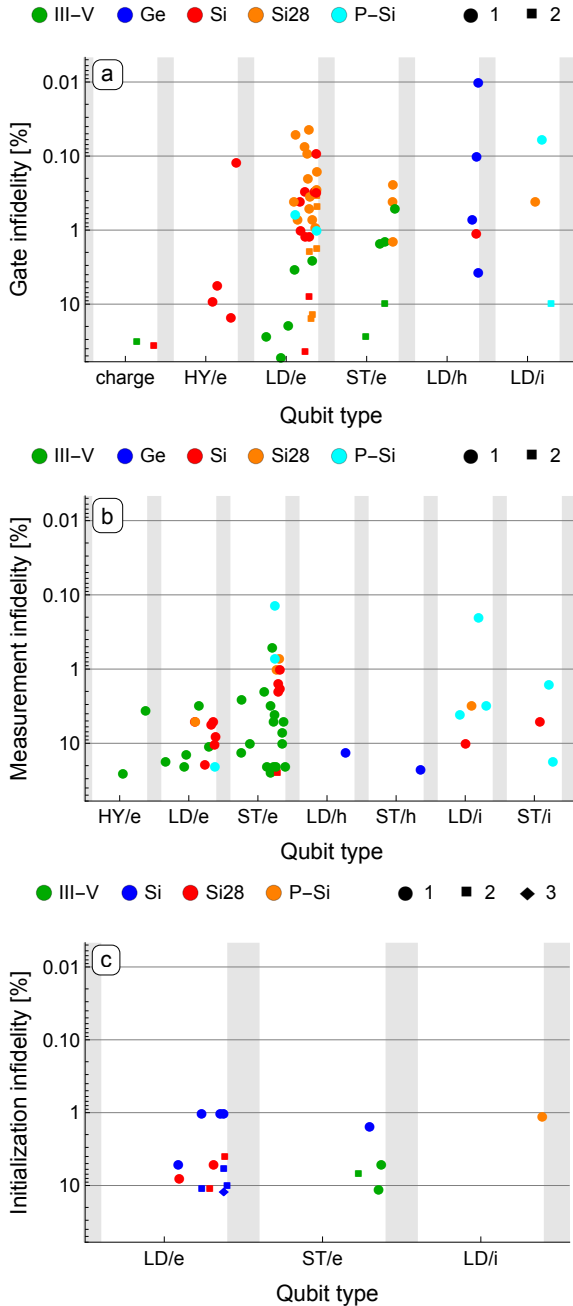


FIG. 8. Operation infidelities: (a) gates, (b) measurements, and (c) initializations. In all panels the horizontal axis shows the qubit type, restricting to those for which infidelity values exist. Within each type, the publication date is reflected by shifting the points laterally, similarly as in Fig. 3. The vertical axis shows the infidelity  $1 - F$  in percent. The point color indicates the material and its symbol the number of qubits involved in the operation, according to the individual panel legend.

the gates, Fig. 8(a), one notes that the qubits based on the electron spin reached the highest fidelities, well above 99.9%. Using silicon, both natural and isotopically purified, was crucial for this achievement. There is one experiment with an impurity spin, and one with a hole spin, which also crossed this

threshold. The singlet-triplet qubits show almost an order of magnitude higher infidelities, and charge or hybrid qubits are further behind. In any case, pushing down the infidelity of single-spin gates is one of the most impressive achievements within the whole spin-qubit field.

Figure 8(b) shows the fidelities of measurements. Until recently, the infidelities remained above few percent. Relying on a “latched” readout in the Pauli spin blockade [25, 193], the infidelities below 1% were achieved with singlet-triplet qubits.

We conclude with a remark on two-qubit fidelities. In all categories, meaning gates, measurements, and initializations, their infidelities remain one to two orders of magnitude above the single-qubit ones. Also, there are much less data published for the two-qubit versions. Concerning initializations, the more-qubit infidelities that we give are initializations into a nontrivial state achieved through some simple quantum algorithm. For example, initializing all individual qubits into single-qubit fiducial states, and then entangling them with gates into the desired entangled multi-qubit state, such as one of the two-qubit Bell states or the three-qubit GHZ state.

## V. QUALITY FACTOR $Q$

The quality factor is another dimensionless measure allowing comparison of diverse qubits, similar to the gate fidelity. The quality factor is a product of a gate frequency and a characteristic time scale. We denote the former by  $f_R$ , with the subscript suggesting the most typical case where the gate is implemented as EDSR-induced Rabi oscillations. There are two usual choices for the characteristic time, resulting in two groups of quality factors reported in the literature.

The first choice is using the inhomogeneous dephasing time. We call the resulting metric the qubit quality-factor,

$$Q = f_R T_2^*. \quad (20)$$

This  $Q$  counts the number of operations which can be performed on a given qubit, before other qubits, waiting idly, loose their coherence. With the possibility of dynamical decoupling, one might consider using other coherence times instead of  $T_2^*$ , as the time for which the other qubits can wait before loosing coherence. However, we know only a single case where a different choice was made for this type of the quality factor,  $T_2^H$  in [56], and therefore stick to Eq. (20).

The second choice is using the gate-signal decay time. Though it is not exclusive to Rabi-induced gates, we denote it using the symbol  $T_2^R$  introduced in Sec. II, again as the most typical scenario. We call the resulting quantity the gate quality-factor,

$$Q = f_R T_2^R. \quad (21)$$

In this form,  $Q$  gives the number of oscillations<sup>14</sup> at frequency  $f_R$  during the decay time  $T_2^R$ . We note that many references

<sup>14</sup> Indeed, Ref. [276] calls  $Q$  defined in Eq. (21) a “number of gate oscillations”, which might have been a better name than a “quality factor”.

reporting the gate quality-factors use Eq. (21) with the right-hand side multiplied by a factor of two. While such a factor is understandable looking at Eq.(9), we adopt Eq. (21) to make it more directly comparable to Eq. 20. As a consequence, we have to divide several of the reported values for the gate quality-factors by two. Finally, we note that the gate quality-factor is related to the gate fidelity, both being a qualitative measure of the gate imperfections. In App. B we derive  $1 - \mathcal{F} \approx 1/4Q$  valid for a large  $Q$  in a toy model with exponential dephasing.

Figure 9(a) shows the published data on quality factors, both gate and qubit ones. The majority of the values is within the range of few to about a hundred. There are some exceptions which crawl toward a thousand. Figure 9(b) makes it easier to compare different qubit types and discriminate the gate and qubit quality-factors. Since among the two dephasing times it is typically  $T_2^*$  being smaller than  $T_2^R$ , one expects that the gate quality-factors will reach higher values than qubit quality-factors. There is some evidence in favor of this expectation, but more data is needed to decide on its generality.

## VI. SIZE OF QUBIT ARRAYS

Scaling up qubit devices is the biggest current challenge of the field. The statement applies to all qubit platforms, not only to semiconducting qubits. For serious applications, being able to build large two-dimensional arrays seems necessary since the fault-tolerant thresholds for error-correction in one-dimensional arrays remain too low (see Tab. VIII in Ref. [55]).

### A. The definition of qubit-array functionality levels

While it is possible to fabricate relatively large gated arrays with semiconductors, making them functional is a different story. Therefore, we discriminate several functionality levels. We note that the assignment of the levels as defined below to a specific experiment is often difficult. This assignment is perhaps the most subjective of all made in this review. The reader is advised to consult the original work to judge the details of the achievements.

We define the following values, in ascending order according to the device functionality:

***N*-qubit device.** A structure capable of hosting  $N$  qubits has been fabricated. The gating and charge sensing work, so that all qubit hosts can be brought into the required charge configuration. On top of this minimal requirement, the articles assigned to this category report a large variation of additional features: single EDSR gates, tunable interdot tunneling or coupling, controllable charge shuffling, spin detection based on Pauli spin blockade, estimations of qubit-qubit interaction strength, and so on.

***N*-qubit simulator.** First of all, the device is stable and tunable enough to search large regions in the high-dimensional

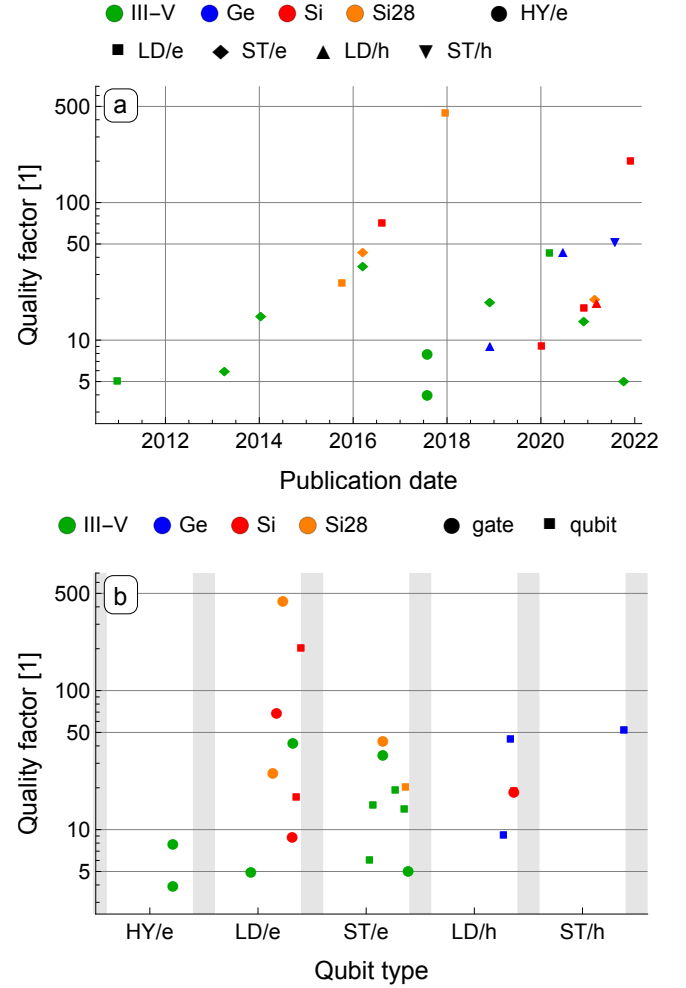


FIG. 9. Quality factors. The two panels show the same data. In (a), according to the publication date, with the point color indicating the material and point symbol the qubit type, according to the panel legend. In (b), the qubit type is on the horizontal axis, the publication date is reflected by shifting the points laterally, similarly as in Fig. 3. The point color indicates the material and its symbol discriminates the qubit and the gate quality-factor as defined in Eq. (20) and Eq. (21), respectively.

charge diagram. For example, aiming at single-electron LD qubits, the structure can be brought into the 1-1-1-...-1 charge state, or the (11)-(11)-...-(11) state for ST qubits. In such a configuration, qubits can interact pair-wisely and all  $N$  qubits are connected by an interaction path. The interactions are tunable. Either one qubit can be measured and manipulated at the single-qubit level, or at least qubit-qubit (being spin-spin) correlations can be measured.

***N*-qubit processor.** Every qubit (or most of them) has a two-axis control and can be measured. Qubits can interact pair-wisely through tunable interactions. The structure can perform  $N$ -qubit algorithms.

To cast more light on the ambiguities that we met and deci-

sions we took on them, let us make a few additional comments.

First, we do not include many-qubit structures which were fabricated but no functionality was demonstrated, no matter what their size was. We do not include experiments where multiple-dot structure was involved without any intention towards using it for qubits (for example, it was used in a transport experiment).

Second, the vast majority of the experiments within the spin-qubit field until now was done with a single dot implementing spin-one-half qubit or a double dot implementing a singlet-triplet qubit. Therefore, we normally do not include these two cases into our tables and figures. One exception is if the experiment is somewhat outstanding, perhaps pioneering a spin qubit in a new material or platform. We included some of these.

Third, the number of qubits is not the same as the number of dots. For example, a double-dot with two-electrons can be viewed both as one singlet-triplet qubit as well as two qubits of spin-one-half with a limited functionality. In these cases, we follow the primary intention of the experiment as we understood it from the reference. For example, a triple dot implementing a resonant-exchange qubit is counted as a single-qubit structure implementing a fully functional resonant-exchange qubit (that is, a hybrid qubit in our nomenclature), and not as a structure implementing three spin-one-half qubits with a limited functionality.

Finally, in Refs. [52, 269] there is no single-qubit gate nor measurement available. Still, we assign it to the quantum-simulator category, as in these experiments a simulation was the primary target and controllable spin-spin interactions played a critical role.

## B. Sizes of qubit arrays achieved experimentally

The sizes of qubit arrays appearing in publications on experiments are displayed in Fig. 10. The panel (a) shows the progress over time. A lot of effort goes into scaling up the spin-qubit structures, with slow but nevertheless steady progress. It took about ten to fifteen years to bring the most basic structure of the spin-qubit field, the double dot, up to the functionality of a quantum processor, as defined in the above list: With the experiments starting around 2005 [218], Refs. [276, 285, 306] could be acknowledged to have reached the “processor” level, and only in the most recent one the fidelities were high enough to run the most elementary quantum circuits. We assign the accomplishment of the first fully-functional “processor” beyond the double dot to the year 2021, with Ref. [257] using electrons in silicon and Ref. [97] using holes in germanium. In Fig. 10(b) one can see that the recent couple of years have brought a surge of results demonstrating progress in building spin-qubit arrays with advanced functionality. The fact that these recent breakthroughs come from many groups and happen in diverse materials and geometries gives excellent reasons for optimism on the scaling-up finally taking off.

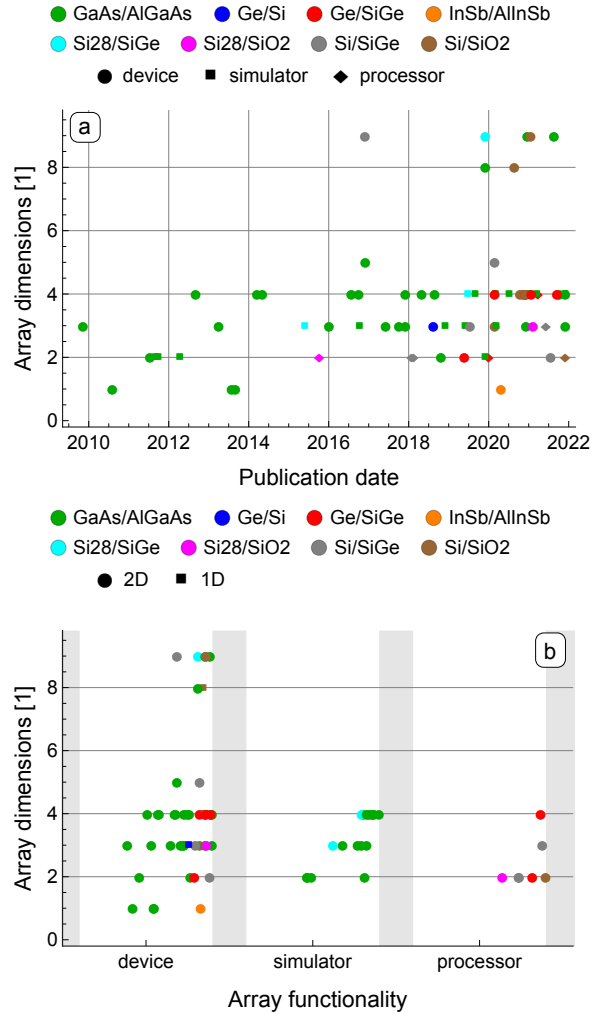


FIG. 10. Size of qubit arrays. The two panels show the same data: in (a) according to the publication date, with the point color indicating the material and point symbol the array functionality (see the text for the definitions), according to the panel legend. In (b), the array functionality is on the horizontal axis, the publication date is reflected by shifting the points laterally, similarly as in Fig. 3. The point color indicates the material and its symbol the host geometry, according to the panel legend.

## VII. ACKNOWLEDGMENTS

We thank Takashi Nakajima, Akito Noiri, Kenta Takeda, and other members of Seigo Tarucha laboratory in RIKEN, for numerous discussions that were invaluable for preparing this review. We also thank Leon Camenzind, Matthieu Delbecq, Georgios Katsaros, Ferdinand Kuemmeth, Tristan Meunier, Andrea Morello, Takashi Nakajima, Akito Noiri, Matthew Reed, and Menno Veldhorst for providing feedback on early versions of the review. Finally, we would like to acknowledge the financial support from CREST JST (JPMJCR1675) and Swiss National Science Foundation (SNSF) and NCCR SPIN.

## Appendix A: Relaxation time notations

To define the notation and give an example of the simplest dephasing form, we state here the result of Markovian (or exponential) decay displayed by the Bloch equations. Let us consider the following two parametrizations of the density matrix of a spin one-half

$$\rho = \begin{pmatrix} \rho_{\uparrow\uparrow} & \rho_{\uparrow\downarrow} \\ \rho_{\downarrow\uparrow} & \rho_{\downarrow\downarrow} \end{pmatrix} = \frac{1}{2} \begin{pmatrix} 1 + s_z & s_x - is_y \\ s_x + is_y & 1 - s_z \end{pmatrix} \equiv \frac{1}{2} (1 + \mathbf{s} \cdot \boldsymbol{\sigma}). \quad (\text{A1})$$

The defining and normalization conditions of a density matrix (trace one, Hermiticity, and positive semi-definiteness), require that the vector  $\mathbf{s}$  is real and its length is not larger than one.

The Bloch equations [13], describing the exponential decay of the density-matrix components, read

$$\partial_t s_x = -\frac{s_x}{T_2}, \quad (\text{A2a})$$

$$\partial_t s_y = -\frac{s_y}{T_2}, \quad (\text{A2b})$$

$$\partial_t s_z = -\frac{s_z - s_{0z}}{T_1}, \quad (\text{A2c})$$

with  $s_{0z}$  being the equilibrium spin polarization. The spin decay is described by two parameters,  $T_1$  and  $T_2$ , called, respectively, the longitudinal and transverse relaxation time in the original work of Bloch. We denote the inverse of these times as rates,  $\Gamma_1 = 1/T_1$  and  $\Gamma_2 = 1/T_2$ , that is, with the indexes corresponding.

We now use the alternative parameterization of the density matrix, where the exponential decay reads

$$\partial_t \rho_{\uparrow\uparrow} = -\Gamma_{ex} \rho_{\uparrow\uparrow} + \Gamma_{rel} \rho_{\downarrow\downarrow}, \quad (\text{A3a})$$

$$\partial_t \rho_{\uparrow\downarrow} = -\left(\frac{\Gamma_{ex} + \Gamma_{rel}}{2} + \Gamma_\varphi\right) \rho_{\uparrow\downarrow}, \quad (\text{A3b})$$

and the remaining matrix elements evolution is fixed by the requirements  $\rho_{\uparrow\uparrow} + \rho_{\downarrow\downarrow} = 1$  and  $\rho_{\uparrow\downarrow} = \rho_{\downarrow\uparrow}^*$ . Here, we use the notation of Ref. [105], which originates in the assumption that the spin-up state is the energy ground state and the equations contain  $\Gamma_{ex}$ , the rate of excitations from the ground state,  $\Gamma_{rel}$  the rate of relaxation into the ground state, and  $\Gamma_\varphi$ , the “pure-dephasing” rate. With the following relations,

$$\frac{1}{T_1} = \Gamma_{ex} + \Gamma_{rel}, \quad (\text{A4a})$$

$$\frac{1}{T_2} = \frac{\Gamma_{ex} + \Gamma_{rel}}{2} + \Gamma_\varphi, \quad (\text{A4b})$$

$$s_{0z} = \frac{\Gamma_{rel} - \Gamma_{ex}}{\Gamma_{rel} + \Gamma_{ex}}, \quad (\text{A4c})$$

the two sets of equations, (A2) and (A3), correspond to each other.

In the above equations for the density matrix evolution, we dropped the coherent part, which would read  $\partial_t \mathbf{s} = (g\mu_B/\hbar)\mathbf{s} \times \mathbf{B}$ , with  $g$  being the electron g-factor and  $\mathbf{B}$  the magnetic field. Equations (A2) are derived in Ref. [64] in a simple model

on p. 707-712. The same reference derives also Eq. (A3) on p. 759-765, considering a spin qubit coupled to phonons as the decay source, following the standard methods of Ref. [16].

## Appendix B: Relation of the gate fidelity and the gate quality factor

The gate quality-factor is closely related to the gate fidelity, as we now illustrate. Let us consider a Rabi-oscillations experiment with a qubit. In the rotating frame, we describe it using a density matrix parameterized by vector  $\mathbf{s}$ . The Rabi oscillations induced by a resonant drive result in a time dependence of this vector. In an ideal scenario without errors or decoherence, the qubit rotates at a fixed frequency  $f$  around certain axis, set by the driving pulse phase. The time evolution is

$$\rho_{ideal}(t) = \frac{1}{2} (1 + \mathbf{s}(t) \cdot \boldsymbol{\sigma}). \quad (\text{B1})$$

The ideal state at certain specific times corresponds to  $|\Psi(t)\rangle\langle\Psi(t)|$ . For example, with the initial state along  $z$ ,  $\mathbf{s}(0) = (0, 0, 1)$  and a rotation axis  $x$ , at time  $t = 1/2f$  an ideal  $\pi$  rotation is performed.

Let us now consider the coherence decay given by Eq. (A2). Assuming, for simplicity, that either the rotation is in the plane of the Bloch sphere perpendicular to the energy-quantization axis, or taking  $T_2 = T_1$  and  $s_{0z} = 0$ , the actual density matrix is described by  $\mathbf{s}(t) \exp(-t/T_2)$ . The amplitude of the oscillating polarization measured as a function of time will decay exponentially, as  $\exp(-t/T_2)$ . The fitted time-scale of the decay is called the “gate decay time”  $T_2^R$  entering Eq. (21). Evaluating the fidelity with Eq. (14) gives

$$\mathcal{F} = \frac{1}{2} (1 + \exp(-t/T_2)). \quad (\text{B2})$$

For a  $\pi$ -rotation gate, implemented imperfectly at time  $t = 1/2f$ , it finally gives

$$\mathcal{F} = \frac{1}{2} (1 + \exp(-1/2Q)) \approx 1 - \frac{1}{4Q}, \quad (\text{B3})$$

where the approximation is valid for small infidelity or large quality factor.

In this toy model, the gate infidelity and the gate quality-factor are in a simple one-to-one correspondence. In reality, the relation is complicated by two facts. First, the dephasing might be more complicated than the Markovian decay described by the Bloch equations. More importantly, the signal decay and the fidelity are influenced differently by unitary gate-errors. The latter are deviations from the desired gate which do not originate in dephasing: for example, if the rotation axis is not exactly along  $x$  or the rotation angle is below the target value  $\pi$ . By definition of the name, the unitary errors are systematic, that is they do not change in time. If known, they could be corrected by additional unitary rotations. Nevertheless, if they are not known, for example due to insufficient calibration, or they could not be corrected, they do diminish the gate fidelity. On the other hand, they do not lead to the

gate-signal decay  $T_2^R$  as extracted experimentally. At most, they diminish the overall signal magnitude, called the visibility. To conclude, because of the unitary errors diminishing the fidelity but not the gate quality-factor, the right hand side in Eq. (B3) becomes only the upper limit for the left hand side.

**Appendix C: List of tables**

Content	Table	Page
Spin coherence	Tab. I	17-20
Charge coherence	Tab. II	22
Operation times	Tab. III	23-24
Operation fidelities	Tab. IV	26-27
Quality factors	Tab. V	28
Qubit arrays	Tab. VI	30-31

Material	Host	Qubit	Coherence	Time	Source	Date	Reference
CNT	1D	LD/e	$T_2^H$	<b>65 ns</b>	p4 and Fig. 4	2013-08	143
CNT	1D	ST/e	$T_2^*$	<b>3.2 ns<sup>a</sup></b>	p3	2009-04	38
CNT	1D	LD/e	$T_2^*$	<b>8 ns</b>	p4 and Fig. 4	2013-08	143
CNT	1D	LD/e	$T_2^*$	<b>64 ns<sup>b</sup></b>	p4	2015-07	277
CNT	1D	LD/e	$T_2^*$	<b>0.64 <math>\mu</math>s</b>	p2 and Fig. 3d	2019-12	48
GaAs/AlGaAs	1D	LD/h	$T_1$	<b>5 ns</b>	p4 and SM pS5	2016-12	282
GaAs/AlGaAs	2D	LD/e	$T_1$	<b>50 <math>\mu</math>s</b>	abstract	2003-11	85
GaAs/AlGaAs	2D	LD/e	$T_1$	<b>0.85 ms</b>	p4	2004-07	59
GaAs/AlGaAs	2D	ST/e	$T_1$	<b>2.3 ms<sup>c</sup></b>	p2	2007-03	180
GaAs/AlGaAs	2D	LD/e	$T_1$	<b>1 s</b>	p4 and Fig. 3c the leftmost blue point	2008-01	2
GaAs/AlGaAs	2D	ST/e	$T_1$	<b>34 <math>\mu</math>s</b>	p3	2009-10	11
GaAs/AlGaAs	2D	ST/e	$T_1$	<b>40 <math>\mu</math>s<sup>d</sup></b>	p5	2012-01	9
GaAs/AlGaAs	2D	LD/e	$T_1$	<b>85 ms</b>	p2 and Fig. 3	2014-12	234
GaAs/AlGaAs	2D	LD/e	$T_1$	<b>3.7 ms</b>	p3 and Fig. 2	2016-07	6
GaAs/AlGaAs	2D	LD/e	$T_1$	<b>10 s</b>	Fig. 2 the lowest green point	2017-10	101
GaAs/AlGaAs	2D	LD/e	$T_1$	<b>57 s</b>	p3 and Fig. 4a	2018-12	29
GaAs/AlGaAs	2D	LD/e	$T_1$	<b>1.5 ms</b>	Fig. 2	2019-06	195
GaAs/AlGaAs	2D	LD/h	$T_1$	<b>60 <math>\mu</math>s</b>	abstract and Fig. 4	2019-12	18
GaAs/AlGaAs	2D	ST/e	$T_2^D$	<b>80 <math>\mu</math>s</b>	p3	2010-12	10
GaAs/AlGaAs	2D	ST/e	$T_2^D$	<b>0.28 ms</b>	Fig. 3	2011-02	15
GaAs/AlGaAs	2D	ST/e	$T_2^D$	<b>0.13 ms<sup>e</sup></b>	Fig. 3b	2012-02	177
GaAs/AlGaAs	2D	HY/e <sup>f</sup>	$T_2^D$	<b>19 <math>\mu</math>s</b>	p3 and Fig. 5 the rightmost point	2013-07	176
GaAs/AlGaAs	2D	ST/e	$T_2^D$	<b>0.87 ms</b>	Fig. 5	2016-10	168
GaAs/AlGaAs	2D	ST/e	$T_2^D$	<b>0.3 ms</b>	Fig. 4c the point n=256	2017-04	167
GaAs/AlGaAs	2D	HY/e <sup>g</sup>	$T_2^D$	<b>1 <math>\mu</math>s</b>	Fig. 5b	2017-07	169
GaAs/AlGaAs	2D	HY/e <sup>h</sup>	$T_2^D$	<b>1 <math>\mu</math>s</b>	Fig. 5b	2017-07	169
GaAs/AlGaAs	2D	ST/e	$T_2^H$	<b>1.2 <math>\mu</math>s</b>	p4 and Fig. 5c	2005-09	218
GaAs/AlGaAs	2D	LD/e	$T_2^H$	<b>0.44 <math>\mu</math>s</b>	p4 and Fig. 4b	2008-06	137
GaAs/AlGaAs	2D	ST/e	$T_2^H$	<b>6 <math>\mu</math>s</b>	p3	2010-12	10
GaAs/AlGaAs	2D	ST/e	$T_2^H$	<b>30 <math>\mu</math>s</b>	abstract and SM p9	2011-02	15
GaAs/AlGaAs	2D	ST/e	$T_2^H$	<b>7 <math>\mu</math>s<sup>i</sup></b>	Fig. 4	2012-02	177
GaAs/AlGaAs	2D	ST/e	$T_2^H$	<b>9 <math>\mu</math>s</b>	p3	2013-04	56
GaAs/AlGaAs	2D	HY/e <sup>f</sup>	$T_2^H$	<b>2 <math>\mu</math>s<sup>j</sup></b>	Fig. 5	2013-07	176
GaAs/AlGaAs	2D	HY/e <sup>k</sup>	$T_2^H$	<b>0.1 <math>\mu</math>s</b>	p3	2013-09	175
GaAs/AlGaAs	2D	ST/e	$T_2^H$	<b>0.18 <math>\mu</math>s</b>	p4	2016-06	32
GaAs/AlGaAs	2D	ST/e	$T_2^H$	<b>8.5 <math>\mu</math>s</b>	Fig. 4c the point n=1	2017-04	167
GaAs/AlGaAs	2D	ST/e	$T_2^H$	<b>7 <math>\mu</math>s</b>	Fig. 2b	2017-12	196
GaAs/AlGaAs	2D	ST/e	$T_2^H$	<b>6.1 <math>\mu</math>s</b>	p4	2020-12	33
GaAs/AlGaAs	2D	LD/e	$T_2^R$	<b>37 ns<sup>l</sup></b>	p3	2014-12	302
GaAs/AlGaAs	2D	LD/e	$T_2^R$	<b>84 ns</b>	Fig. 3	2016-04	201
GaAs/AlGaAs	2D	HY/e <sup>g</sup>	$T_2^R$	<b>40 ns<sup>m</sup></b>	Fig. 4c	2017-07	169
GaAs/AlGaAs	2D	HY/e <sup>h</sup>	$T_2^R$	<b>80 ns<sup>m</sup></b>	Fig. 4c	2017-07	169
GaAs/AlGaAs	2D	ST/e	$T_2^R$	<b>0.7 <math>\mu</math>s</b>	p3 and Fig. 2b	2017-12	196
GaAs/AlGaAs	2D	LD/e	$T_2^R$	<b>0.53 <math>\mu</math>s</b>	Fig. 2	2019-06	195
GaAs/AlGaAs	2D	LD/e	$T_2^R$	<b>1.3 <math>\mu</math>s</b>	Fig. 6	2020-03	194
GaAs/AlGaAs	2D	HY/e	$T_2^R$	<b>37 ns</b>	Fig. 3b	2021-06	109
GaAs/AlGaAs	2D	ST/e	$T_2^R$	<b>86 ns</b>	p3	2021-12	133
GaAs/AlGaAs	2D	ST/e	$T_2^*$	<b>9 ns</b>	p3	2005-06	115
GaAs/AlGaAs	2D	ST/e	$T_2^*$	<b>25 ns</b>	p5	2005-08	134
GaAs/AlGaAs	2D	ST/e	$T_2^*$	<b>10 ns</b>	p3 and Fig. 3b	2005-09	218

TABLE I-1. Spin coherence times (part 1). Superscripts stand for the following. <sup>a</sup>: Carbon nanotube made from  $^{13}\text{C}$  isotope. <sup>b</sup>: From linewidth. <sup>c</sup>: A single-dot singlet. <sup>d</sup>: From several relaxation times defined, we take the inverse of the "bare triplet relaxation rate"  $1/\Gamma_T = 40 \mu\text{s}$ . <sup>e</sup>: (estimated) Fig. 3b the rightmost point. <sup>f</sup>: RX qubit. <sup>g</sup>: At a partial sweet spot. <sup>h</sup>: At a full sweet spot. <sup>i</sup>: (estimated) Fig. 4 the leftmost point. <sup>j</sup>: (estimated) Fig. 5 the leftmost point. <sup>k</sup>: EO qubit. <sup>l</sup>: At Rabi frequency  $f_R = 85.9 \text{ MHz}$ . <sup>m</sup>: Approximate value at  $f_R = 100 \text{ MHz}$ .

Material	Host	Qubit	Coherence	Time	Source	Date	Reference
GaAs/AlGaAs	2D	ST/e	$T_2^*$	<b>14 ns</b>	p1	2006-07	144
GaAs/AlGaAs	2D	LD/e	$T_2^*$	<b>20 ns</b>	p1	2007-09	136
GaAs/AlGaAs	2D	LD/e	$T_2^*$	<b>30 ns</b>	p2	2008-06	137
GaAs/AlGaAs	2D	ST/e	$T_2^*$	<b>15 ns</b>	p2 and Fig. 1e	2008-12	227
GaAs/AlGaAs	2D	ST/e	$T_2^*$	<b>27 ns</b>	p4	2009-10	11
GaAs/AlGaAs	2D	ST/e	$T_2^*$	<b>15 ns</b>	p2 and Fig. 1	2010-06	228
GaAs/AlGaAs	2D	ST/e	$T_2^*$	<b>5.6 ns</b>	p4	2010-08	214
GaAs/AlGaAs	2D	ST/e	$T_2^*$	<b>14 ns<sup>a</sup></b>	p2 and Fig. 3a	2010-11	14
GaAs/AlGaAs	2D	ST/e	$T_2^*$	<b>94 ns<sup>b</sup></b>	Fig. 3b	2010-11	14
GaAs/AlGaAs	2D	ST/e	$T_2^*$	<b>16 ns</b>	SM SFig. 1	2011-02	15
GaAs/AlGaAs	2D	ST/e	$T_2^*$	<b>40 ns<sup>b</sup></b>	SM SFig. 1	2011-02	15
GaAs/AlGaAs	2D	HY/e <sup>c</sup>	$T_2^*$	<b>18 ns</b>	p2	2011-11	75
GaAs/AlGaAs	2D	ST/e	$T_2^*$	<b>90 ns</b>	p2	2013-04	56
GaAs/AlGaAs	2D	HY/e <sup>c</sup>	$T_2^*$	<b>25 ns</b>	p3	2013-09	175
GaAs/AlGaAs	2D	ST/e	$T_2^*$	<b>2.1 <math>\mu</math>s<sup>b</sup></b>	p4 and Fig. 3b	2014-10	247
GaAs/AlGaAs	2D	LD/e	$T_2^*$	<b>61 ns<sup>d</sup></b>	p3	2014-12	302
GaAs/AlGaAs	2D	ST/e	$T_2^*$	<b>80 ns<sup>e</sup></b>	Fig. 4d	2015-08	12
GaAs/AlGaAs	2D	ST/e	$T_2^*$	<b>0.6 <math>\mu</math>s<sup>f</sup></b>	p3	2016-01	54
GaAs/AlGaAs	2D	HY/e	$T_2^*$	<b>8.1 ns</b>	p4 and Fig. 4d	2016-02	31
GaAs/AlGaAs	2D	ST/e	$T_2^*$	<b>0.1 <math>\mu</math>s<sup>b</sup></b>	p2	2017-12	196
GaAs/AlGaAs	2D	ST/e	$T_2^*$	<b>14 ns</b>	p2	2017-12	74
GaAs/AlGaAs	2D	ST/e	$T_2^*$	<b>80 ns<sup>g</sup></b>	p3	2017-12	68
GaAs/AlGaAs	2D	LD/h	$T_2^*$	<b>0.12 ns<sup>h</sup></b>	p4	2018-05	19
GaAs/AlGaAs	2D	HY/e <sup>i</sup>	$T_2^*$	<b>16 ns<sup>j</sup></b>	p2	2018-08	146
GaAs/AlGaAs	2D	ST/e	$T_2^*$	<b>0.21 <math>\mu</math>s</b>	p4	2018-12	197
GaAs/AlGaAs	2D	ST/e	$T_2^*$	<b>0.89 ns<sup>i</sup></b>	p2	2019-05	148
GaAs/AlGaAs	2D	LD/e	$T_2^*$	<b>0.21 <math>\mu</math>s</b>	Fig. 2	2019-06	195
GaAs/AlGaAs	2D	HY/e <sup>i</sup>	$T_2^*$	<b>29 ns<sup>j</sup></b>	p3	2019-12	147
GaAs/AlGaAs	2D	LD/e	$T_2^*$	<b>0.77 <math>\mu</math>s<sup>b</sup></b>	p3 and Fig. 3b	2020-03	194
GaAs/AlGaAs	2D	LD/e	$T_2^*$	<b>28 ns</b>	p2 and Fig. 2c	2020-03	194
GaAs/AlGaAs	2D	ST/e	$T_2^*$	<b>15 ns</b>	p4	2020-12	111
GaAs/AlGaAs	2D	ST/e	$T_2^*$	<b>22 ns</b>	Fig. 2a the green trace	2020-12	110
GaAs/AlGaAs	2D	ST/e	$T_2^*$	<b>12 ns</b>	p1 and Fig. 2b	2021-05	108
GaAs/AlGaAs	2D	HY/e	$T_2^*$	<b>7 ns</b>	p4 and Fig. 3c	2021-06	109
GaAs/AlGaAs	2D	LD/e	$T_2^*$	<b>0.12 <math>\mu</math>s<sup>k</sup></b>	Fig. 5f the topmost point	2021-08	188
GaAs/AlGaAs	2D	ST/e	$T_2^*$	<b>22 ns</b>	Fig. 2c Qubit 2	2021-10	65
GaAs/AlGaAs	2D	ST/e	$T_2^*$	<b>21 ns</b>	p5	2021-12	133
Ge/Si	1D	LD/h	$T_1$	<b>86 <math>\mu</math>s</b>	p3 and Fig. 3c the leftmost point	2018-11	281
Ge/Si	1D	LD/h	$T_1$	<b>3.7 <math>\mu</math>s</b>	p6	2020-06	284
Ge/Si	1D	LD/h	$T_2^H$	<b>0.52 <math>\mu</math>s</b>	p8 and Fig. 3f	2020-06	284
Ge/Si	1D	LD/h	$T_2^H$	<b>0.25 <math>\mu</math>s</b>	Fig. 2e	2021-01	71
Ge/Si	1D	LD/h	$T_2^R$	<b>60 ns</b>	Fig. 3d	2021-01	71
Ge/Si	1D	LD/h	$T_2^*$	<b>0.18 <math>\mu</math>s</b>	p3	2014-06	100
Ge/Si	1D	LD/h	$T_2^*$	<b>0.13 <math>\mu</math>s</b>	p4 and Fig. 6d	2018-12	288
Ge/Si	1D	LD/h	$T_2^*$	<b>82 ns</b>	p7 and Fig. 3	2020-06	284
Ge/Si	1D	LD/h	$T_2^*$	<b>11 ns</b>	Fig. 2e	2021-01	71
Ge/SiGe	2D	LD/h	$T_1$	<b>9 <math>\mu</math>s</b>	p3 and Fig. 2f	2020-01	95
Ge/SiGe	2D	LD/h	$T_1$	<b>32 ms</b>	p3	2020-08	152
Ge/SiGe	2D	LD/h	$T_1$	<b>1.2 ms</b>	p4 and Fig. 3a	2020-12	96
Ge/SiGe	2D	LD/h	$T_1$	<b>16 ms</b>	Fig. S5 dot 3	2021-03	97

TABLE I-2. Spin coherence times (part 2). Superscripts stand for the following. <sup>a</sup>: Without feedback. <sup>b</sup>: With feedback. <sup>c</sup>: EO qubit. <sup>d</sup>: From ESR linewidth. <sup>e</sup>: (estimated) from Fig. 4d. <sup>f</sup>: In non-ergodic regime. <sup>g</sup>: Dephasing of transported spin. <sup>h</sup>: Using LZ interference. <sup>i</sup>: RX qubit. <sup>j</sup>: From linewidth. <sup>k</sup>: The value of the point, 118 ns, is from T. Meunier, private communication.

Material	Host	Qubit	Coherence	Time	Source	Date	Reference
Ge/SiGe	2D	LD/h	$T_2^D$	<b>0.1 ms</b>	Fig. S6 dot 3	2021-03	97
Ge/SiGe	2D	ST/h	$T_2^D$	<b>0.16 ms</b>	p6 and Fig. 5	2021-08	112
Ge/SiGe	2D	LD/h	$T_2^H$	<b>1.9 <math>\mu</math>s</b>	p2 and Fig. 2f	2020-01	95
Ge/SiGe	2D	LD/h	$T_2^H$	<b>3.8 <math>\mu</math>s</b>	Fig. S6 dot 3	2021-03	97
Ge/SiGe	2D	ST/h	$T_2^H$	<b>1.8 <math>\mu</math>s<sup>a</sup></b>	Fig. 5 of arXiv-v3	2021-08	112
Ge/SiGe	2D	LD/h	$T_2^*$	<b>0.83 <math>\mu</math>s</b>	p2 and Fig. 2f	2020-01	95
Ge/SiGe	2D	LD/h	$T_2^*$	<b>0.33 <math>\mu</math>s</b>	p4 and Fig. 4b	2020-12	96
Ge/SiGe	2D	LD/h	$T_2^*$	<b>0.45 <math>\mu</math>s</b>	Fig. S6 dot 3	2021-03	97
Ge/SiGe	2D	ST/h	$T_2^*$	<b>0.7 <math>\mu</math>s</b>	Fig. 3f 1.0 mT trace	2021-08	112
Ge/SiGe	2D	LD/h	$T_2^*$	<b>0.47 <math>\mu</math>s<sup>b</sup></b>	Fig. 1 caption	2021-09	153
InAs	1D	LD/e	$T_1$	<b>1 <math>\mu</math>s</b>	Fig. 4d	2012-10	212
InAs	1D	LD/e	$T_2^D$	<b>0.15 <math>\mu</math>s</b>	Fig. 4a inset the highest point	2010-12	192
InAs	1D	LD/e	$T_2^H$	<b>50 ns</b>	p3	2010-12	192
InAs	1D	LD/e	$T_2^*$	<b>8 ns</b>	p3	2010-12	192
InGaAs/AlGaAs	2D	ST/e	$T_1$	<b>0.2 ms</b>	p3 and Fig. 3e	2002-09	73
InSb	1D	LD/e	$T_2^H$	<b>34 ns</b>	p3	2013-02	266
InSb	1D	LD/e	$T_2^*$	<b>8 ns</b>	p3	2013-02	266
P-Si	imp	LD/i	$T_1$	<b>6 s</b>	p2	2010-10	186
P-Si	imp	LD/i	$T_1$	<b>30 s</b>	Fig. 2b the lowest point	2017-03	286
P-Si	imp	LD/i	$T_1$	<b>1.3 s</b>	p3 and Fig. 2b	2018-12	289
P-Si	imp	LD/e	$T_1$	<b>9.8 s</b>	Fig. 2c	2019-05	261
P-Si	imp	LD/e	$T_2^D$	<b>10 ms</b>	p4 and Fig. 3j	2015-04	150
P-Si	imp	LD/e	$T_2^H$	<b>0.97 ms</b>	p4 and Fig. 3h	2015-04	150
P-Si28	imp	LD/i <sup>c</sup>	$T_1$	<b>1.3 s</b>	p4	2016-10	149
P-Si28	imp	LD/i	$T_1$	<b>3 s</b>	p3	2016-10	50
P-Si28	imp	LD/e	$T_1$	<b>3.1 ms</b>	ED Fig. 3 first column	2021-07	162
P-Si28	imp	LD/i	$T_1$	<b>3.4 s</b>	p6 and SFig. 3c	2021-12	164
P-Si28	imp	LD/i <sup>c</sup>	$T_2^D$	<b>23 ms</b>	p4	2016-10	149
P-Si28	imp	LD/i	$T_2^H$	<b>0.31 ms</b>	Fig. 4d	2016-02	264
P-Si28	imp	LD/i <sup>c</sup>	$T_2^H$	<b>9.2 ms</b>	p4	2016-10	149
P-Si28	imp	LD/i	$T_2^H$	<b>1.7 ms</b>	Fig. 3	2020-07	163
P-Si28	imp	LD/e	$T_2^H$	<b>0.85 ms</b>	ED Fig. 3 first column	2021-07	162
P-Si28	imp	LD/i	$T_2^H$	<b>0.12 ms</b>	SFig. 3b	2021-12	164
P-Si28	imp	LD/i	$T_2^*$	<b>18 <math>\mu</math>s</b>	Fig. 4c	2016-02	264
P-Si28	imp	LD/i <sup>c</sup>	$T_2^*$	<b>2.4 ms</b>	p4	2016-10	149
P-Si28	imp	ST/e <sup>d</sup>	$T_2^*$	<b>1.3 <math>\mu</math>s</b>	p4	2017-12	89
P-Si28	imp	LD/i	$T_2^*$	<b>0.11 ms</b>	Fig. 2b and i	2020-07	163
P-Si28	imp	LD/e	$T_2^*$	<b>0.12 ms</b>	ED Fig. 3 first column	2021-07	162
P-Si28	imp	LD/i	$T_2^*$	<b>9 <math>\mu</math>s</b>	p7 and SFig. 3a	2021-12	164
Si28/SiGe	2D	LD/e	$T_1$	<b>0.13 s</b>	p4	2019-12	249
Si28/SiGe	2D	LD/e	$T_1$	<b>1 s</b>	p6 and Fig. 4a	2020-03	102
Si28/SiGe	2D	LD/e	$T_2^D$	<b>3.1 ms</b>	Fig. 4a	2017-12	304
Si28/SiGe	2D	ST/e	$T_2^H$	<b>70 <math>\mu</math>s</b>	Fig. S2 the topmost red point	2015-05	60
Si28/SiGe	2D	LD/e	$T_2^H$	<b>99 <math>\mu</math>s</b>	p3 and Fig. 3c	2017-12	304
Si28/SiGe	2D	LD/e	$T_2^H$	<b>0.11 ms</b>	Tab. 1	2019-06	248
Si28/SiGe	2D	LD/e	$T_2^H$	<b>0.13 ms</b>	Fig. 2d	2020-12	253
Si28/SiGe	2D	LD/e	$T_2^H$	<b>1 ms</b>	p6 and Fig. 5	2021-03	125
Si28/SiGe	2D	LD/e	$T_2^H$	<b>32 <math>\mu</math>s</b>	ED Fig. 2i the topmost trace	2021-08	199
Si28/SiGe	2D	ST/e	$T_2^R$	<b>0.28 <math>\mu</math>s<sup>e</sup></b>	p3, Fig. 4a and b	2016-03	225
Si28/SiGe	2D	LD/e	$T_2^R$	<b>0.11 ms</b>	p2	2017-12	304

TABLE I-3. Spin coherence times (part 3). Superscripts stand for the following. <sup>a</sup>: arXiv:2011.13755v3. <sup>b</sup>: We take the value for qubit 3 at 0.6 Tesla. <sup>c</sup>: Qubit defined in the rotating frame. <sup>d</sup>: Impurity-gated dot hybrid qubit. <sup>e</sup>: (derived) from  $T = hN_R/J$  with  $J/h = 160$  MHz and  $N_R = 44$ .

Material	Host	Qubit	Coherence	Time	Source	Date	Reference
Si28/SiGe	2D	LD/e <sup>a</sup>	$T_2^R$	<b>0.4 <math>\mu</math>s<sup>b</sup></b>	Fig. S2c	2019-08	3
Si28/SiGe	2D	ST/e	$T_2^R$	<b>6 <math>\mu</math>s</b>	p3	2020-03	258
Si28/SiGe	2D	LD/e	$T_2^R$	<b>0.1 ms<sup>c</sup></b>	ED Fig. 2l the topmost trace	2021-08	199
Si28/SiGe	2D	ST/e	$T_2^*$	<b>2.3 <math>\mu</math>s</b>	p3	2015-05	60
Si28/SiGe	2D	LD/e	$T_2^*$	<b>20 <math>\mu</math>s</b>	p3 and Fig. 3a	2017-12	304
Si28/SiGe	2D	LD/e	$T_2^*$	<b>0.13 <math>\mu</math>s<sup>d</sup></b>	p3 and Fig. 3b	2018-02	182
Si28/SiGe	2D	LD/e	$T_2^*$	<b>9.4 <math>\mu</math>s</b>	Tab.1	2019-06	248
Si28/SiGe	2D	LD/e <sup>a</sup>	$T_2^*$	<b>2 <math>\mu</math>s<sup>e</sup></b>	Fig. S2a	2019-08	3
Si28/SiGe	2D	LD/e	$T_2^*$	<b>10 <math>\mu</math>s</b>	p4	2019-12	249
Si28/SiGe	2D	ST/e	$T_2^*$	<b>1.3 <math>\mu</math>s</b>	Fig. 3c	2020-03	258
Si28/SiGe	2D	LD/e	$T_2^*$	<b>21 <math>\mu</math>s</b>	Fig. 3b	2020-12	253
Si28/SiGe	2D	LD/e	$T_2^*$	<b>6.8 <math>\mu</math>s</b>	Fig. 6 the blue point	2021-03	125
Si28/SiGe	2D	LD/e	$T_2^*$	<b>20 <math>\mu</math>s</b>	Fig. 3c	2021-07	296
Si28/SiGe	2D	LD/e	$T_2^*$	<b>7.4 <math>\mu</math>s</b>	ED Fig. 2f the topmost trace	2021-08	199
Si28/SiO2	2D	LD/e	$T_1$	<b>0.15 s<sup>f</sup></b>	p2 and p4	2018-08	215
Si28/SiO2	2D	LD/e	$T_1$	<b>2.8 ms<sup>g</sup></b>	p4 and Fig. 3a	2018-08	215
Si28/SiO2	2D	LD/e	$T_1$	<b>1 s</b>	p2	2018-10	34
Si28/SiO2	2D	LD/e <sup>h</sup>	$T_1$	<b>3.7 ms</b>	p2	2020-04	216
Si28/SiO2	2D	ST/e	$T_1$	<b>0.5 s<sup>i</sup></b>	Fig. 4 the leftmost black point	2020-04	300
Si28/SiO2	2D	ST/e	$T_1$	<b>15 ms<sup>j</sup></b>	Fig. 4 the rightmost black point	2020-04	300
Si28/SiO2	2D	LD/e	$T_1$	<b>1.6 s</b>	p3 and Fig. 3b	2021-01	310
Si28/SiO2	2D	ST/e	$T_1$	<b>0.2 ms<sup>k</sup></b>	p4 and Fig. 1d	2021-01	241
Si28/SiO2	2D	ST/e	$T_1$	<b>5 ms<sup>l</sup></b>	p4 and Fig. 1d	2021-01	241
Si28/SiO2	2D	LD/e	$T_2^D$	<b>28 ms</b>	p2 and Fig. 3c	2014-10	274
Si28/SiO2	2D	LD/e	$T_2^D$	<b>28 ms</b>	p1	2015-10	276
Si28/SiO2	2D	LD/e	$T_2^D$	<b>6.7 ms</b>	p2	2018-10	34
Si28/SiO2	2D	LD/e	$T_2^D$	<b>3.7 ms</b>	p4 and Fig. 4b	2021-01	310
Si28/SiO2	2D	ST/e	$T_2^D$	<b>20 <math>\mu</math>s<sup>m</sup></b>	Fig. 4c the rightmost blue point	2021-02	114
Si28/SiO2	2D	LD/e	$T_2^H$	<b>1.2 ms</b>	p2 and Fig. 3b	2014-10	274
Si28/SiO2	2D	LD/e	$T_2^H$	<b>0.4 ms</b>	p2	2018-10	34
Si28/SiO2	2D	ST/e	$T_2^H$	<b>8.4 <math>\mu</math>s</b>	p6 and Fig. 4f	2018-12	113
Si28/SiO2	2D	LD/e	$T_2^H$	<b>0.29 ms</b>	p3 and ExtData Fig. 1b	2019-05	103
Si28/SiO2	2D	ST/e	$T_2^H$	<b>0.2 ms<sup>i</sup></b>	Fig. 4 the leftmost blue point	2020-04	300
Si28/SiO2	2D	ST/e	$T_2^H$	<b>7 <math>\mu</math>s<sup>j</sup></b>	Fig. 4 the rightmost blue point	2020-04	300
Si28/SiO2	2D	ST/e	$T_2^H$	<b>5 <math>\mu</math>s<sup>n</sup></b>	Fig. 4c	2021-02	114
Si28/SiO2	2D	LD/e	$T_2^R$	<b>19 <math>\mu</math>s</b>	p3 and Fig. 2d	2019-12	308
Si28/SiO2	2D	LD/e	$T_2^*$	<b>0.12 ms</b>	p2 and Fig. 3a	2014-10	274
Si28/SiO2	2D	LD/e	$T_2^*$	<b>0.12 ms</b>	p1	2015-10	276
Si28/SiO2	2D	LD/e <sup>o</sup>	$T_2^*$	<b>70 <math>\mu</math>s</b>	p2 and Fig. 2b	2015-11	275
Si28/SiO2	2D	LD/e	$T_2^*$	<b>33 <math>\mu</math>s</b>	p2	2018-10	34
Si28/SiO2	2D	ST/e	$T_2^*$	<b>1.6 <math>\mu</math>s</b>	p6	2018-12	113
Si28/SiO2	2D	LD/e	$T_2^*$	<b>24 <math>\mu</math>s</b>	p3 and ExtData Fig. 1a	2019-05	103
Si28/SiO2	2D	LD/e	$T_2^*$	<b>3.4 <math>\mu</math>s</b>	p2	2019-05	88
Si28/SiO2	2D	LD/e	$T_2^*$	<b>8.2 <math>\mu</math>s</b>	p5 and Fig. 3b	2019-05	260
Si28/SiO2	2D	LD/e	$T_2^*$	<b>3.3 <math>\mu</math>s</b>	Tab. 1	2019-12	308
Si28/SiO2	2D	LD/e <sup>h</sup>	$T_2^*$	<b>2.7 <math>\mu</math>s</b>	p2 and Fig. 2e	2020-04	216
Si28/SiO2	2D	ST/e	$T_2^*$	<b>12 <math>\mu</math>s<sup>i</sup></b>	Fig. 3c	2020-04	300
Si28/SiO2	2D	ST/e	$T_2^*$	<b>2 <math>\mu</math>s<sup>j</sup></b>	Fig. 3g	2020-04	300
Si28/SiO2	2D	LD/e	$T_2^*$	<b>24 <math>\mu</math>s</b>	p3 and ED Fig. 8b	2021-01	310
Si28/SiO2	2D	LD/e	$T_2^*$	<b>0.12 ms</b>	p13 and Fig. 4a	2021-02	35

TABLE I-4. Spin coherence times (part 4). Superscripts stand for the following. <sup>a</sup>: EO qubit. <sup>b</sup>: (estimated) from Fig. S2c as the signal decay by factor  $1/e$ . <sup>c</sup>: The Rabi decay time  $T_2^R = 100 \mu$ s is obtained by fitting the Rabi decay data to a function with two parameters,  $T_2^R$  and  $T_2^*$ . <sup>d</sup>: From linewidth. <sup>e</sup>: (estimated) from Fig. S2a as the signal decay by factor  $1/e$ . <sup>f</sup>: At 0.1 Kelvin. <sup>g</sup>: At 1.1 Kelvin. <sup>h</sup>: At 1 Kelvin. <sup>i</sup>: At 0.04 Kelvin. <sup>j</sup>: At 1.5 Kelvin. <sup>k</sup>: Lifetime of  $T_0$  state. <sup>l</sup>: Lifetime of  $T_-$  state. <sup>m</sup>: (estimated) from Fig. 4c. <sup>n</sup>: (estimated) from Fig. 4c the blue points extrapolation to  $N_\pi = 1$ . <sup>o</sup>: A three-electron qubit.

Material	Host	Qubit	Coherence	Time	Source	Date	Reference
Si28/SiO2	2D	ST/e	$T_2^*$	<b>0.1 <math>\mu</math>s<sup>a</sup></b>	p4 and Fig. 2e-g	2021-02	114
Si28/SiO2	imp	LD/i	$T_1$	<b>5 ms</b>	p3 and Fig. 3b	2021-01	132
Si28/SiO2	imp	LD/i	$T_2^D$	<b>0.56 s</b>	p2 and Fig. 2e	2014-10	189
Si28/SiO2	imp	LD/i	$T_2^D$	<b>9.2 ms</b>	p3 and Fig. 4	2021-01	132
Si28/SiO2	imp	LD/i	$T_2^H$	<b>1 ms</b>	p2 and Fig. 2d	2014-10	189
Si28/SiO2	imp	LD/i	$T_2^H$	<b>0.92 ms</b>	p3 and Fig. 3a	2021-01	132
Si28/SiO2	imp	LD/i	$T_2^*$	<b>0.27 ms</b>	p1 and Fig. 2b	2014-10	189
Si/SiGe	2D	LD/e	$T_1$	<b>0.6 s<sup>b</sup></b>	Fig. 5	2009-08	92
Si/SiGe	2D	ST/e	$T_1$	<b>3 s</b>	p4	2012-01	220
Si/SiGe	2D	ST/e	$T_1$	<b>0.14 s</b>	Fig. 2d	2012-04	243
Si/SiGe	2D	LD/e	$T_1$	<b>0.17 s</b>	Fig. 6	2016-11	305
Si/SiGe	2D	LD/e	$T_1$	<b>50 ms</b>	p1 and ED Fig. 3b	2018-02	285
Si/SiGe	2D	LD/e	$T_1$	<b>0.16 s<sup>c</sup></b>	Fig. 2	2019-04	23
Si/SiGe	2D	LD/e	$T_1$	<b>5 s<sup>d</sup></b>	p4	2019-04	23
Si/SiGe	2D	LD/e	$T_1$	<b>1.3 ms</b>	p1 for Q3	2021-06	257
Si/SiGe	2D	LD/e	$T_2^D$	<b>44 <math>\mu</math>s</b>	Fig. 4b	2014-08	123
Si/SiGe	2D	HY/e	$T_2^D$	<b>0.15 <math>\mu</math>s</b>	abstract and Fig. 3d	2015-12	129
Si/SiGe	2D	LD/e	$T_2^D$	<b>0.4 ms</b>	p3	2016-10	122
Si/SiGe	2D	LD/e	$T_2^H$	<b>37 <math>\mu</math>s</b>	p4 and Fig. 4a	2014-08	123
Si/SiGe	2D	LD/e	$T_2^H$	<b>11 <math>\mu</math>s<sup>e</sup></b>	p3 and Fig. 2c	2016-08	256
Si/SiGe	2D	LD/e	$T_2^H$	<b>19 <math>\mu</math>s</b>	p1 and ED Fig. 3e	2018-02	285
Si/SiGe	2D	LD/e	$T_2^H$	<b>2 <math>\mu</math>s</b>	Fig. 4	2020-06	24
Si/SiGe	2D	LD/e	$T_2^H$	<b>46 <math>\mu</math>s</b>	p1 for Q3	2021-06	257
Si/SiGe	2D	LD/e	$T_2^R$	<b>7 <math>\mu</math>s<sup>f</sup></b>	p3	2016-08	256
Si/SiGe	2D	HY/e <sup>g</sup>	$T_2^R$	<b>1 <math>\mu</math>s</b>	Fig. 3g	2017-12	263
Si/SiGe	2D	LD/e	$T_2^R$	<b>1.4 <math>\mu</math>s</b>	p4	2020-01	46
Si/SiGe	2D	ST/e	$T_2^*$	<b>0.36 <math>\mu</math>s</b>	p3	2012-01	173
Si/SiGe	2D	HY/e	$T_2^*$	<b>3.7 ns</b>	p2	2014-01	245
Si/SiGe	2D	HY/e	$T_2^*$	<b>10 ns</b>	p1	2014-07	127
Si/SiGe	2D	LD/e	$T_2^*$	<b>0.84 <math>\mu</math>s<sup>h</sup></b>	p2	2014-08	123
Si/SiGe	2D	ST/e	$T_2^*$	<b>0.24 <math>\mu</math>s</b>	Fig. 2d the blue trace	2014-08	292
Si/SiGe	2D	HY/e	$T_2^*$	<b>11 ns</b>	Fig. 2c	2015-12	129
Si/SiGe	2D	LD/e	$T_2^*$	<b>1.8 <math>\mu</math>s</b>	p3 and Fig. 2c	2016-08	256
Si/SiGe	2D	LD/e	$T_2^*$	<b>1 <math>\mu</math>s<sup>h</sup></b>	p3	2016-10	122
Si/SiGe	2D	LD/e	$T_2^*$	<b>0.11 <math>\mu</math>s<sup>i</sup></b>	Fig. 3a	2017-04	233
Si/SiGe	2D	LD/e	$T_2^*$	<b>1 <math>\mu</math>s<sup>j</sup></b>	p2	2017-04	233
Si/SiGe	2D	HY/e <sup>g</sup>	$T_2^*$	<b>45 ns</b>	Fig. 2i the blue trace	2017-12	263
Si/SiGe	2D	LD/e	$T_2^*$	<b>1 <math>\mu</math>s</b>	p1 and ED Fig. 3d	2018-02	285
Si/SiGe	2D	LD/e	$T_2^*$	<b>0.18 <math>\mu</math>s<sup>j</sup></b>	p1	2018-03	230
Si/SiGe	2D	LD/e	$T_2^*$	<b>68 ns<sup>j</sup></b>	p1	2020-01	22
Si/SiGe	2D	LD/e	$T_2^*$	<b>0.97 <math>\mu</math>s</b>	p3	2020-06	24
Si/SiGe	2D	LD/e	$T_2^*$	<b>1.7 <math>\mu</math>s</b>	p1 for Q3	2021-06	257
Si/SiGe	2D	ST/e	$T_2^*$	<b>1 <math>\mu</math>s</b>	p3	2021-08	158
Si/SiO2	1D	LD/e	$T_1$	<b>9 s</b>	p3 and Fig. 3a the leftmost blue point	2021-03	39
Si/SiO2	1D	LD/h <sup>k</sup>	$T_2^D$	<b>5.4 <math>\mu</math>s</b>	p7 and Fig. 4a	2021-03	28
Si/SiO2	1D	LD/h	$T_2^H$	<b>0.25 <math>\mu</math>s</b>	p5 and Fig. 4b	2016-11	174
Si/SiO2	1D	LD/h <sup>k</sup>	$T_2^H$	<b>1.5 <math>\mu</math>s<sup>l</sup></b>	Fig. 4a	2021-03	28
Si/SiO2	1D	LD/h	$T_2^*$	<b>59 ns</b>	p4 and Fig. 3a	2016-11	174
Si/SiO2	1D	LD/h <sup>k</sup>	$T_2^*$	<b>0.44 <math>\mu</math>s</b>	p8 and SM Sec. 9	2021-03	28
Si/SiO2	2D	LD/e	$T_1$	<b>40 ms</b>	p4 and Fig. 4 the leftmost red point	2010-03	293

TABLE I-5. Spin coherence times (part 5). Superscripts stand for the following. <sup>a</sup>: (derived) from  $T_2^* = Q/f$  with  $f = 200$  MHz and  $Q = 20$ . <sup>b</sup>: (estimated) Fig. 5 the lowest point. <sup>c</sup>: With micromagnet. <sup>d</sup>: No micromagnet. <sup>e</sup>: Measured in Ref. [259]. <sup>f</sup>: From  $Q = 140$  and  $f_R = 10$  MHz. <sup>g</sup>: Tunable between spin- and charge- qubit. <sup>h</sup>: From EDSR linewidth. <sup>i</sup>: Valley and spin flip. <sup>j</sup>: From linewidth. <sup>k</sup>: At temperature 1.5 K. <sup>l</sup>: (estimated) we take the value for  $n = 2$  CPMG sequence, which seems comparable to the Hahn echo data according to Fig. S12.

Material	Host	Qubit	Coherence	Time	Source	Date	Reference
Si/SiO <sub>2</sub>	2D	LD/e	$T_1$	<b>2.6 s</b>	p3	2013-06	301
Si/SiO <sub>2</sub>	2D	LD/e	$T_1$	<b>90 ms</b>	Fig. 1c	2020-06	307
Si/SiO <sub>2</sub>	2D	LD/e <sup>a</sup>	$T_2^H$	<b>22 <math>\mu</math>s</b>	SM Tab. I	2020-12	155
Si/SiO <sub>2</sub>	2D	LD/e <sup>a</sup>	$T_2^*$	<b>16 <math>\mu</math>s</b>	SM Tab. I	2020-12	155
Si/SiO <sub>2</sub>	imp	LD/i	$T_1$	<b>0.7 s</b>	p3	2012-09	219
Si/SiO <sub>2</sub>	imp	ST/i	$T_1$	<b>4.1 ms</b>		2014-06	51
Si/SiO <sub>2</sub>	imp	LD/i	$T_2^D$	<b>0.41 <math>\mu</math>s</b>	p3	2012-09	219
Si/SiO <sub>2</sub>	imp	LD/i	$T_2^H$	<b>0.21 ms</b>	p3	2012-09	219
Si/SiO <sub>2</sub>	imp	LD/i	$T_2^*$	<b>55 ns</b>	p2	2012-09	219

TABLE I-6. Spin coherence times (part 6). Superscripts stand for the following. <sup>a</sup>: In a five-electron dot configuration.

Material	Host	Qubit	Coherence	Time	Source	Date	Reference
CNT	1D	charge	$T_1$	<b>48 ns</b>	p4 and Fig. 3c	2017-05	210
CNT	1D	charge	$T_2^*$	<b>0.35 ns<sup>a</sup></b>	p4	2015-07	277
CNT	1D	charge	$T_2^*$	<b>5 ns<sup>a</sup></b>	p4 and Fig. 3b	2017-05	210
CNT	1D	charge	$T_2^*$	<b>0.24 ns<sup>a</sup></b>	p2	2019-12	48
GaAs/AlGaAs	2D	charge	$T_1$	<b>16 ns</b>	p3 and Fig. 4	2004-10	217
GaAs/AlGaAs	2D	charge	$T_1$	<b>10 ns</b>	p2	2010-12	213
GaAs/AlGaAs	2D	charge	$T_1$	<b>19 ns</b>	p4	2015-12	157
GaAs/AlGaAs	2D	charge	$T_1$	<b>42 ns</b>	p4 and Fig. 5d	2019-05	236
GaAs/AlGaAs	2D	charge	$T_2^D$	<b>4 ns<sup>b</sup></b>	p5	2013-06	30
GaAs/AlGaAs	2D	charge	$T_2^H$	<b>43 ns</b>	p4 and Fig. 5e	2019-05	236
GaAs/AlGaAs	2D	charge	$T_2^*$	<b>1 ns</b>	p3	2003-11	91
GaAs/AlGaAs	2D	charge	$T_2^*$	<b>0.4 ns<sup>a</sup></b>	p4 and Fig. 4	2004-10	217
GaAs/AlGaAs	2D	charge	$T_2^*$	<b>1.1 ns<sup>a</sup></b>	p3	2010-08	214
GaAs/AlGaAs	2D	charge	$T_2^*$	<b>7 ns</b>	p4	2010-12	213
GaAs/AlGaAs	2D	charge	$T_2^*$	<b>60 ps</b>	p2	2011-10	57
GaAs/AlGaAs	2D	charge	$T_2^*$	<b>0.35 ns<sup>a</sup></b>	p4	2012-01	70
GaAs/AlGaAs	2D	charge	$T_2^*$	<b>1.2 ns</b>	p4	2015-12	157
GaAs/AlGaAs	2D	charge	$T_2^*$	<b>4 ns<sup>a</sup></b>	p5	2017-03	252
GaAs/AlGaAs	2D	charge	$T_2^*$	<b>11 ns<sup>a</sup></b>	p4	2018-08	146
GaAs/AlGaAs	2D	charge	$T_2^*$	<b>66 ns<sup>a</sup></b>	p2	2018-10	272
GaAs/AlGaAs	2D	charge	$T_2^*$	<b>23 ns</b>	p4 and Fig. 5c	2019-05	236
GaAs/AlGaAs	2D	charge	$T_2^*$	<b>0.12 <math>\mu</math>s<sup>a</sup></b>	p2	2019-12	235
GaAs/AlGaAs	2D	charge	$T_2^*$	<b>9.9 ns<sup>a</sup></b>	p3	2020-06	138
GaAs/AlGaAs	2D	charge	$T_2^*$	<b>6 ns<sup>a</sup></b>	p5 and Fig. 4a	2021-02	139
InGaAs/AlGaAs	2D	charge	$T_1$	<b>10 ns</b>	p1 and Fig. 2d	2002-09	73
Si/SiGe	2D	charge	$T_1$	<b>45 <math>\mu</math>s</b>	p3 and Fig. 3c	2013-07	283
Si/SiGe	2D	charge	$T_2^H$	<b>0.76 <math>\mu</math>s</b>	Fg. 2	2013-08	244
Si/SiGe	2D	charge	$T_2^H$	<b>2.2 ns</b>	p3	2015-03	128
Si/SiGe	2D	charge	$T_2^*$	<b>2.2 ns</b>	abstract and Fig. 1	2013-08	244
Si/SiGe	2D	charge	$T_2^*$	<b>1.5 ns</b>	p1	2015-03	128
Si/SiGe	2D	charge	$T_2^*$	<b>0.12 <math>\mu</math>s<sup>a</sup></b>	p2	2017-01	183
Si/SiGe	2D	charge	$T_2^*$	<b>8 ns<sup>a</sup></b>	p5	2017-01	184
Si/SiGe	2D	charge	$T_2^*$	<b>8.8 ns<sup>a</sup></b>	Fig. 3b	2020-06	21
Si/SiGe	2D	charge	$T_2^*$	<b>80 ps</b>	p3	2020-12	161
Si/SiO <sub>2</sub>	1D	charge	$T_2^*$	<b>32 ps<sup>a</sup></b>	p4	2021-05	104

TABLE II. Charge coherence times. Superscripts stand for the following. <sup>a</sup>: From linewidth. <sup>b</sup>: From Landau-Zener interference.

Material	Host	Qubit	Operation	Qubit #	Time	Source	Date	Reference
CNT	1D	LD/e	gate	1	<b>5 ns<sup>a</sup></b>	Fig. 3b	2013-08	143
GaAs/AlGaAs	2D	ST/e	gate	1	<b>0.35 ns</b>	p3 and Fig. 5d	2005-09	218
GaAs/AlGaAs	2D	LD/e	gate	1	<b>54 ns</b>	p4	2006-08	135
GaAs/AlGaAs	2D	LD/e	gate	1	<b>63 ns<sup>b</sup></b>	p3	2007-09	136
GaAs/AlGaAs	2D	LD/e	gate	1	<b>0.11 <math>\mu</math>s</b>	p3	2007-11	202
GaAs/AlGaAs	2D	LD/e	gate	1	<b>0.28 <math>\mu</math>s<sup>c</sup></b>	p3 and Fig. 3b	2007-12	142
GaAs/AlGaAs	2D	LD/e	gate	1	<b>60 ns</b>	Fig. 2b the blue trace	2008-06	137
GaAs/AlGaAs	2D	LD/e	gate	1	<b>0.25 <math>\mu</math>s<sup>d</sup></b>	Fig 2b	2011-09	26
GaAs/AlGaAs	2D	LD/e	gate	2	<b>10 ns<sup>e</sup></b>	p4	2011-09	26
GaAs/AlGaAs	2D	ST/e	gate	2	<b>0.14 <math>\mu</math>s</b>	p3	2012-04	246
GaAs/AlGaAs	2D	LD/e	gate	1	<b>2.5 <math>\mu</math>s<sup>f</sup></b>	p3	2013-03	242
GaAs/AlGaAs	2D	charge	gate	1	<b>50 ps</b>	p4	2013-06	30
GaAs/AlGaAs	2D	HY/e <sup>g</sup>	gate	1	<b>15 ns</b>	Fig. 4 the blue set	2013-07	176
GaAs/AlGaAs	2D	HY/e <sup>h</sup>	gate	1	<b>11 ps</b>	p2	2013-09	175
GaAs/AlGaAs	2D	ST/e	gate	1	<b>0.25 ns</b>	Fig. 4a and Fig. 3d	2014-01	99
GaAs/AlGaAs	2D	LD/e	gate	1	<b>4.1 ns</b>	p2	2014-12	302
GaAs/AlGaAs	2D	ST/e	gate	1	<b>0.83 ns<sup>i</sup></b>	Fig. 4d	2016-03	171
GaAs/AlGaAs	2D	LD/e	gate	1	<b>20 ns</b>	p4 and Fig. 3	2016-04	201
GaAs/AlGaAs	2D	HY/e <sup>j</sup>	gate	1	<b>5 ns</b>	Fig. 4c	2017-07	169
GaAs/AlGaAs	2D	HY/e <sup>k</sup>	gate	1	<b>5 ns</b>	Fig. 4c	2017-07	169
GaAs/AlGaAs	2D	LD/e	gate	1	<b>94 ns</b>	p3 and Fig. 3b	2018-08	107
GaAs/AlGaAs	2D	ST/e	gate	2	<b>5.5 ns<sup>l</sup></b>	p4 and Fig. 3	2018-12	197
GaAs/AlGaAs	2D	LD/e	gate	1	<b>92 ns</b>	Fig. 2	2019-06	195
GaAs/AlGaAs	2D	ST/e	gate	2	<b>2 ns</b>	Fig. 2c	2019-12	170
GaAs/AlGaAs	2D	LD/e	gate	1	<b>15 ns</b>	Fig. 6	2020-03	194
GaAs/AlGaAs	2D	ST/e	gate	1	<b>1.6 ns</b>	Fig. 2a the green trace	2020-12	110
GaAs/AlGaAs	2D	ST/e	gate	1	<b>1 ns</b>	p4	2020-12	111
GaAs/AlGaAs	2D	ST/e	gate	1	<b>4.2 ns</b>	p4	2020-12	33
GaAs/AlGaAs	2D	HY/e	gate	1	<b>5 ns</b>	p3 and Fig. 3a	2021-06	109
GaAs/AlGaAs	2D	ST/e	gate	1	<b>15 ns</b>	p3	2021-10	65
GaAs/AlGaAs	2D	ST/e	gate	1	<b>38 ns</b>	p3	2021-12	133
Ge/Si	1D	LD/h	gate	1	<b>7.1 ns</b>	Fig. 5d the point at 11 Db	2018-12	288
Ge/Si	1D	LD/h	gate	1	<b>0.92 ns</b>	p5	2020-06	284
Ge/Si	1D	LD/h	gate	1	<b>1.1 ns</b>	Fig. 4	2021-01	71
Ge/SiGe	2D	LD/h	gate	1	<b>20 ns</b>	p2	2020-01	95
Ge/SiGe	2D	LD/h	gate	2	<b>55 ns</b>	p4	2020-01	95
Ge/SiGe	2D	LD/h	gate	1	<b>8.8 ns</b>	p4 and Fig. 3b	2020-12	96
Ge/SiGe	2D	LD/h	gate	2	<b>9 ns</b>	Tab. S2	2021-03	97
Ge/SiGe	2D	ST/h	gate	1	<b>5 ns</b>	p2 and Fig. 3e	2021-08	112
Ge/SiGe	2D	LD/h	gate	1	<b>10 ns<sup>m</sup></b>	Fig. 2g	2021-09	153
Ge/SiGe	2D	LD/h	gate	1	<b>96 ns</b>	p3	2021-09	153
InAs	1D	LD/e	gate	1	<b>8.6 ns</b>	p2	2010-12	192
InAs	1D	LD/e	gate	1	<b>17 ns<sup>n</sup></b>	p3 and Fig. 4f	2012-10	212
InSb	1D	LD/e	gate	1	<b>4.8 ns</b>	Fig. 2c	2013-02	266
P-Si	imp	LD/i	gate	2	<b>0.8 ns</b>	Fig. 3 and abstract	2019-07	93
P-Si28	imp	LD/i <sup>o</sup>	gate	1	<b>0.16 ms</b>	p3 and Fig. 3d	2016-10	149
P-Si28	imp	LD/i	gate	1	<b>3 <math>\mu</math>s</b>	p3	2016-10	50
P-Si28	imp	LD/e	gate	1	<b>0.83 <math>\mu</math>s</b>	ED Fig. 3 first column	2021-07	162
P-Si28	imp	LD/i	gate	2	<b>5.6 <math>\mu</math>s<sup>p</sup></b>	Fig. 5c	2021-12	164
Si28/SiGe	2D	ST/e	gate	1	<b>3.1 ns</b>	Fig. 4a	2016-03	225
Si28/SiGe	2D	LD/e	gate	1	<b>0.13 <math>\mu</math>s</b>	p2	2017-12	304

TABLE III-1. Operation times (part 1). Superscripts stand for the following. <sup>a</sup>: (estimated) from Fig. 3b the rightmost point. <sup>b</sup>: Using  $T_R = 4\pi\hbar/g\mu_B B_{ac}$  with  $B_{ac} = 2.5$  mT and  $g = 0.44$ . <sup>c</sup>: Nuclear-driven EDSR. <sup>d</sup>: (estimated) from Fig. 2b. <sup>e</sup>: SWAP time. <sup>f</sup>: EDSR without a micromagnet. <sup>g</sup>: RX qubit. <sup>h</sup>: EO qubit. <sup>i</sup>: (estimated) from Fig. 4d the rightmost red point. <sup>j</sup>: At a partial sweet spot. <sup>k</sup>: At a full sweet spot. <sup>l</sup>: Gate between a single-spin and a singlet-triplet qubit. <sup>m</sup>: (estimated) Fig. 2g the leftmost point. <sup>n</sup>: Driving through the cavity. <sup>o</sup>: Qubit defined in the rotating frame. <sup>p</sup>: Fidelity not measured; signal visibility was 50%.

Material	Host	Qubit	Operation	Qubit #	Time	Source	Date	Reference
Si28/SiGe	2D	LD/e	gate	2	<b>0.27 <math>\mu</math>s</b>	Fig. 4d	2019-06	248
Si28/SiGe	2D	LD/e <sup>a</sup>	gate	1	<b>10 ns</b>	Fig. 4c caption	2019-08	3
Si28/SiGe	2D	LD/e	gate	2	<b>0.3 <math>\mu</math>s</b>	p5	2019-12	249
Si28/SiGe	2D	ST/e	gate	1	<b>0.13 <math>\mu</math>s</b>	p3	2020-03	258
Si28/SiGe	2D	LD/e	gate	2	<b>0.1 <math>\mu</math>s</b>	p6	2021-07	296
Si28/SiGe	2D	LD/e	gate	1	<b>0.1 <math>\mu</math>s</b>	p4	2021-08	199
Si28/SiO2	2D	LD/e	gate	1	<b>1.6 <math>\mu</math>s<sup>b</sup></b>	Fig. 4 and Fig. 2d	2014-10	274
Si28/SiO2	2D	LD/e	gate	1	<b>2.4 <math>\mu</math>s</b>	p5	2015-10	276
Si28/SiO2	2D	LD/e	gate	2	<b>0.16 <math>\mu</math>s</b>	p4	2015-10	276
Si28/SiO2	2D	LD/e	gate	1	<b>1.5 <math>\mu</math>s</b>	Tab. 1	2019-12	308
Si28/SiO2	2D	LD/e	gate	1	<b>0.56 <math>\mu</math>s</b>	p3 and ED Fig. 11e	2021-01	310
Si28/SiO2	2D	ST/e	gate	1	<b>2.5 ns</b>	p4 and Fig. 2e the rightmost point	2021-02	114
Si28/SiO2	imp	LD/e	gate	1	<b>3 <math>\mu</math>s</b>	Fig. 3c the topmost point	2015-04	190
Si/SiGe	2D	HY/e	gate	1	<b>45 ps</b>	Fig. 2b	2014-07	127
Si/SiGe	2D	LD/e	gate	1	<b>0.15 <math>\mu</math>s<sup>c</sup></b>	Fig. 3b	2014-08	123
Si/SiGe	2D	ST/e	gate	1	<b>36 ns</b>	p3	2014-08	292
Si/SiGe	2D	HY/e	gate	1	<b>4.5 ns</b>	Fig. 1g	2015-12	129
Si/SiGe	2D	LD/e	gate	1	<b>50 ns</b>	p3	2016-08	256
Si/SiGe	2D	LD/e	gate	1	<b>0.37 <math>\mu</math>s</b>	p3	2016-10	122
Si/SiGe	2D	LD/e	gate	1	<b>0.5 <math>\mu</math>s</b>	p2	2017-04	233
Si/SiGe	2D	LD/e	gate	1	<b>50 <math>\mu</math>s<sup>d</sup></b>	p7	2017-04	233
Si/SiGe	2D	HY/e <sup>e</sup>	gate	1	<b>36 ns</b>	Fig. 3g	2017-12	263
Si/SiGe	2D	LD/e	gate	1	<b>0.1 <math>\mu</math>s</b>	p2	2018-01	306
Si/SiGe	2D	LD/e	gate	2	<b>0.13 <math>\mu</math>s</b>	p2	2018-01	306
Si/SiGe	2D	LD/e	gate	1	<b>0.25 <math>\mu</math>s</b>	p1	2018-02	285
Si/SiGe	2D	LD/e	gate	2	<b>0.17 <math>\mu</math>s<sup>f</sup></b>	ED Fig. 9	2018-02	285
Si/SiGe	2D	LD/e	gate	1	<b>83 ns</b>	p4	2020-01	46
Si/SiGe	2D	charge	gate	2	<b>74 ps</b>	p4	2020-12	161
Si/SiGe	2D	LD/e	gate	2	<b>0.53 <math>\mu</math>s</b>	p3	2020-12	303
Si/SiGe	2D	LD/e	gate	1	<b>83 ns</b>	p1	2021-06	257
Si/SiGe	2D	ST/e	gate	1	<b>91 ns</b>	p3	2021-08	158
Si/SiO2	1D	LD/h	gate	1	<b>5.9 ns</b>	p4	2016-11	174
Si/SiO2	1D	LD/h	gate	1	<b>18 ns<sup>g</sup></b>	Fig. 1d	2018-03	45
Si/SiO2	1D	LD/e	gate	1	<b>42 ns</b>	Fig. 4b	2018-12	42
Si/SiO2	1D	LD/h	gate	1	<b>33 ns</b>	p5 and Fig. 4d	2019-12	44
Si/SiO2	1D	LD/h <sup>h</sup>	gate	1	<b>11 ns<sup>i</sup></b>	p7 and Fig. 3e	2021-03	28
Si/SiO2	1D	LD/h <sup>h</sup>	gate	1	<b>3.4 ns</b>	p4	2021-03	28
Si/SiO2	2D	LD/e <sup>j</sup>	gate	1	<b>5 <math>\mu</math>s</b>	SM Fig. 4a at around 50 nV	2020-12	155
Si/SiO2	2D	LD/e	gate	2	<b>2.5 <math>\mu</math>s</b>	Fig. 2j the rightmost point	2021-12	154
Si/SiO2	imp	LD/i	gate	1	<b>0.15 <math>\mu</math>s</b>	p2 and Fig. 2	2012-09	219
GaAs/AlGaAs	2D	LD/e	measure	1	<b>0.4 <math>\mu</math>s</b>	Fig. 3	2003-11	85
GaAs/AlGaAs	2D	ST/e	measure	1	<b>10 <math>\mu</math>s</b>	p2	2005-09	218
GaAs/AlGaAs	2D	ST/e	measure	1	<b>20 <math>\mu</math>s</b>	p2	2006-11	181
GaAs/AlGaAs	2D	ST/e	measure	1	<b>6 <math>\mu</math>s</b>	p3	2009-10	11
GaAs/AlGaAs	2D	ST/e	measure	1	<b>0.1 <math>\mu</math>s<sup>k</sup></b>	p3 and Fig. 3	2010-04	8
GaAs/AlGaAs	2D	ST/e	measure	1	<b>4 ms<sup>l</sup></b>	p4	2010-08	214
GaAs/AlGaAs	2D	ST/e	measure	1	<b>1 <math>\mu</math>s</b>	p1	2012-04	246
GaAs/AlGaAs	2D	ST/e	measure	1	<b>0.2 <math>\mu</math>s<sup>m</sup></b>	SM Fig. S1d	2014-01	99
GaAs/AlGaAs	2D	ST/e	measure	1	<b>1 <math>\mu</math>s</b>	p2	2014-10	247
GaAs/AlGaAs	2D	ST/e	measure	1	<b>20 ms</b>	p3	2016-11	130

TABLE III-2. Operation times (part 2). Superscripts stand for the following. <sup>a</sup>: EO qubit. <sup>b</sup>: (estimated) from Fig. 2d: 9 oscillations in 30  $\mu$ s at resonance. <sup>c</sup>:  $2 \times 75$  ns. <sup>d</sup>: Valley and spin flip. <sup>e</sup>: Tunable between spin- and charge- qubit. <sup>f</sup>: The reference gives also the “decay time of the CZ operation” of 1.6  $\mu$ s in ED Fig. 9, which would correspond to a gate quality factor of 4.8. <sup>g</sup>: (derived) from Fig. 1d showing 11 oscillations in 400 ns. <sup>h</sup>: At temperature 1.5 K. <sup>i</sup>: Z-gate. <sup>j</sup>: In a five-electron dot configuration. <sup>k</sup>: SNR  $\sim$ 3. <sup>l</sup>: The reference estimates this time as required for SNR = 1. <sup>m</sup>: SNR = 4.1.

Material	Host	Qubit	Operation	Qubit #	Time	Source	Date	Reference
GaAs/AlGaAs	2D	ST/e	measure	1	<b>2 ms</b>	p3	2016-11	130
GaAs/AlGaAs	2D	ST/e	measure	1	<b>4 <math>\mu</math>s</b>	p2 and SM p1	2017-07	193
GaAs/AlGaAs	2D	ST/e	measure	1	<b>0.8 <math>\mu</math>s</b>	p4	2018-04	191
GaAs/AlGaAs	2D	ST/e	measure	1	<b>2 <math>\mu</math>s</b>	Fig. 4b the rightmost point	2018-09	207
GaAs/AlGaAs	2D	LD/e	measure	1	<b>0.7 ms</b>	Fig. 1f	2019-06	195
GaAs/AlGaAs	2D	ST/e	measure	1	<b>0.22 ms</b>	Fig. 2a caption	2021-05	108
GaAs/AlGaAs	2D	HY/e	measure	1	<b>0.17 ms<sup>a</sup></b>	p3	2021-06	109
GaAs/AlGaAs	2D	ST/e	measure	1	<b>10 <math>\mu</math>s<sup>b</sup></b>	p3	2021-10	65
Ge/SiGe	2D	ST/h	measure	1	<b>6 <math>\mu</math>s</b>	p4	2020-12	96
Ge/SiGe	2D	LD/h	measure	1	<b>10 <math>\mu</math>s</b>	p1	2021-09	153
P-Si	imp	LD/i	measure	1	<b>0.2 s</b>	p3	2017-03	286
P-Si	imp	ST/i	measure	1	<b>18 ms<sup>c</sup></b>	p3	2017-07	25
P-Si	imp	ST/e <sup>d</sup>	measure	1	<b>0.15 ms</b>	Tab. II	2018-05	87
P-Si	imp	ST/e <sup>d</sup>	measure	1	<b>65 <math>\mu</math>s<sup>e</sup></b>	Tab. II	2018-05	87
P-Si	imp	ST/i	measure	1	<b>0.3 ms</b>	p2	2018-11	209
P-Si	imp	LD/i	measure	1	<b>1.5 <math>\mu</math>s</b>	p4	2019-10	124
Si/SiGe	2D	LD/e	measure	1	<b>4 ms</b>	p1	2014-08	123
Si/SiGe	2D	ST/e	measure	1	<b>13 <math>\mu</math>s<sup>f</sup></b>	p3 and p6	2019-07	117
Si/SiGe	2D	LD/e	measure	1	<b>24 <math>\mu</math>s<sup>g</sup></b>	p7	2019-08	279
Si/SiGe	2D	ST/e	measure	1	<b>6 <math>\mu</math>s</b>	p3 and Fig. 3f	2019-08	309
Si/SiGe	2D	ST/e	measure	1	<b>0.8 <math>\mu</math>s<sup>h</sup></b>	Fig. 3c	2020-01	200
Si/SiGe	2D	ST/e	measure	1	<b>0.8 <math>\mu</math>s</b>	Fig. 5b	2020-02	41
Si/SiGe	2D	ST/e	measure	1	<b>1.7 <math>\mu</math>s</b>	p6	2020-02	41
Si/SiGe	2D	LD/e	measure	1	<b>49 ms<sup>i</sup></b>	p3	2020-04	294
Si/SiO <sub>2</sub>	1D	ST/e	measure	1	<b>0.5 ms</b>	abstract	2019-08	265
Si/SiO <sub>2</sub>	1D	ST/e	measure	1	<b>33 <math>\mu</math>s<sup>j</sup></b>	p6 and Fig. 7e	2020-12	20
Si/SiO <sub>2</sub>	1D	ST/e	measure	1	<b>50 ns<sup>k</sup></b>	p5 and Fig. 3	2021-05	104
Si/SiO <sub>2</sub>	1D	LD/e	measure	1	<b>1 ms</b>	p2	2021-09	251
Si/SiO <sub>2</sub>	2D	ST/e	measure	2	<b>2.6 ms</b>	p3	2019-03	290
Si/SiO <sub>2</sub>	2D	charge	measure	1	<b>1 <math>\mu</math>s<sup>l</sup></b>	p5 and Fig. 4c the leftmost green point	2020-02	237
GaAs/AlGaAs	2D	ST/e	initialize	1	<b>50 ns</b>	p1	2012-04	246
GaAs/AlGaAs	2D	ST/e	initialize	1	<b>20 ns<sup>m</sup></b>	p2	2014-10	247
P-Si28	imp	LD/i	initialize	1	<b>10 ms</b>	p5	2021-10	116
Si/SiGe	2D	LD/e	initialize	1	<b>4 ms</b>	p1	2014-08	123
Si/SiGe	2D	LD/e	initialize	1	<b>50 <math>\mu</math>s<sup>n</sup></b>	ED Fig. 2	2018-02	285
Si/SiO <sub>2</sub>	1D	ST/e	initialize	1	<b>20 ms<sup>o</sup></b>	Fig. 3	2019-08	265

TABLE III-3. Operation times (part 3). Superscripts stand for the following. <sup>a</sup>: 32  $\mu$ s+140  $\mu$ s. <sup>b</sup>: SNR = 5. <sup>c</sup>: Latched readout; SNR = 6.4. <sup>d</sup>: Hybrid ST qubit: impurity – gated dot. <sup>e</sup>: Latched readout. <sup>f</sup>: SNR = 6.5. <sup>g</sup>: SNR = 3.4. <sup>h</sup>: SNR = 6. <sup>i</sup>: 15 QND measurements, each taking 3.263 ms. <sup>j</sup>: Detecting single electron transfer between neighboring dots. <sup>k</sup>: SNR = 3.3 for an interdot charge transition “mimicking the singlet-triplet readout scheme”. <sup>l</sup>: Dot-donor transition; SNR  $\approx$  5. <sup>m</sup>: Into singlet. <sup>n</sup>: Using spin hot-spot. <sup>o</sup>: Into triplet.

Material	Host	Qubit	Operation	Qubit #	Infidelity	Source	Date	Reference
GaAs/AlGaAs	2D	LD/e	gate	1	27 %	p5	2006-08	135
GaAs/AlGaAs	2D	ST/e	gate	2	28 % <sup>a</sup>	p3	2012-04	246
GaAs/AlGaAs	2D	LD/e	gate	1	3.4 %	p2	2014-12	302
GaAs/AlGaAs	2D	charge	gate	2	32 %	p4	2015-12	157
GaAs/AlGaAs	2D	ST/e	gate	1	1.5 %	p4	2016-06	32
GaAs/AlGaAs	2D	ST/e	gate	1	1.4 %	p3 and Fig. 2c	2017-12	196
GaAs/AlGaAs	2D	ST/e	gate	2	10 %	p4 and Fig. 4e	2017-12	196
GaAs/AlGaAs	2D	LD/e	gate	1	2.5 %	p3 and Fig. 4e	2020-03	194
GaAs/AlGaAs	2D	ST/e	gate	1	0.5 %	Fig. 3	2020-12	33
Ge/SiGe	2D	LD/h	gate	1	0.7 %	p2 and Fig. 2d	2020-01	95
Ge/SiGe	2D	LD/h	gate	1	0.1 %	Fig. S4 dot 3	2021-03	97
Ge/SiGe	2D	LD/h	gate	1	0.01 %	p2 and Fig. 2k	2021-09	153
Ge/SiGe	2D	LD/h	gate	1	3.7 % <sup>b</sup>	Fig. 2g	2021-09	153
InAs	1D	LD/e	gate	1	52 %	p2	2010-12	192
InSb	1D	LD/e	gate	1	19 %	p3	2013-02	266
P-Si	imp	LD/e	gate	1	0.6 %	p4 and Fig. 4a	2015-04	150
P-Si	imp	LD/i	gate	2	10 %	p3	2019-07	93
P-Si28	imp	LD/i	gate	1	0.058 %	p6 and Fig. 3	2016-10	50
P-Si28	imp	LD/e	gate	1	1 % <sup>c</sup>	p3	2021-07	162
Si28/SiGe	2D	LD/e	gate	1	0.074 %	p4 and Fig. 5	2017-12	304
Si28/SiGe	2D	LD/e	gate	1	0.2 %	p5	2018-12	259
Si28/SiGe	2D	LD/e <sup>d</sup>	gate	1	0.35 %	abstract	2019-08	3
Si28/SiGe	2D	LD/e	gate	2	16 % <sup>e</sup>	p6	2019-12	249
Si28/SiGe	2D	ST/e	gate	1	0.4 %	p4	2020-03	258
Si28/SiGe	2D	LD/e	gate	1	0.28 %	p3	2021-07	296
Si28/SiGe	2D	LD/e	gate	2	0.35 % <sup>f</sup>	p3 and ED Fig. 5	2021-07	296
Si28/SiGe	2D	LD/e	gate	1	0.16 %	p4 and Fig. 2c	2021-08	199
Si28/SiGe	2D	LD/e	gate	2	0.49 % <sup>g</sup>	p4 and Fig. 2g	2021-08	199
Si28/SiO2	2D	LD/e	gate	1	0.4 %	p2 and Fig. 4	2014-10	274
Si28/SiO2	2D	LD/e <sup>h</sup>	gate	1	0.7 %	p4 and Fig. 4c	2015-11	275
Si28/SiO2	2D	LD/e	gate	1	0.09 %	p3	2018-10	34
Si28/SiO2	2D	LD/e	gate	1	0.043 %	abstract	2019-04	299
Si28/SiO2	2D	LD/e	gate	1	0.5 %	ED Tab. 2	2019-05	103
Si28/SiO2	2D	LD/e	gate	2	2 %	p4 and Fig. 4	2019-05	103
Si28/SiO2	2D	LD/e <sup>i</sup>	gate	1	0.7 %	p3 and Fig. 2g	2020-04	216
Si28/SiO2	2D	LD/e <sup>i</sup>	gate	2	14 %	p3 and Fig. 3d	2020-04	216
Si28/SiO2	2D	ST/e	gate	1	0.24 % <sup>j</sup>	Fig. 3d	2020-04	300
Si28/SiO2	2D	ST/e	gate	1	1.4 % <sup>k</sup>	Fig. 3h	2020-04	300
Si28/SiO2	2D	LD/e	gate	1	0.9 %	p3 and ED Fig. 10f	2021-01	310
Si28/SiO2	2D	LD/e	gate	2	1.8 %	p4 and Fig. 3a	2021-07	62
Si28/SiO2	imp	LD/i	gate	1	0.4 %	p2	2014-10	189
Si28/SiO2	imp	LD/e	gate	1	0.05 %	p6	2015-04	190
Si/SiGe	2D	HY/e	gate	1	9 %	p3	2014-07	127
Si/SiGe	2D	HY/e	gate	1	5.5 % <sup>l</sup>	p5 and Fig. 4e and g	2015-12	129
Si/SiGe	2D	LD/e	gate	1	0.4 %	p4	2016-08	256
Si/SiGe	2D	LD/e	gate	1	1 %	p5	2016-10	122
Si/SiGe	2D	LD/e	gate	1	0.3 %	p2	2018-01	306
Si/SiGe	2D	LD/e	gate	2	44 % <sup>m</sup>	p3	2018-01	306
Si/SiGe	2D	LD/e	gate	1	1.2 %	p1 and ED Fig. 4	2018-02	285
Si/SiGe	2D	LD/e	gate	1	1.2 %	p7	2019-04	297

TABLE IV-1. Operation infidelities (part 1). Superscripts stand for the following. <sup>a</sup>: Fidelity of a Bell state produced using CPHASE. <sup>b</sup>: (estimated) Fig. 2g the leftmost point. <sup>c</sup>: Lower limit. <sup>d</sup>: EO qubit. <sup>e</sup>: SWAP. <sup>f</sup>: CPHASE. <sup>g</sup>: CNOT. <sup>h</sup>: A three-electron qubit. <sup>i</sup>: At 1 Kelvin. <sup>j</sup>: At 0.04 Kelvin. <sup>k</sup>: At 1.5 Kelvin. <sup>l</sup>: Average of  $\mathcal{F}[X_\pi] = 93\%$  and  $\mathcal{F}[Z_\pi] = 96\%$ . <sup>m</sup>: Resonantly induced CNOT.

Material	Host	Qubit	Operation	Qubit #	Infidelity	Source	Date	Reference
Si/SiGe	2D	LD/e	gate	2	8 %	p7	2019-04	297
Si/SiGe	2D	HY/e <sup>a</sup>	gate	1	15 %	p4	2019-12	211
Si/SiGe	2D	charge	gate	2	37 %	p4	2020-12	161
Si/SiGe	2D	LD/e <sup>b</sup>	gate	1	0.31 %	p4	2021-05	295
Si/SiGe	2D	LD/e	gate	1	0.09 %	p1 for Q3	2021-06	257
Si/SiGe	2D	HY/e	gate	1	0.12 % <sup>c</sup>	p4	2021-07	82
Si/SiO <sub>2</sub>	1D	LD/h <sup>d</sup>	gate	1	1.1 %	p6 and Fig. 3b	2021-03	28
Si/SiO <sub>2</sub>	2D	LD/e <sup>e</sup>	gate	1	0.3 %	SM Fig. 3	2020-12	155
GaAs/AlGaAs	2D	LD/e	measure	1	18 % <sup>f</sup>	p4	2004-07	59
GaAs/AlGaAs	2D	ST/e	measure	1	13 %	p2	2006-11	181
GaAs/AlGaAs	2D	ST/e	measure	1	2.5 %	p3	2006-12	179
GaAs/AlGaAs	2D	ST/e	measure	1	10 %	p3	2009-10	11
GaAs/AlGaAs	2D	LD/e	measure	1	14 %	p4	2011-09	203
GaAs/AlGaAs	2D	HY/e <sup>g</sup>	measure	1	25 %	p4	2013-09	175
GaAs/AlGaAs	2D	ST/e	measure	1	2 %	p2	2014-10	247
GaAs/AlGaAs	2D	ST/e	measure	1	20 %	p3	2015-08	12
GaAs/AlGaAs	2D	LD/e	measure	1	3 %	abstract	2016-01	7
GaAs/AlGaAs	2D	ST/e	measure	1	24 % <sup>h</sup>	p4	2016-11	130
GaAs/AlGaAs	2D	ST/e	measure	1	3 % <sup>i</sup>	p4	2016-11	130
GaAs/AlGaAs	2D	ST/e	measure	1	0.5 % <sup>j</sup>	p4	2017-07	193
GaAs/AlGaAs	2D	ST/e	measure	1	20 %	p2	2017-12	68
GaAs/AlGaAs	2D	ST/e	measure	1	5 %	p2	2017-12	74
GaAs/AlGaAs	2D	ST/e	measure	1	4 %	p4	2018-04	191
GaAs/AlGaAs	2D	ST/e	measure	1	20 %	p4	2018-09	207
GaAs/AlGaAs	2D	LD/e	measure	1	11 %	p3	2019-06	195
GaAs/AlGaAs	2D	ST/e	measure	1	10 %	p4	2020-12	111
GaAs/AlGaAs	2D	ST/e	measure	1	7 %	p5 and SM Fig. 11	2020-12	223
GaAs/AlGaAs	2D	ST/e	measure	1	5 %	p1	2021-05	108
GaAs/AlGaAs	2D	HY/e	measure	1	3.6 %	p4 and Fig. 2d	2021-06	109
GaAs/AlGaAs	2D	ST/e	measure	1	20 %	p2 and p3	2021-12	133
Ge/Si	1D	LD/h	measure	1	13 % <sup>k</sup>	p3	2018-11	281
Ge/SiGe	2D	ST/h	measure	1	22 % <sup>l</sup>	p4	2020-12	96
InAs	1D	LD/e	measure	1	20 %	p1	2010-12	192
P-Si	imp	LD/i	measure	1	4 %	p4 and Fig. 4c	2010-10	186
P-Si	imp	LD/i	measure	1	0.2 %	p3 and p4	2017-03	286
P-Si	imp	ST/i	measure	1	1.6 % <sup>j</sup>	p3 and abstract	2017-07	25
P-Si	imp	ST/e <sup>m</sup>	measure	1	0.14 % <sup>j</sup>	Tab. II	2018-05	87
P-Si	imp	ST/e <sup>m</sup>	measure	1	0.7 %	Tab. II	2018-05	87
P-Si	imp	ST/i	measure	1	17 %	p4	2018-11	209
P-Si	imp	LD/i	measure	1	3 %	p4	2019-10	124
P-Si28	imp	LD/e	measure	1	20 %	p9	2021-07	162
Si28/SiO <sub>2</sub>	2D	LD/e	measure	1	5 %	p2	2014-10	274
Si28/SiO <sub>2</sub>	2D	ST/e	measure	1	1 %	p2	2018-12	69
Si28/SiO <sub>2</sub>	2D	ST/e	measure	1	0.7 %	p2	2019-12	308
Si28/SiO <sub>2</sub>	imp	LD/i	measure	1	3 %	p2	2014-10	189
Si/SiGe	2D	LD/e	measure	1	5 %	p1	2014-08	123
Si/SiGe	2D	LD/e	measure	1	19 %	p1	2018-02	285
Si/SiGe	2D	ST/e	measure	1	2 %	p3 and Fig. 3f	2019-08	309
Si/SiGe	2D	ST/e	measure	1	1.8 %	Fig. 5b	2020-02	41
Si/SiGe	2D	ST/e	measure	1	1 %	p6	2020-02	41

TABLE IV-2. Operation infidelities (part 2). Superscripts stand for the following. <sup>a</sup>: Electron-valley qubit. <sup>b</sup>: With the control chip inside the fridge. <sup>c</sup>: Per Clifford gate. <sup>d</sup>: At temperature 1.5 K. <sup>e</sup>: In a five-electron dot configuration. <sup>f</sup>: Average of 93% and 72%. <sup>g</sup>: EO qubit. <sup>h</sup>:  $S/T_0/T_+$  ternary result. <sup>i</sup>: S/T binary result. <sup>j</sup>: Latched readout. <sup>k</sup>: Average of 90.7% and 83.3%. <sup>l</sup>: (derived) from visibility  $1 - \mathcal{F} = [1 - v]/2$  with  $v = 0.56$ . <sup>m</sup>: Hybrid ST qubit: impurity – gated dot.

Material	Host	Qubit	Operation	Qubit #	Infidelity	Source	Date	Reference
Si/SiGe	2D	LD/e	measure	1	5.5 %	abstract and p3	2020-04	294
Si/SiGe	2D	LD/e	measure	1	5 %	p5	2020-12	303
Si/SiGe	2D	LD/e	measure	1	10 %	p1 for Q3	2021-06	257
Si/SiO <sub>2</sub>	1D	ST/e	measure	1	1.5 % <sup>a</sup>	abstract and p2	2019-08	265
Si/SiO <sub>2</sub>	1D	LD/e	measure	1	8 %	p2	2021-09	251
Si/SiO <sub>2</sub>	2D	ST/e	measure	2	25 %	p3	2019-03	290
Si/SiO <sub>2</sub>	imp	LD/i	measure	1	10 %	p3	2012-09	219
Si/SiO <sub>2</sub>	imp	ST/i	measure	1	5 %	p3	2014-06	51
GaAs/AlGaAs	2D	ST/e	initialize	2	7 % <sup>b</sup>	p4	2017-12	196
GaAs/AlGaAs	2D	ST/e	initialize	1	11 %	p5	2020-12	223
GaAs/AlGaAs	2D	ST/e	initialize	1	5 %	p1	2021-05	108
P-Si28	imp	LD/i	initialize	1	1.1 %	p5 and Fig. 3	2021-10	116
Si28/SiGe	2D	LD/e	initialize	1	5 %	p1	2019-12	249
Si28/SiO <sub>2</sub>	2D	LD/e	initialize	1	8 %	p2	2014-10	274
Si28/SiO <sub>2</sub>	2D	LD/e	initialize	2	11 % <sup>b</sup>	p3	2019-05	103
Si28/SiO <sub>2</sub>	2D	LD/e	initialize	2	4 % <sup>c</sup>	p6 and Fig. 3b	2021-07	62
Si/SiGe	2D	LD/e	initialize	1	5 %	p1	2014-08	123
Si/SiGe	2D	LD/e	initialize	1	1 % <sup>d</sup>	p1	2018-02	285
Si/SiGe	2D	LD/e	initialize	2	11 % <sup>b</sup>	p3	2018-02	285
Si/SiGe	2D	LD/e	initialize	1	1 %	p5	2020-12	303
Si/SiGe	2D	LD/e	initialize	1	1 %	p1	2021-06	257
Si/SiGe	2D	LD/e	initialize	2	5.9 % <sup>b</sup>	p2	2021-06	257
Si/SiGe	2D	LD/e	initialize	3	12 % <sup>e</sup>	p4	2021-06	257
Si/SiO <sub>2</sub>	1D	ST/e	initialize	1	1.5 % <sup>f</sup>	p3	2019-08	265
Si/SiO <sub>2</sub>	2D	LD/e	initialize	2	10 % <sup>b</sup>	Fig. 3 caption	2021-12	154

TABLE IV-3. Operation infidelities (part 3). Superscripts stand for the following. <sup>a</sup>: Average of 99.6% and 97.3%; latched readout. <sup>b</sup>: Into a Bell state using a two-qubit algorithm. <sup>c</sup>: Fidelity of a Bell state; the article gives a range 94.6–98.3%. The value 96% was (*estimated*) from Fig. 3b. <sup>d</sup>: Using spin hot-spot. <sup>e</sup>: Initialization into the GHZ state through a quantum algorithm. <sup>f</sup>: Into triplet.

Material	Host	Qubit	Quality factor	Qubit #	Source	Date	Reference
GaAs/AlGaAs	2D	ST/e	6 <sup>a</sup>	1	p3	2013-04	56
GaAs/AlGaAs	2D	ST/e	15 <sup>b</sup>	1	abstract and Fig. 4a	2014-01	99
GaAs/AlGaAs	2D	ST/e	19 <sup>c</sup>	2	p4	2018-12	197
GaAs/AlGaAs	2D	ST/e	14 <sup>d</sup>	1	p4	2020-12	111
Ge/Si	1D	LD/h	9.1 <sup>e</sup>	1	p4	2018-12	288
Ge/Si	1D	LD/h	44 <sup>f</sup>	1	p11	2020-06	284
Ge/SiGe	2D	ST/h	52	1	p4 and SM Fig. 15c	2021-08	112
Si28/SiO <sub>2</sub>	2D	ST/e	20	1	p4 and Fig. 2g the rightmost point	2021-02	114
Si/SiO <sub>2</sub>	1D	LD/h <sup>g</sup>	19 <sup>h</sup>	1	SM Fig. S11	2021-03	28
Si/SiO <sub>2</sub>	2D	LD/e <sup>i</sup>	17 <sup>d</sup>	1	SM Fig. 4c	2020-12	155
Si/SiO <sub>2</sub>	2D	LD/e	200 <sup>j</sup>	2	Fig. 2j the rightmost point	2021-12	154

TABLE V-1. Quality factors (qubit). Superscripts stand for the following. <sup>a</sup>: The reference defines  $Q = T_2^H J / 2\pi\hbar$ , giving the maximal value  $Q = 600$  for  $T_2^H = 9 \mu\text{s}$ . Converting to our definition results in the quality factor at least hundred times smaller, since the maximal  $T_2^*$  was 90 ns, see Fig. 4b. <sup>b</sup>: The reference defines  $Q = [J/2\pi\hbar]/\Gamma_\Sigma$  with  $J/2\pi\hbar \approx 1.5 \text{ GHz}$  and  $\Gamma_\Sigma \approx 100 \text{ MHz}$  from Fig. 3d. <sup>c</sup>: The reference defines  $Q = 2JT_2^*/\hbar$ . To convert to our definition, we divide by 2. <sup>d</sup>: The reference defines  $Q = T_2^*/T_{op}$ . To convert to our definition, we divide by 2. <sup>e</sup>: The reference defines "the ratio  $T_2^*/T_{op}$ ", without using the term "quality factor" explicitly. To convert to our definition, we divide by 2 and use  $f_R = 70 \text{ MHz}$  and  $T_2^* = 130 \text{ ns}$ . <sup>f</sup>: (*derived*) the reference defines  $Q = 2f_R T_2^*$ . To convert to our definition, we divide by 2 and use  $f_R = 542 \text{ MHz}$  and  $T_2^* = 82 \text{ ns}$ . <sup>g</sup>: At temperature 1.5 K. <sup>h</sup>: The reference defines  $Q^* = 2f_R T_2^*$  and reports up to  $Q^* = 37.6$  (*estimated*) as the rightmost blue point in Fig. S11. To convert to our definition, we divide by 2. <sup>i</sup>: In a five-electron dot configuration. <sup>j</sup>: The reference defines  $Q = JT_2^{CZ}$ , with  $T_2^{CZ}$  the decay time of the controlled-Z two-qubit gate.

Material	Host	Qubit	Quality factor	Qubit #	Source	Date	Reference
GaAs/AlGaAs	2D	HY/e <sup>a</sup>	<b>4<sup>b</sup></b>	1	Fig. 4c	2017-07	169
GaAs/AlGaAs	2D	HY/e <sup>c</sup>	<b>8<sup>b</sup></b>	1	Fig. 4c	2017-07	169
GaAs/AlGaAs	2D	LD/e	<b>43<sup>d</sup></b>	1	Fig. 6	2020-03	194
GaAs/AlGaAs	2D	ST/e	<b>35<sup>e</sup></b>	1	p2 and Fig. 4d	2016-03	171
GaAs/AlGaAs	2D	ST/e	<b>5.1</b>	1	Fig. 2c Qubit 2	2021-10	65
InAs	1D	LD/e	<b>5<sup>f</sup></b>	1	p2 and Fig. 2d	2010-12	192
Si28/SiGe	2D	LD/e	<b>440<sup>g</sup></b>	1	p2	2017-12	304
Si28/SiGe	2D	ST/e	<b>44</b>	1	Fig. 4b the topmost red point	2016-03	225
Si28/SiO2	2D	LD/e	<b>26<sup>h</sup></b>	2	p4	2015-10	276
Si/SiGe	2D	LD/e	<b>70<sup>d</sup></b>	1	p3	2016-08	256
Si/SiGe	2D	LD/e	<b>9<sup>i</sup></b>	1	p4	2020-01	46
Si/SiO2	1D	LD/h <sup>j</sup>	<b>44<sup>k</sup></b>	1	p5	2021-03	28

TABLE V-2. Quality factors (gate). Superscripts stand for the following. <sup>a</sup>: At a partial sweet spot. <sup>b</sup>: Approximate value at  $f_R = 100$  MHz. <sup>c</sup>: At a full sweet spot. <sup>d</sup>: The reference defines  $Q = 2f_R T_2^R$ . To convert to our definition, we divide by 2. <sup>e</sup>: The reference defines the quality factor as "the number of [exchange-induced singlet-triplet] oscillations before the [oscillation-signal] amplitude decays to 1/e of its initial value", corresponding qualitatively to  $f_R T_2^R$ . <sup>f</sup>: Rough approximation, given as "number of resolved Rabi oscillation periods". <sup>g</sup>: The reference defines  $Q = 2f_R T_2^R$ . To convert to our definition, we divide 2, and use  $f_R = 3.9$  MHz and  $T_2^R = 113 \mu\text{s}$  to get  $Q = 444$ . <sup>h</sup>: The reference defines  $N_{CZ} = f_{CZ} T_2^{CZ}$  with  $T_2^{CZ} = 8.3 \mu\text{s}$ . <sup>i</sup>: The reference defines  $Q = 2T_2^R f_R$ . To convert to our definition, we divide by 2. <sup>j</sup>: At temperature 1.5 K. <sup>k</sup>: The reference defines  $Q = 2f_R T_2^R$  and finds  $Q \gg 87$ . To convert to our definition, we divide by 2 and take the stated lower limit.

Material	Host	Qubit	Dimensions	Functionality	Date	Reference
GaAs/AlGaAs	2D	HY/e <sup>a</sup>	1	device	2010-08	145
GaAs/AlGaAs	2D	HY/e <sup>b</sup>	1	device	2013-07	176
GaAs/AlGaAs	2D	HY/e <sup>a</sup>	1	device	2013-09	175
InSb/AlInSb	2D	LD/e	1	device	2020-04	141
GaAs/AlGaAs	2D	LD/e	2 × 2	device	2012-09	262
GaAs/AlGaAs	2D	LD/e	2 × 2	device	2018-04	191
GaAs/AlGaAs	2D	ST/e	2 × 2	device	2021-10	65
Ge/SiGe	2D	LD/h	2 × 2	device	2020-02	151
Ge/SiGe	2D	LD/h	2 × 2	device	2020-12	96
Ge/SiGe	2D	LD/h	2 × 2	device	2021-01	270
Ge/SiGe	2D	LD/h	2 × 2	device	2021-09	153
Si/SiO <sub>2</sub>	1D	LD/e	2 × 2	device	2020-10	58
Si/SiO <sub>2</sub>	1D	LD/e	2 × 2	device	2020-11	77
Si/SiO <sub>2</sub>	1D	LD/e	2 × 2	device	2020-12	4
Si/SiO <sub>2</sub>	1D	LD/e	2 × 2	device	2020-12	20
GaAs/AlGaAs	2D	ST/e	2	device	2011-07	271
GaAs/AlGaAs	2D	ST/e	2	device	2018-10	47
Ge/SiGe	2D	LD/h	2	device	2019-05	86
Si/SiGe	2D	HY/e	2	device	2021-07	82
GaAs/AlGaAs	2D	LD/e	3 × 3	device	2020-12	187
GaAs/AlGaAs	2D	LD/e	3 × 3	device	2021-08	188
Si/SiO <sub>2</sub>	2D	LD/e	3 × 3	device	2021-01	229
GaAs/AlGaAs	2D	LD/e	3	device	2009-11	76
GaAs/AlGaAs	2D	LD/e	3	device	2013-04	27
GaAs/AlGaAs	2D	LD/e	3	device	2016-01	7
GaAs/AlGaAs	2D	LD/e	3	device	2017-06	67
GaAs/AlGaAs	2D	LD/e	3	device	2017-10	198
GaAs/AlGaAs	2D	LD/e	3	device	2017-12	68
GaAs/AlGaAs	2D	ST/e	3	device	2020-12	110
GaAs/AlGaAs	2D	LD/e	3	device	2021-12	133
Ge/Si	1D	LD/h	3	device	2018-08	72
Si <sub>28</sub> /SiO <sub>2</sub>	2D	LD/e	3	device	2021-02	35
Si/SiGe	2D	LD/e	3	device	2019-07	117
Si/SiO <sub>2</sub>	2D	LD/e	3	device	2020-02	151
Si/SiO <sub>2</sub>	1D	LD/e	4 × 2	device	2020-08	36
GaAs/AlGaAs	2D	LD/e	4	device	2014-03	255
GaAs/AlGaAs	2D	LD/e	4	device	2014-05	53
GaAs/AlGaAs	2D	LD/e	4	device	2016-07	6
GaAs/AlGaAs	2D	LD/e	4	device	2016-10	208
GaAs/AlGaAs	2D	LD/e	4	device	2017-12	74

TABLE VI-1. Qubit arrays (part 1). Superscripts stand for the following. <sup>a</sup>: EO qubit. <sup>b</sup>: RX qubit.

Material	Host	Qubit	Dimensions	Functionality	Date	Reference
GaAs/AlGaAs	2D	LD/e	<b>4</b>	<b>device</b>	2018-08	107
GaAs/AlGaAs	2D	LD/e	<b>4</b>	<b>device</b>	2021-12	268
GaAs/AlGaAs	2D	LD/e	<b>5</b>	<b>device</b>	2016-12	106
Si/SiGe	2D	LD/e	<b>5</b>	<b>device</b>	2020-02	151
GaAs/AlGaAs	2D	LD/e	<b>8</b>	<b>device</b>	2019-12	280
Si28/SiGe	2D	LD/e	<b>9</b>	<b>device</b>	2019-12	185
Si/SiGe	2D	LD/e	<b>9</b>	<b>device</b>	2016-11	305
GaAs/AlGaAs	2D	LD/e	<b>2 × 2</b>	<b>simulator</b>	2020-03	52
GaAs/AlGaAs	2D	LD/e	<b>2</b>	<b>simulator</b>	2011-09	26
GaAs/AlGaAs	2D	LD/e	<b>2</b>	<b>simulator</b>	2011-09	203
GaAs/AlGaAs	2D	ST/e	<b>2</b>	<b>simulator</b>	2012-04	246
GaAs/AlGaAs	2D	ST/e	<b>2</b>	<b>simulator</b>	2019-12	170
GaAs/AlGaAs	2D	LD/e	<b>3</b>	<b>simulator</b>	2016-10	5
GaAs/AlGaAs	2D	LD/e	<b>3</b>	<b>simulator</b>	2018-12	197
GaAs/AlGaAs	2D	LD/e	<b>3</b>	<b>simulator</b>	2019-06	195
GaAs/AlGaAs	2D	LD/e	<b>3</b>	<b>simulator</b>	2020-03	194
Si28/SiGe	2D	LD/e	<b>3</b>	<b>simulator</b>	2015-05	60
GaAs/AlGaAs	2D	LD/e	<b>4</b>	<b>simulator</b>	2019-09	119
GaAs/AlGaAs	2D	LD/e	<b>4</b>	<b>simulator</b>	2020-07	221
GaAs/AlGaAs	2D	LD/e	<b>4</b>	<b>simulator</b>	2020-12	223
GaAs/AlGaAs	2D	LD/e	<b>4</b>	<b>simulator</b>	2021-01	222
GaAs/AlGaAs	2D	LD/e	<b>4</b>	<b>simulator</b>	2021-03	269
GaAs/AlGaAs	2D	LD/e	<b>4</b>	<b>simulator</b>	2021-12	120
Si28/SiGe	2D	LD/e	<b>4</b>	<b>simulator</b>	2019-06	248
Ge/SiGe	2D	LD/h	<b>2 × 2</b>	<b>processor</b>	2021-03	97
Ge/SiGe	2D	LD/h	<b>2</b>	<b>processor</b>	2020-01	95
Si28/SiO <sub>2</sub>	2D	LD/e	<b>2</b>	<b>processor</b>	2015-10	276
Si/SiGe	2D	LD/e	<b>2</b>	<b>processor</b>	2018-01	306
Si/SiGe	2D	LD/e	<b>2</b>	<b>processor</b>	2018-02	285
Si/SiO <sub>2</sub>	2D	LD/e	<b>2</b>	<b>processor</b>	2021-12	154
Si/SiGe	2D	LD/e	<b>3</b>	<b>processor</b>	2021-06	257

TABLE VI-2. Qubit arrays (part 2).

## Appendix D: Glossary

This section defines keywords with specific meaning used in plots and tables. Some are defined in the text, some are defined only here.

---

First, we define the following special keywords.

---

**(derived)**: The value is not stated in the reference. We derived it as described in the *note*.

**(estimated)**: The value is not stated in the reference. We estimated it from available information, most often from a figure. The estimate is only rough, with a typical error of order one.

**attribute**: A generic attribute. Several *values* belong under it.

**value**: A generic value. It belongs under a unique *attribute*.

---

The list of the *attributes* and *values*, the latter for the case when the allowed values are from a small set of enumerated alternatives.

**ID**: The quantum dot host is quasi-one-dimensional, such as a nanowire. This is one of the values of *Host*.

**2D**: The quantum dot host is quasi-two-dimensional, such as a two-dimensional electron (or hole) gas of a quantum well, an epilayer, or a similar heterostructure. This is one of the values of *Host*.

**charge**: The qubit basis is represented by two different orbitals of a confined particle. Most often, the orbitals differ in their centers (positions), for example a pair of states localized each in one minimum of a double-well potential of a double dot. Unlike for spin-related qubits, we do not discriminate the carrier, be it electron, hole, or impurity. However, most charge-qubit experiments use electrons. This is one of the values of *Qubit*.

**Coherence**: It describes in what type of experiment the corresponding coherence time has been measured. This attribute can have the following values:  $T_1$ ,  $T_2^*$ ,  $T_2^H$ ,  $T_2^D$ , and  $T_2^R$ .

**Date**: Publication date. In tables, the year and month are given. In plots, the full date down to a day (if available) is used in sorting and horizontal shifts. If the reference is unpublished (only an arxiv version exists), we use the submission date of the first arxiv version.

**device**: The array functionality is at the lowest level out of those spanning the range from fabricating a sample to implementing a fully functional quantum processor. See

Sec. VI A for details. This is one of the values of *Functionality*.

**Dimensions**: The single dimension of a one-dimensional array, or the two dimensions of a two-dimensional array starting with the larger one.

**Functionality**: What functionality is available for the qubit-array initialization, manipulation, and measurement. See Sec. VI A. This attribute can have the following values: *device*, *simulator*, and *processor*.

**gate**: The operation is a gate. This is one of the values of *Operation*.

**Host**: Where are the dots defined. This attribute can have the following values: *2D*, *1D*, and *imp*.

**HY/e**: The qubit basis is represented by electron states having hybrid character, most often differing in both the spin and charge degrees of freedom. This is one of the values of *Qubit*.

**imp**: The quantum dot host is an impurity. In this review we include only experiments on gated impurities accessed electrically. This is one of the values of *Host*.

**Infidelity**: Operation infidelity (one minus fidelity). See Sec. IV A for details.

**initialize**: The operation is an initialization. This is one of the values of *Operation*.

**LD/e**: The qubit basis is represented by the spin-up and spin-down state of a confined conduction-band electron (or many-electron) state [159]. This is one of the values of *Qubit*.

**LD/h**: The same as *LD/e* but using valence-band holes instead of conduction-band electrons. This is one of the values of *Qubit*.

**LD/i**: The same as *LD/e* but using impurity-bound electrons instead of conduction-band electrons confined by gates [121]. This is one of the values of *Qubit*.

**Material**: Material of the device. Most of the structures used in experiments are composites, for example a heterostructure with GaAs and AlGaAs layers is given as GaAs/AlGaAs. In some plots we merge groups of materials by retaining only the primary material where the qubit host particle is located. For example, under such a contraction both "Si/SiO" and "Si/Ge" become "Si". When merging in this way, we further merge binary and ternary alloys of Al, Ga, In, As, and Sb under the key "III-V". Finally, we denote isotopically purified silicon by appending the number 28, such as in "Si28".

**measure**: The operation is a measurement. This is one of the values of *Operation*.

**Note**: Additional information concerning the *value* exists, indicated by a superscript. The corresponding note is given in the table caption.

**Operation:** The operation type. This attribute can have the following values: *gate*, *measure*, and *initialize*.

**processor:** The array functionality is at the highest level out of those spanning the range from fabricating a sample to implementing a fully functional quantum processor. See Sec. VI A for details. This is one of the values of *Functionality*.

**Quality factor:** (For a gate). The number of gate-signal oscillations before the signal amplitude drops to  $1/e$ . See Sec. V for details.

**Quality factor:** (For a qubit). The number of gate-signal oscillations within the inhomogeneous dephasing time. See Sec. V for details.

**Qubit:** Which degree of freedom defines the qubit. It includes the carrier (such as the electron, hole, or impurity) and the subspace representing the qubit states' pair, such as the spin one-half (the LD qubit), the singlet and triplet (the ST qubit), orbitals (the charge qubit), and their hybrids. This attribute can have the following values: *charge*, *HY/e*, *LD/e*, *ST/e*, *LD/h*, *ST/h*, *LD/i*, and *ST/i*.

**Qubit #:** Number of qubits that the operation involves.

**Reference:** The number referring to the bibliography at the end of the document. The bibliography is sorted alphabetically in first authors' names.

**simulator:** The array functionality is at the second level out of those spanning the range from fabricating a sample to implementing a fully functional quantum processor. See Sec. VI A for details. This is one of the values of *Functionality*.

**Source:** Where in the reference the value can be found. Typical sources are page X, denoted as *pX*, or figure Y, denoted as Fig. Y. Multiple places might be given, if relevant. An example of the value source is "p3 and Fig. 2a".

**ST/e:** The qubit basis is represented by the spin-singlet and spin-triplet state of a confined conduction-band electron pair [156]. This is one of the values of *Qubit*.

**ST/h:** The same as *ST/e* but using valence-band holes instead of conduction-band electrons. This is one of the values of *Qubit*.

**ST/i:** The same as *ST/e* but using impurity-bound electrons instead of conduction-band electrons confined by gates. This is one of the values of *Qubit*.

**$T_1$ :** Energy relaxation. The decay of population of the energy basis state(s) was measured. This is one of the values of *Coherence*.

**$T_2^*$ :** Inhomogeneous dephasing. The experiment measured the decay of phase of an idling qubit without any echos. Most often, it corresponds to a Ramsey sequence: initialization –  $\pi/2$  pulse – free precession for time  $\tau - \pi/2$  pulse – measurement. This is one of the values of *Coherence*.

**$T_2^D$ :** Dephasing under a dynamical decoupling protocol. The experiment measured the decay of phase of a qubit applying more than one echo-pulse. While there are several families of pulse sequences, we do not discriminate them. This is one of the values of *Coherence*.

**$T_2^H$ :** Dephasing under Hahn echo. The experiment measured the decay of phase of a qubit applying a single echo-pulse. A typical sequence is: initialization –  $\pi/2$  pulse – free precession for time  $\tau/2 - \pi$  pulse – free precession for time  $\tau/2 - \pi/2$  pulse – measurement. This is one of the values of *Coherence*.

**$T_2^R$ :** Dephasing of a driven qubit. Strictly speaking, this time should describe the decay of the relative phase of the two quasi-energy states in the rotating frame of reference. Usually, it is extracted as the observed decay time of Rabi oscillations. This is one of the values of *Coherence*.

**Time:** (In tables on coherence). The timescale of the coherence decay observed in a certain type of experiment. The type is described by *Coherence*.

**Time:** (In tables on operation times) The duration of the operation. If the reference gives a frequency  $f$  for a gate signal, we convert it to time  $t$  using  $t = 1/2f$ , see Eq. 9.

- [1] G. A. Álvarez, A. Ajoy, X. Peng, and D. Suter. Performance comparison of dynamical decoupling sequences for a qubit in a rapidly fluctuating spin bath. *Physical Review A*, 82(4):042306, Oct. 2010.
- [2] S. Amasha, K. MacLean, I. P. Radu, D. M. Zumbühl, M. A. Kastner, M. P. Hanson, and A. C. Gossard. Electrical Control of Spin Relaxation in a Quantum Dot. *Physical Review Letters*, 100(4), Jan. 2008.
- [3] R. W. Andrews, C. Jones, M. D. Reed, A. M. Jones, S. D. Ha, M. P. Jura, J. Kerckhoff, M. Levendorf, S. Meenehan, S. T. Merkel, A. Smith, B. Sun, A. J. Weinstein, M. T. Rakher, T. D. Ladd, and M. G. Borselli. Quantifying error and leakage in an encoded Si/SiGe triple-dot qubit. *Nature Nanotechnology*, 14(8):747–750, Aug. 2019.

- [4] F. Ansaloni, A. Chatterjee, H. Bohuslavskyi, B. Bertrand, L. Hutin, M. Vinet, and F. Kuemmeth. Single-electron operations in a foundry-fabricated array of quantum dots. *Nature Communications*, 11(1):6399, Dec. 2020.
- [5] T. A. Baart, T. Fujita, C. Reichl, W. Wegscheider, and L. M. K. Vandersypen. Coherent spin-exchange via a quantum mediator. *Nature Nanotechnology*, 12(1):26–30, Oct. 2016.
- [6] T. A. Baart, N. Jovanovic, C. Reichl, W. Wegscheider, and L. M. K. Vandersypen. Nanosecond-timescale spin transfer using individual electrons in a quadruple-quantum-dot device. *Applied Physics Letters*, 109(4):043101, July 2016.
- [7] T. A. Baart, M. Shafiei, T. Fujita, C. Reichl, W. Wegscheider,

- and L. M. K. Vandersypen. Single-spin CCD. *Nature Nanotechnology*, 11(4):330–334, Jan. 2016.
- [8] C. Barthel, M. Kjærgaard, J. Medford, M. Stopa, C. M. Marcus, M. P. Hanson, and A. C. Gossard. Fast sensing of double-dot charge arrangement and spin state with a radio-frequency sensor quantum dot. *Physical Review B*, 81(16):161308, Apr. 2010.
- [9] C. Barthel, J. Medford, H. Bluhm, A. Yacoby, C. M. Marcus, M. P. Hanson, and A. C. Gossard. Relaxation and readout visibility of a singlet-triplet qubit in an Overhauser field gradient. *Physical Review B*, 85(3), Jan. 2012.
- [10] C. Barthel, J. Medford, C. M. Marcus, M. P. Hanson, and A. C. Gossard. Interlaced Dynamical Decoupling and Coherent Operation of a Singlet-Triplet Qubit. *Physical Review Letters*, 105(26), Dec. 2010.
- [11] C. Barthel, D. J. Reilly, C. M. Marcus, M. P. Hanson, and A. C. Gossard. Rapid Single-Shot Measurement of a Singlet-Triplet Qubit. *Physical Review Letters*, 103(16), Oct. 2009.
- [12] B. Bertrand, H. Flentje, S. Takada, M. Yamamoto, S. Tarucha, A. Ludwig, A. D. Wieck, C. Bäuerle, and T. Meunier. Quantum Manipulation of Two-Electron Spin States in Isolated Double Quantum Dots. *Physical Review Letters*, 115(9), Aug. 2015.
- [13] F. Bloch. Nuclear Induction. *Physical Review*, 70(7-8):460–474, Oct. 1946.
- [14] H. Bluhm, S. Foletti, D. Mahalu, V. Umansky, and A. Yacoby. Enhancing the Coherence of a Spin Qubit by Operating it as a Feedback Loop That Controls its Nuclear Spin Bath. *Physical Review Letters*, 105(21), Nov. 2010.
- [15] H. Bluhm, S. Foletti, I. Neder, M. Rudner, D. Mahalu, V. Umansky, and A. Yacoby. Dephasing time of GaAs electron-spin qubits coupled to a nuclear bath exceeding 200  $\mu$ s. *Nature Physics*, 7(2):109–113, Feb. 2011.
- [16] K. Blum. *Density Matrix Theory and Applications*. Springer US, Boston, MA, 1996. OCLC: 905455687.
- [17] R. Blume-Kohout, J. K. Gamble, E. Nielsen, K. Rudinger, J. Mizrahi, K. Fortier, and P. Maunz. Demonstration of qubit operations below a rigorous fault tolerance threshold with gate set tomography. *Nature Communications*, 8(1):14485, Apr. 2017.
- [18] A. Bogan, S. Studenikin, M. Korkusinski, L. Gaudreau, P. Zawadzki, A. Sachrajda, L. Tracy, J. Reno, and T. Hargett. Single hole spin relaxation probed by fast single-shot latched charge sensing. *Communications Physics*, 2(1):17, Dec. 2019.
- [19] A. Bogan, S. Studenikin, M. Korkusinski, L. Gaudreau, P. Zawadzki, A. S. Sachrajda, L. Tracy, J. Reno, and T. Hargett. Landau-Zener-Stückelberg-Majorana Interferometry of a Single Hole. *Physical Review Letters*, 120(20), May 2018.
- [20] H. Bohuslavskyi, F. Ansaloni, A. Chatterjee, F. Fedele, T. Rasmussen, B. Brovang, J. Li, L. Hutin, B. Venitucci, B. Bertrand, M. Vinet, Y.-M. Niquet, and F. Kuemmeth. Reflectometry of charge transitions in a silicon quadruple dot. *arXiv:2012.04791 [cond-mat, physics:quant-ph]*, Dec. 2020. arXiv: 2012.04791.
- [21] F. Borjans, X. Croot, S. Putz, X. Mi, S. M. Quinn, A. Pan, J. Kerckhoff, E. J. Pritchett, C. A. Jackson, L. F. Edge, R. S. Ross, T. D. Ladd, M. G. Borselli, M. F. Gyure, and J. R. Petta. Split-gate cavity coupler for silicon circuit quantum electrodynamics. *Applied Physics Letters*, 116(23):234001, June 2020.
- [22] F. Borjans, X. G. Croot, X. Mi, M. J. Gullans, and J. R. Petta. Resonant microwave-mediated interactions between distant electron spins. *Nature*, 577(7789):195–198, Jan. 2020.
- [23] F. Borjans, D. Zajac, T. Hazard, and J. Petta. Single-Spin Relaxation in a Synthetic Spin-Orbit Field. *Physical Review Applied*, 11(4):044063, Apr. 2019.
- [24] J. M. Boter, X. Xue, T. Krähenmann, T. F. Watson, V. N. Premakumar, D. R. Ward, D. E. Savage, M. G. Lagally, M. Friesen, S. N. Coppersmith, M. A. Eriksson, R. Joynt, and L. M. K. Vandersypen. Spatial noise correlations in a Si/SiGe two-qubit device from Bell state coherences. *Physical Review B*, 101(23):235133, June 2020.
- [25] M. A. Broome, T. F. Watson, D. Keith, S. K. Gorman, M. G. House, J. G. Keizer, S. J. Hile, W. Baker, and M. Y. Simmons. High-Fidelity Single-Shot Singlet-Triplet Readout of Precision-Placed Donors in Silicon. *Physical Review Letters*, 119(4), July 2017.
- [26] R. Brunner, Y.-S. Shin, T. Obata, M. Pioro-Ladrière, T. Kubo, K. Yoshida, T. Taniyama, Y. Tokura, and S. Tarucha. Two-Qubit Gate of Combined Single-Spin Rotation and Interdot Spin Exchange in a Double Quantum Dot. *Physical Review Letters*, 107(14), Sept. 2011.
- [27] M. Busl, G. Granger, L. Gaudreau, R. Sánchez, A. Kam, M. Pioro-Ladrière, S. A. Studenikin, P. Zawadzki, Z. R. Wasilewski, A. S. Sachrajda, and G. Platero. Bipolar spin blockade and coherent state superpositions in a triple quantum dot. *Nature Nanotechnology*, 8(4):261–265, Apr. 2013.
- [28] L. C. Camenzind, S. Geyer, A. Fuhrer, R. J. Warburton, D. M. Zumbühl, and A. V. Kuhlmann. A spin qubit in a fin field-effect transistor. *arXiv:2103.07369 [cond-mat, physics:quant-ph]*, Mar. 2021. arXiv: 2103.07369.
- [29] L. C. Camenzind, L. Yu, P. Stano, J. D. Zimmerman, A. C. Gossard, D. Loss, and D. M. Zumbühl. Hyperfine-phonon spin relaxation in a single-electron GaAs quantum dot. *Nature Communications*, 9(1):3454, Dec. 2018.
- [30] G. Cao, H.-O. Li, T. Tu, L. Wang, C. Zhou, M. Xiao, G.-C. Guo, H.-W. Jiang, and G.-P. Guo. Ultrafast universal quantum control of a quantum-dot charge qubit using Landau-Zener-Stückelberg interference. *Nature Communications*, 4(1):1401, June 2013.
- [31] G. Cao, H.-O. Li, G.-D. Yu, B.-C. Wang, B.-B. Chen, X.-X. Song, M. Xiao, G.-C. Guo, H.-W. Jiang, X. Hu, and G.-P. Guo. Tunable Hybrid Qubit in a GaAs Double Quantum Dot. *Physical Review Letters*, 116(8), Feb. 2016.
- [32] P. Cerfontaine, T. Botzem, S. S. Humpohl, D. Schuh, D. Bougeard, and H. Bluhm. Feedback-tuned noise-resilient gates for encoded spin qubits. *arXiv preprint arXiv:1606.01897*, June 2016. arXiv: 1606.01897.
- [33] P. Cerfontaine, T. Botzem, J. Ritzmann, S. S. Humpohl, A. Ludwig, D. Schuh, D. Bougeard, A. D. Wieck, and H. Bluhm. Closed-loop control of a GaAs-based singlet-triplet spin qubit with 99.5% gate fidelity and low leakage. *Nature Communications*, 11(1):4144, Dec. 2020.
- [34] K. W. Chan, W. Huang, C. H. Yang, J. C. C. Hwang, B. Hensen, T. Tanttu, F. E. Hudson, K. M. Itoh, A. Laucht, A. Morello, and A. S. Dzurak. Assessment of a Silicon Quantum Dot Spin Qubit Environment via Noise Spectroscopy. *Physical Review Applied*, 10(4), Oct. 2018.
- [35] K. W. Chan, H. Sahasrabudhe, W. Huang, Y. Wang, H. C. Yang, M. Veldhorst, J. C. C. Hwang, F. A. Mohiyaddin, F. E. Hudson, K. M. Itoh, A. Saraiva, A. Morello, A. Laucht, R. Rahman, and A. S. Dzurak. Exchange coupling in a linear chain of three quantum-dot spin qubits in silicon. *Nano Letters*, 21(3):1517–1522, Feb. 2021. arXiv: 2004.07666.
- [36] E. Chanrion, D. J. Niegemann, B. Bertrand, C. Spence, B. Jadot, J. Li, P.-A. Mortemousque, L. Hutin, R. Maurand, X. Jehl, M. Sanquer, S. De Franceschi, C. Bäuerle, F. Balestro, Y.-M. Niquet, M. Vinet, T. Meunier, and M. Urdampilleta. Charge Detection in an Array of CMOS Quantum Dots. *Physical Review Applied*, 14(2):024066, Aug. 2020.
- [37] A. Chatterjee, P. Stevenson, S. De Franceschi, A. Morello,

- N. P. de Leon, and F. Kuemmeth. Semiconductor qubits in practice. *Nature Reviews Physics*, 3(3):157–177, Mar. 2021.
- [38] H. O. H. Churchill, F. Kuemmeth, J. W. Harlow, A. J. Bestwick, E. I. Rashba, K. Flensberg, C. H. Stwertka, T. Taychatanapat, S. K. Watson, and C. M. Marcus. Relaxation and Dephasing in a Two-Electron C 13 Nanotube Double Quantum Dot. *Physical Review Letters*, 102(16):166802, Apr. 2009.
- [39] V. N. Ciriano-Tejel, M. A. Fogarty, S. Schaal, L. Hutin, B. Bertrand, L. Ibberson, M. F. Gonzalez-Zalba, J. Li, Y.-M. Niquet, M. Vinet, and J. J. Morton. Spin Readout of a CMOS Quantum Dot by Gate Reflectometry and Spin-Dependent Tunneling. *PRX Quantum*, 2(1):010353, Mar. 2021.
- [40] J. I. Colless, A. C. Mahoney, J. M. Hornibrook, A. C. Doherty, H. Lu, A. C. Gossard, and D. J. Reilly. Dispersive Readout of a Few-Electron Double Quantum Dot with Fast rf Gate Sensors. *Physical Review Letters*, 110(4), Jan. 2013.
- [41] E. J. Connors, J. Nelson, and J. M. Nichol. Rapid High-Fidelity Spin-State Readout in Si / Si - Ge Quantum Dots via rf Reflectometry. *Physical Review Applied*, 13(2), Feb. 2020.
- [42] A. Corna, L. Bourdet, R. Maurand, A. Crippa, D. Kotekar-Patil, H. Bohuslavskyi, R. Laviéville, L. Hutin, S. Barraud, X. Jehl, M. Vinet, S. De Franceschi, Y.-M. Niquet, and M. Sanquer. Electrically driven electron spin resonance mediated by spin-valley-orbit coupling in a silicon quantum dot. *npj Quantum Information*, 4(1), Dec. 2018.
- [43] A. Cottet, M. C. Dartailh, M. M. Desjardins, T. Cubaynes, L. C. Contamin, M. Delbecq, J. J. Viennot, L. E. Bruhat, B. Douçot, and T. Kontos. Cavity QED with hybrid nanocircuits: from atomic-like physics to condensed matter phenomena. *Journal of Physics: Condensed Matter*, 29(43):433002, Nov. 2017.
- [44] A. Crippa, R. Ezzouch, A. Aprá, A. Amisse, R. Laviéville, L. Hutin, B. Bertrand, M. Vinet, M. Urdampilleta, T. Meunier, M. Sanquer, X. Jehl, R. Maurand, and S. De Franceschi. Gate-reflectometry dispersive readout and coherent control of a spin qubit in silicon. *Nature Communications*, 10(1):2776, Dec. 2019.
- [45] A. Crippa, R. Maurand, L. Bourdet, D. Kotekar-Patil, A. Amisse, X. Jehl, M. Sanquer, R. Laviéville, H. Bohuslavskyi, L. Hutin, S. Barraud, M. Vinet, Y.-M. Niquet, and S. De Franceschi. Electrical Spin Driving by g -Matrix Modulation in Spin-Orbit Qubits. *Physical Review Letters*, 120(13):137702, Mar. 2018.
- [46] X. Croot, X. Mi, S. Putz, M. Benito, F. Borjans, G. Burkard, and J. R. Petta. Flopping-mode electric dipole spin resonance. *Physical Review Research*, 2(1):012006, Jan. 2020. arXiv: 1905.00346.
- [47] X. Croot, S. Pauka, J. Watson, G. Gardner, S. Fallahi, M. Manfra, and D. Reilly. Device Architecture for Coupling Spin Qubits via an Intermediate Quantum State. *Physical Review Applied*, 10(4), Oct. 2018.
- [48] T. Cubaynes, M. R. Delbecq, M. C. Dartailh, R. Assouly, M. M. Desjardins, L. C. Contamin, L. E. Bruhat, Z. Leghtas, F. Mallet, A. Cottet, and T. Kontos. Highly coherent spin states in carbon nanotubes coupled to cavity photons. *npj Quantum Information*, 5(1):47, Dec. 2019.
- [49] Ł. Cywiński, R. M. Lutchyn, C. P. Nave, and S. Das Sarma. How to enhance dephasing time in superconducting qubits. *Physical Review B*, 77(17):174509, May 2008.
- [50] J. P. Dehollain, J. T. Muhonen, R. Blume-Kohout, K. M. Rudinger, J. K. Gamble, E. Nielsen, A. Laucht, S. Simmons, R. Kalra, A. S. Dzurak, and A. Morello. Optimization of a solid-state electron spin qubit using gate set tomography. *New Journal of Physics*, 18(10):103018, Oct. 2016.
- [51] J. P. Dehollain, J. T. Muhonen, K. Y. Tan, A. Saraiva, D. N. Jamieson, A. S. Dzurak, and A. Morello. Single-Shot Readout and Relaxation of Singlet and Triplet States in Exchange-Coupled P 31 Electron Spins in Silicon. *Physical Review Letters*, 112(23), June 2014.
- [52] J. P. Dehollain, U. Mukhopadhyay, V. P. Michal, Y. Wang, B. Wunsch, C. Reichl, W. Wegscheider, M. S. Rudner, E. Demler, and L. M. K. Vandersypen. Nagaoka ferromagnetism observed in a quantum dot plaquette. *Nature*, Mar. 2020.
- [53] M. R. Delbecq, T. Nakajima, T. Otsuka, S. Amaha, J. D. Watson, M. J. Manfra, and S. Tarucha. Full control of quadruple quantum dot circuit charge states in the single electron regime. *Applied Physics Letters*, 104(18):183111, May 2014.
- [54] M. R. Delbecq, T. Nakajima, P. Stano, T. Otsuka, S. Amaha, J. Yoneda, K. Takeda, G. Allison, A. Ludwig, A. D. Wieck, and S. Tarucha. Quantum Dephasing in a Gated GaAs Triple Quantum Dot due to Nonergodic Noise. *Physical Review Letters*, 116(4):046802, Jan. 2016.
- [55] S. J. Devitt, K. Nemoto, and W. J. Munro. Quantum Error Correction for Beginners. *Reports on Progress in Physics*, 76(7):076001, July 2013. arXiv: 0905.2794.
- [56] O. E. Dial, M. D. Shulman, S. P. Harvey, H. Bluhm, V. Umansky, and A. Yacoby. Charge Noise Spectroscopy Using Coherent Exchange Oscillations in a Singlet-Triplet Qubit. *Physical Review Letters*, 110(14), Apr. 2013.
- [57] Y. Dovzhenko, J. Stehlík, K. D. Petersson, J. R. Petta, H. Lu, and A. C. Gossard. Nonadiabatic quantum control of a semiconductor charge qubit. *Physical Review B*, 84(16):161302, Oct. 2011.
- [58] J. Duan, M. A. Fogarty, J. Williams, L. Hutin, M. Vinet, and J. J. L. Morton. Remote Capacitive Sensing in Two-Dimensional Quantum-Dot Arrays. *Nano Letters*, 20(10):7123–7128, Oct. 2020.
- [59] J. M. Elzerman, R. Hanson, L. H. Willems van Beveren, B. Witkamp, L. M. K. Vandersypen, and L. P. Kouwenhoven. Single-shot read-out of an individual electron spin in a quantum dot. *Nature*, 430(6998):431–435, July 2004.
- [60] K. Eng, T. D. Ladd, A. Smith, M. G. Borselli, A. A. Kislev, B. H. Fong, K. S. Holabird, T. M. Hazard, B. Huang, P. W. Deelman, I. Milosavljevic, A. E. Schmitz, R. S. Ross, M. F. Gyure, and A. T. Hunter. Isotopically enhanced triple-quantum-dot qubit. *Science Advances*, 1(4):e1500214–e1500214, May 2015.
- [61] J. M. Epstein, A. W. Cross, E. Magesan, and J. M. Gambetta. Investigating the limits of randomized benchmarking protocols. *Physical Review A*, 89(6):062321, June 2014.
- [62] T. J. Evans, W. Huang, J. Yoneda, R. Harper, T. Tanttu, K. W. Chan, F. E. Hudson, K. M. Itoh, A. Saraiva, C. H. Yang, A. S. Dzurak, and S. D. Bartlett. Fast Bayesian tomography of a two-qubit gate set in silicon. arXiv:2107.14473 [quant-ph], July 2021. arXiv: 2107.14473.
- [63] R. Ezzouch, S. Zihlmann, V. P. Michal, J. Li, A. Aprá, B. Bertrand, L. Hutin, M. Vinet, M. Urdampilleta, T. Meunier, X. Jehl, Y.-M. Niquet, M. Sanquer, S. De Franceschi, and R. Maurand. Dispersively probed microwave spectroscopy of a silicon hole double quantum dot. arXiv:2012.15588 [cond-mat], Jan. 2021. arXiv: 2012.15588.
- [64] J. Fabian, A. Matos-Abiague, C. Ertler, P. Stano, and I. Žutić. Semiconductor spintronics. *Acta Physica Slovaca. Reviews and Tutorials*, 57(4-5), Aug. 2007.
- [65] F. Fedele, A. Chatterjee, S. Fallahi, G. C. Gardner, M. J. Manfra, and F. Kuemmeth. Simultaneous Operations in a Two-Dimensional Array of Singlet-Triplet Qubits. *PRX Quantum*, 2(4):040306, Oct. 2021.

- [66] J. Fischer and D. Loss. Dealing with Decoherence. *Science*, 324(5932):1277–1278, June 2009.
- [67] H. Flentje, B. Bertrand, P.-A. Mortemousque, V. Thiney, A. Ludwig, A. D. Wieck, C. Bäuerle, and T. Meunier. A linear triple quantum dot system in isolated configuration. *Applied Physics Letters*, 110(23):233101, June 2017.
- [68] H. Flentje, P.-A. Mortemousque, R. Thalineau, A. Ludwig, A. D. Wieck, C. Bäuerle, and T. Meunier. Coherent long-distance displacement of individual electron spins. *Nature Communications*, 8(1), Dec. 2017.
- [69] M. A. Fogarty, K. W. Chan, B. Hensen, W. Huang, T. Tanttu, C. H. Yang, A. Laucht, M. Veldhorst, F. E. Hudson, K. M. Itoh, D. Culcer, T. D. Ladd, A. Morello, and A. S. Dzurak. Integrated silicon qubit platform with single-spin addressability, exchange control and single-shot singlet-triplet readout. *Nature Communications*, 9(1), Dec. 2018.
- [70] T. Frey, P. J. Leek, M. Beck, A. Blais, T. Ihn, K. Ensslin, and A. Wallraff. Dipole Coupling of a Double Quantum Dot to a Microwave Resonator. *Physical Review Letters*, 108(4), Jan. 2012.
- [71] F. N. M. Froning, L. C. Camenzind, O. A. H. van der Molen, A. Li, E. P. A. M. Bakkers, D. M. Zumbühl, and F. R. Braakman. Ultrafast hole spin qubit with gate-tunable spin-orbit switch functionality. *Nature Nanotechnology*, 16:308–312, Jan. 2021.
- [72] F. N. M. Froning, M. K. Rehmann, J. Ridderbos, M. Brauns, F. A. Zwanenburg, A. Li, E. P. A. M. Bakkers, D. M. Zumbühl, and F. R. Braakman. Single, double, and triple quantum dots in Ge/Si nanowires. *Applied Physics Letters*, 113(7):073102, Aug. 2018.
- [73] T. Fujisawa, D. G. Austing, Y. Tokura, Y. Hirayama, and S. Tarucha. Allowed and forbidden transitions in artificial hydrogen and helium atoms. *Nature*, 419(6904):278–281, Sept. 2002.
- [74] T. Fujita, T. A. Baart, C. Reichl, W. Wegscheider, and L. M. K. Vandersypen. Coherent shuttle of electron-spin states. *npj Quantum Information*, 3(1), Dec. 2017.
- [75] L. Gaudreau, G. Granger, A. Kam, G. C. Aers, S. A. Studenikin, P. Zawadzki, M. Pioro-Ladrière, Z. R. Wasilewski, and A. S. Sachrajda. Coherent control of three-spin states in a triple quantum dot. *Nature Physics*, 8(1):54–58, Nov. 2011.
- [76] L. Gaudreau, A. Kam, G. Granger, S. A. Studenikin, P. Zawadzki, and A. S. Sachrajda. A tunable few electron triple quantum dot. *Applied Physics Letters*, 95(19):193101, Nov. 2009.
- [77] W. Gilbert, A. Saraiva, W. H. Lim, C. H. Yang, A. Laucht, B. Bertrand, N. Rambal, L. Hutin, C. C. Escott, M. Vinet, and A. S. Dzurak. Single-electron operation of a silicon-CMOS 2x2 quantum dot array with integrated charge sensing. *Nano Letters*, 20(11):7882–7888, Nov. 2020. arXiv: 2004.11558.
- [78] A. Gilchrist, N. K. Langford, and M. A. Nielsen. Distance measures to compare real and ideal quantum processes. *Physical Review A*, 71(6):062310, June 2005.
- [79] M. F. Gonzalez-Zalba, S. Barraud, A. J. Ferguson, and A. C. Betz. Probing the limits of gate-based charge sensing. *Nature Communications*, 6(1):6084, May 2015.
- [80] M. F. Gonzalez-Zalba, S. de Franceschi, E. Charbon, T. Meunier, M. Vinet, and A. S. Dzurak. Scaling silicon-based quantum computing using CMOS technology: State-of-the-art, Challenges and Perspectives. *arXiv:2011.11753 [cond-mat, physics:quant-ph]*, Nov. 2020. arXiv: 2011.11753.
- [81] D. Gottesman. Theory of fault-tolerant quantum computation. *Physical Review A*, 57(1):127–137, Jan. 1998.
- [82] W. Ha, S. D. Ha, M. D. Choi, Y. Tang, A. E. Schmitz, M. P. Levendorf, K. Lee, J. M. Chappell, T. S. Adams, D. R. Hulbert, E. Acuna, R. S. Noah, J. W. Matten, M. P. Jura, J. A. Wright, M. T. Rakher, and M. G. Borselli. A flexible design platform for Si/SiGe exchange-only qubits with low disorder. *arXiv:2107.10916 [cond-mat, physics:quant-ph]*, July 2021. arXiv: 2107.10916.
- [83] E. L. Hahn. Spin Echoes. *Physical Review*, 80(4):580–594, Nov. 1950.
- [84] R. Hanson, L. P. Kouwenhoven, J. R. Petta, S. Tarucha, and L. M. K. Vandersypen. Spins in few-electron quantum dots. *Reviews of Modern Physics*, 79(4):1217–1265, Oct. 2007.
- [85] R. Hanson, B. Witkamp, L. M. K. Vandersypen, L. H. W. van Beveren, J. M. Elzerman, and L. P. Kouwenhoven. Zeeman Energy and Spin Relaxation in a One-Electron Quantum Dot. *Physical Review Letters*, 91(19), Nov. 2003.
- [86] W. J. Hardy, C. T. Harris, Y.-H. Su, Y. Chuang, J. Moussa, L. N. Maurer, J.-Y. Li, T.-M. Lu, and D. R. Luhman. Single and double hole quantum dots in strained Ge/SiGe quantum wells. *Nanotechnology*, 30(21):215202, May 2019.
- [87] P. Harvey-Collard, B. D’Anjou, M. Rudolph, N. T. Jacobson, J. Dominguez, G. A. Ten Eyck, J. R. Wendt, T. Pluym, M. P. Lilly, W. A. Coish, M. Pioro-Ladrière, and M. S. Carroll. High-Fidelity Single-Shot Readout for a Spin Qubit via an Enhanced Latching Mechanism. *Physical Review X*, 8(2):021046, May 2018.
- [88] P. Harvey-Collard, N. T. Jacobson, C. Bureau-Oxton, R. M. Jock, V. Srinivasa, A. M. Mounce, D. R. Ward, J. M. Anderson, R. P. Manginell, J. R. Wendt, T. Pluym, M. P. Lilly, D. R. Luhman, M. Pioro-Ladrière, and M. S. Carroll. Spin-orbit Interactions for Singlet-Triplet Qubits in Silicon. *Physical Review Letters*, 122(21):217702, May 2019.
- [89] P. Harvey-Collard, N. T. Jacobson, M. Rudolph, J. Dominguez, G. A. Ten Eyck, J. R. Wendt, T. Pluym, J. K. Gamble, M. P. Lilly, M. Pioro-Ladrière, and M. S. Carroll. Coherent coupling between a quantum dot and a donor in silicon. *Nature Communications*, 8(1), Dec. 2017.
- [90] J. Hauss, A. Fedorov, C. Hutter, A. Shnirman, and G. Schön. Single-Qubit Lasing and Cooling at the Rabi Frequency. *Physical Review Letters*, 100(3):037003, Jan. 2008.
- [91] T. Hayashi, T. Fujisawa, H. D. Cheong, Y. H. Jeong, and Y. Hirayama. Coherent Manipulation of Electronic States in a Double Quantum Dot. *Physical Review Letters*, 91(22), Nov. 2003.
- [92] R. R. Hayes, A. A. Kiselev, M. G. Borselli, S. S. Bui, E. T. Croke III, P. W. Deelman, B. M. Maune, I. Milosavljevic, J.-S. Moon, and R. S. Ross. Lifetime measurements (T1) of electron spins in Si/SiGe quantum dots. *arXiv preprint arXiv:0908.0173*, Aug. 2009. arXiv: 0908.0173.
- [93] Y. He, S. K. Gorman, D. Keith, L. Kranz, J. G. Keizer, and M. Y. Simmons. A two-qubit gate between phosphorus donor electrons in silicon. *Nature*, 571(7765):371–375, July 2019.
- [94] T. Heinosaari and M. Ziman. Guide to mathematical concepts of quantum theory. *Acta Physica Slovaca*, 58(4):487–674, 2008.
- [95] N. W. Hendrickx, D. P. Franke, A. Sammak, G. Scappucci, and M. Veldhorst. Fast two-qubit logic with holes in germanium. *Nature*, 577(7791):487–491, Jan. 2020.
- [96] N. W. Hendrickx, W. I. L. Lawrie, L. Petit, A. Sammak, G. Scappucci, and M. Veldhorst. A single-hole spin qubit. *Nature Communications*, 11(1):3478, Dec. 2020.
- [97] N. W. Hendrickx, W. I. L. Lawrie, M. Russ, F. van Riggelen, S. L. de Snoo, R. N. Schouten, A. Sammak, G. Scappucci, and M. Veldhorst. A four-qubit germanium quantum processor. *Nature*, 591(7851):580–585, Mar. 2021.
- [98] B. Hensen, W. Wei Huang, C.-H. Yang, K. Wai Chan,

- J. Yoneda, T. Tanttu, F. E. Hudson, A. Laucht, K. M. Itoh, T. D. Ladd, A. Morello, and A. S. Dzurak. A silicon quantum-dot-coupled nuclear spin qubit. *Nature Nanotechnology*, Dec. 2019.
- [99] A. P. Higginbotham, F. Kuemmeth, M. P. Hanson, A. C. Gossard, and C. M. Marcus. Coherent Operations and Screening in Multielectron Spin Qubits. *Physical Review Letters*, 112(2):026801, Jan. 2014.
- [100] A. P. Higginbotham, T. W. Larsen, J. Yao, H. Yan, C. M. Lieber, C. M. Marcus, and F. Kuemmeth. Hole Spin Coherence in a Ge/Si Heterostructure Nanowire. *Nano Letters*, 14(6):3582–3586, June 2014.
- [101] A. Hofmann, V. F. Maisi, T. Krähenmann, C. Reichl, W. Wegscheider, K. Ensslin, and T. Ihn. Anisotropy and Suppression of Spin-Orbit Interaction in a GaAs Double Quantum Dot. *Physical Review Letters*, 119(17), Oct. 2017.
- [102] A. Hollmann, T. Struck, V. Langrock, A. Schmidbauer, F. Schauer, T. Leonhardt, K. Sawano, H. Riemann, N. V. Abrosimov, D. Bougeard, and L. R. Schreiber. Large, Tunable Valley Splitting and Single-Spin Relaxation Mechanisms in a Si / Si x Ge 1 - x Quantum Dot. *Physical Review Applied*, 13(3):034068, Mar. 2020.
- [103] W. Huang, C. H. Yang, K. W. Chan, T. Tanttu, B. Hensen, R. C. C. Leon, M. A. Fogarty, J. C. C. Hwang, F. E. Hudson, K. M. Itoh, A. Morello, A. Laucht, and A. S. Dzurak. Fidelity benchmarks for two-qubit gates in silicon. *Nature*, 569(7757):532–536, May 2019.
- [104] D. J. Ibberson, T. Lundberg, J. A. Haigh, L. Hutin, B. Bertrand, S. Barraud, C.-M. Lee, N. A. Stelmashenko, G. A. Oakes, L. Cochrane, J. W. Robinson, M. Vinet, M. F. Gonzalez-Zalba, and L. A. Ibberson. Large Dispersive Interaction between a CMOS Double Quantum Dot and Microwave Photons. *PRX Quantum*, 2(2):020315, May 2021.
- [105] G. Ithier, E. Collin, P. Joyez, P. J. Meeson, D. Vion, D. Esteve, F. Chiarello, A. Shnirman, Y. Makhlin, J. Schriefl, and G. Schön. Decoherence in a superconducting quantum bit circuit. *Physical Review B*, 72(13), Oct. 2005.
- [106] T. Ito, T. Otsuka, S. Amaha, M. R. Delbecq, T. Nakajima, J. Yoneda, K. Takeda, G. Allison, A. Noiri, K. Kawasaki, and S. Tarucha. Detection and control of charge states in a quintuple quantum dot. *Scientific Reports*, 6(1), Dec. 2016.
- [107] T. Ito, T. Otsuka, T. Nakajima, M. R. Delbecq, S. Amaha, J. Yoneda, K. Takeda, A. Noiri, G. Allison, A. Ludwig, A. D. Wieck, and S. Tarucha. Four single-spin Rabi oscillations in a quadruple quantum dot. *Applied Physics Letters*, 113(9):093102, Aug. 2018.
- [108] B. Jadot, P.-A. Mortemousque, E. Chanrion, V. Thiney, A. Ludwig, A. D. Wieck, M. Urdampilleta, C. Bäuerle, and T. Meunier. Distant spin entanglement via fast and coherent electron shuttling. *Nature Nanotechnology*, 16(5):570–575, May 2021.
- [109] W. Jang, M.-K. Cho, H. Jang, J. Kim, J. Park, G. Kim, B. Kang, H. Jung, V. Umansky, and D. Kim. Single-Shot Readout of a Driven Hybrid Qubit in a GaAs Double Quantum Dot. *Nano Letters*, 21(12):4999–5005, June 2021.
- [110] W. Jang, M.-K. Cho, J. Kim, H. Chung, V. Umansky, and D. Kim. Individual two-axis control of three singlet-triplet qubits in a micromagnet integrated quantum dot array. *Applied Physics Letters*, 117(23):234001, Dec. 2020.
- [111] W. Jang, J. Kim, M.-K. Cho, H. Chung, S. Park, J. Eom, V. Umansky, Y. Chung, and D. Kim. Robust energy-selective tunneling readout of singlet-triplet qubits under large magnetic field gradient. *npj Quantum Information*, 6(1), Dec. 2020.
- [112] D. Jirovec, A. Hofmann, A. Ballabio, P. M. Mutter, G. Tavani, M. Botifoll, A. Crippa, J. Kukucka, O. Sagi, F. Martins, J. Saez-Mollejo, I. Prieto, M. Borovkov, J. Arbiol, D. Chrastina, G. Isella, and G. Katsaros. A singlet-triplet hole spin qubit in planar Ge. *Nature Materials*, 20(8):1106–1112, Aug. 2021.
- [113] R. M. Jock, N. T. Jacobson, P. Harvey-Collard, A. M. Mounce, V. Srinivasa, D. R. Ward, J. Anderson, R. Manginell, J. R. Wendt, M. Rudolph, T. Pluym, J. K. Gamble, A. D. Baczewski, W. M. Witzel, and M. S. Carroll. A silicon metal-oxide-semiconductor electron spin-orbit qubit. *Nature Communications*, 9(1), Dec. 2018.
- [114] R. M. Jock, N. T. Jacobson, M. Rudolph, D. R. Ward, M. S. Carroll, and D. R. Luhman. A silicon singlet-triplet qubit driven by spin-valley coupling. *arXiv:2102.12068 [cond-mat, physics:quant-ph]*, Feb. 2021. arXiv: 2102.12068.
- [115] A. C. Johnson, J. R. Petta, J. M. Taylor, A. Yacoby, M. D. Lukin, C. M. Marcus, M. P. Hanson, and A. C. Gossard. Triplet–singlet spin relaxation via nuclei in a double quantum dot. *Nature*, 435(7044):925–928, June 2005.
- [116] M. A. I. Johnson, M. T. Mądzik, F. E. Hudson, K. M. Itoh, A. M. Jakob, D. N. Jamieson, A. Dzurak, and A. Morello. Beating the thermal limit of qubit initialization with a Bayesian ‘Maxwell’s demon’. *arXiv:2110.02046 [cond-mat, physics:quant-ph]*, Oct. 2021. arXiv: 2110.02046.
- [117] A. Jones, E. Pritchett, E. Chen, T. Keating, R. Andrews, J. Blumoff, L. De Lorenzo, K. Eng, S. Ha, A. Kiselev, S. Meenehan, S. Merkel, J. Wright, L. Edge, R. Ross, M. Rakher, M. Borselli, and A. Hunter. Spin-Blockade Spectroscopy of Si / Si - Ge Quantum Dots. *Physical Review Applied*, 12(1):014026, July 2019.
- [118] R. Jozsa. Fidelity for Mixed Quantum States. *Journal of Modern Optics*, 41(12):2315–2323, Dec. 1994.
- [119] Y. P. Kandel, H. Qiao, S. Fallahi, G. C. Gardner, M. J. Manfra, and J. M. Nichol. Coherent spin-state transfer via Heisenberg exchange. *Nature*, 573(7775):553–557, Sept. 2019.
- [120] Y. P. Kandel, H. Qiao, S. Fallahi, G. C. Gardner, M. J. Manfra, and J. M. Nichol. Adiabatic quantum state transfer in a semiconductor quantum-dot spin chain. *Nature Communications*, 12(1):2156, Dec. 2021.
- [121] B. E. Kane. A silicon-based nuclear spin quantum computer. *Nature*, 393(6681):133–137, May 1998.
- [122] E. Kawakami, T. Jullien, P. Scarlino, D. R. Ward, D. E. Savage, M. G. Lagally, V. V. Dobrovitski, M. Friesen, S. N. Coppersmith, M. A. Eriksson, and L. M. K. Vandersypen. Gate fidelity and coherence of an electron spin in an Si/SiGe quantum dot with micromagnet. *Proceedings of the National Academy of Sciences*, 113(42):11738–11743, Oct. 2016.
- [123] E. Kawakami, P. Scarlino, D. R. Ward, F. R. Braakman, D. E. Savage, M. G. Lagally, M. Friesen, S. N. Coppersmith, M. A. Eriksson, and L. M. K. Vandersypen. Electrical control of a long-lived spin qubit in a Si/SiGe quantum dot. *Nature Nanotechnology*, 9(9):666–670, Aug. 2014.
- [124] D. Keith, M. G. House, M. B. Donnelly, T. F. Watson, B. Weber, and M. Y. Simmons. Single-Shot Spin Readout in Semiconductors Near the Shot-Noise Sensitivity Limit. *Physical Review X*, 9(4):041003, Oct. 2019.
- [125] J. Kerckhoff, B. Sun, B. Fong, C. Jones, A. Kiselev, D. Barnes, R. Noah, E. Acuna, M. Akmal, S. Ha, J. Wright, B. Thomas, C. Jackson, L. Edge, K. Eng, R. Ross, and T. Ladd. Magnetic Gradient Fluctuations from Quadrupolar 73 Ge in Si / Si Ge Exchange-Only Qubits. *PRX Quantum*, 2(1):010347, Mar. 2021.
- [126] A. V. Khaetskii, D. Loss, and L. Glazman. Electron Spin Decoherence in Quantum Dots due to Interaction with Nuclei. *Phys-*

- ical Review Letters*, 88(18), Apr. 2002.
- [127] D. Kim, Z. Shi, C. B. Simmons, D. R. Ward, J. R. Prance, T. S. Koh, J. K. Gamble, D. E. Savage, M. G. Lagally, M. Friesen, S. N. Coppersmith, and M. A. Eriksson. Quantum control and process tomography of a semiconductor quantum dot hybrid qubit. *Nature*, 511(7507):70–74, July 2014.
- [128] D. Kim, D. R. Ward, C. B. Simmons, J. K. Gamble, R. Blume-Kohout, E. Nielsen, D. E. Savage, M. G. Lagally, M. Friesen, S. N. Coppersmith, and M. A. Eriksson. Microwave-driven coherent operation of a semiconductor quantum dot charge qubit. *Nature Nanotechnology*, 10(3):243–247, Mar. 2015.
- [129] D. Kim, D. R. Ward, C. B. Simmons, D. E. Savage, M. G. Lagally, M. Friesen, S. N. Coppersmith, and M. A. Eriksson. High-fidelity resonant gating of a silicon-based quantum dot hybrid qubit. *npj Quantum Information*, 1(1):15004, Dec. 2015.
- [130] H. Kiyama, T. Nakajima, S. Teraoka, A. Oiwa, and S. Tarucha. Single-Shot Ternary Readout of Two-Electron Spin States in a Quantum Dot Using Spin Filtering by Quantum Hall Edge States. *Physical Review Letters*, 117(23), Nov. 2016.
- [131] C. Kloeffel and D. Loss. Prospects for Spin-Based Quantum Computing in Quantum Dots. *Annual Review of Condensed Matter Physics*, 4(1):51–81, Apr. 2013.
- [132] T. Kobayashi, J. Salfi, C. Chua, J. van der Heijden, M. G. House, D. Culcer, W. D. Hutchison, B. C. Johnson, J. C. McCallum, H. Riemann, N. V. Abrosimov, P. Becker, H.-J. Pohl, M. Y. Simmons, and S. Rogge. Engineering long spin coherence times of spin-orbit qubits in silicon. *Nature Materials*, 20(1):38–42, Jan. 2021.
- [133] Y. Kojima, T. Nakajima, A. Noiri, J. Yoneda, T. Otsuka, K. Takeda, S. Li, S. D. Bartlett, A. Ludwig, A. D. Wieck, and S. Tarucha. Probabilistic teleportation of a quantum dot spin qubit. *npj Quantum Information*, 7(1):68, Dec. 2021.
- [134] F. H. L. Koppens. Control and Detection of Singlet-Triplet Mixing in a Random Nuclear Field. *Science*, 309(5739):1346–1350, Aug. 2005.
- [135] F. H. L. Koppens, C. Buizert, K. J. Tielrooij, I. T. Vink, K. C. Nowack, T. Meunier, L. P. Kouwenhoven, and L. M. K. Vandersypen. Driven coherent oscillations of a single electron spin in a quantum dot. *Nature*, 442(7104):766–771, Aug. 2006.
- [136] F. H. L. Koppens, D. Klauser, W. A. Coish, K. C. Nowack, L. P. Kouwenhoven, D. Loss, and L. M. K. Vandersypen. Universal Phase Shift and Nonexponential Decay of Driven Single-Spin Oscillations. *Physical Review Letters*, 99(10), Sept. 2007.
- [137] F. H. L. Koppens, K. C. Nowack, and L. M. K. Vandersypen. Spin Echo of a Single Electron Spin in a Quantum Dot. *Physical Review Letters*, 100(23), June 2008.
- [138] J. V. Koski, A. J. Landig, M. Russ, J. C. Abadillo-Uriel, P. Scarlino, B. Kratochwil, C. Reichl, W. Wegscheider, G. Burkard, M. Friesen, S. N. Coppersmith, A. Wallraff, K. Ensslin, and T. Ihn. Strong photon coupling to the quadrupole moment of an electron in a solid-state qubit. *Nature Physics*, 16(6):642–646, June 2020.
- [139] B. Kratochwil, J. V. Koski, A. J. Landig, P. Scarlino, J. C. Abadillo-Uriel, C. Reichl, S. N. Coppersmith, W. Wegscheider, M. Friesen, A. Wallraff, T. Ihn, and K. Ensslin. Charge qubit in a triple quantum dot with tunable coherence. *Physical Review Research*, 3(1):013171, Feb. 2021.
- [140] F. Kuemmeth and H. Bluhm. Roadmap for gallium arsenide spin qubits. *arXiv:2011.13907 [cond-mat, physics:quant-ph]*, Nov. 2020. arXiv: 2011.13907.
- [141] I. Kulesh, C. T. Ke, C. Thomas, S. Karwal, C. M. Moehle, S. Metti, R. Kallaher, G. C. Gardner, M. J. Manfra, and S. Goswami. Quantum Dots in an In Sb Two-Dimensional Electron Gas. *Physical Review Applied*, 13(4):041003, Apr. 2020.
- [142] E. A. Laird, C. Barthel, E. I. Rashba, C. M. Marcus, M. P. Hanson, and A. C. Gossard. Hyperfine-Mediated Gate-Driven Electron Spin Resonance. *Physical Review Letters*, 99(24), Dec. 2007.
- [143] E. A. Laird, F. Pei, and L. P. Kouwenhoven. A valley–spin qubit in a carbon nanotube. *Nature Nanotechnology*, 8(8):565–568, Aug. 2013.
- [144] E. A. Laird, J. R. Petta, A. C. Johnson, C. M. Marcus, A. Yacoby, M. P. Hanson, and A. C. Gossard. Effect of Exchange Interaction on Spin Dephasing in a Double Quantum Dot. *Physical Review Letters*, 97(5), July 2006.
- [145] E. A. Laird, J. M. Taylor, D. P. DiVincenzo, C. M. Marcus, M. P. Hanson, and A. C. Gossard. Coherent spin manipulation in an exchange-only qubit. *Physical Review B*, 82(7), Aug. 2010.
- [146] A. J. Landig, J. V. Koski, P. Scarlino, U. C. Mendes, A. Blais, C. Reichl, W. Wegscheider, A. Wallraff, K. Ensslin, and T. Ihn. Coherent spin–photon coupling using a resonant exchange qubit. *Nature*, 560(7717):179–184, Aug. 2018.
- [147] A. J. Landig, J. V. Koski, P. Scarlino, C. Müller, J. C. Abadillo-Uriel, B. Kratochwil, C. Reichl, W. Wegscheider, S. N. Coppersmith, M. Friesen, A. Wallraff, T. Ihn, and K. Ensslin. Virtual-photon-mediated spin-qubit–transmon coupling. *Nature Communications*, 10(1):5037, Dec. 2019.
- [148] A. J. Landig, J. V. Koski, P. Scarlino, C. Reichl, W. Wegscheider, A. Wallraff, K. Ensslin, and T. Ihn. Microwave-Cavity-Detected Spin Blockade in a Few-Electron Double Quantum Dot. *Physical Review Letters*, 122(21):213601, May 2019.
- [149] A. Laucht, R. Kalra, S. Simmons, J. P. Dehollain, J. T. Muhonen, F. A. Mohiyaddin, S. Freer, F. E. Hudson, K. M. Itoh, D. N. Jamieson, J. C. McCallum, A. S. Dzurak, and A. Morello. A dressed spin qubit in silicon. *Nature Nanotechnology*, 12(1):61–66, Oct. 2016.
- [150] A. Laucht, J. T. Muhonen, F. A. Mohiyaddin, R. Kalra, J. P. Dehollain, S. Freer, F. E. Hudson, M. Veldhorst, R. Rahman, G. Klimeck, K. M. Itoh, D. N. Jamieson, J. C. McCallum, A. S. Dzurak, and A. Morello. Electrically controlling single-spin qubits in a continuous microwave field. *Science Advances*, 1(3):e1500022–e1500022, Apr. 2015.
- [151] W. I. L. Lawrie, H. G. J. Eenink, N. W. Hendrickx, J. M. Boter, L. Petit, S. V. Amitonov, M. Lodari, B. Paquelet Wuetz, C. Volk, S. G. J. Philips, G. Droulers, N. Kalhor, F. van Riggelen, D. Brousse, A. Sammak, L. M. K. Vandersypen, G. Scappucci, and M. Veldhorst. Quantum dot arrays in silicon and germanium. *Applied Physics Letters*, 116(8):080501, Feb. 2020.
- [152] W. I. L. Lawrie, N. W. Hendrickx, F. van Riggelen, M. Russ, L. Petit, A. Sammak, G. Scappucci, and M. Veldhorst. Spin relaxation benchmarks and individual qubit addressability for holes in quantum dots. *Nano Letters*, page acs.nanolett.0c02589, Aug. 2020. arXiv: 2006.12563.
- [153] W. I. L. Lawrie, M. Russ, F. van Riggelen, N. W. Hendrickx, S. L. de Snoo, A. Sammak, G. Scappucci, and M. Veldhorst. Simultaneous driving of semiconductor spin qubits at the fault-tolerant threshold. *arXiv:2109.07837 [cond-mat]*, Sept. 2021. arXiv: 2109.07837.
- [154] R. C. C. Leon, C. H. Yang, J. C. C. Hwang, J. Camirand Lemyre, T. Tanttu, W. Huang, J. Y. Huang, F. E. Hudson, K. M. Itoh, A. Laucht, M. Piñor-Ladrière, A. Saraiva, and A. S. Dzurak. Bell-state tomography in a silicon many-electron artificial molecule. *Nature Communications*, 12(1):3228, Dec. 2021.
- [155] R. C. C. Leon, C. H. Yang, J. C. C. Hwang, J. C. Lemyre, T. Tanttu, W. Huang, K. W. Chan, K. Y. Tan, F. E. Hud-

- son, K. M. Itoh, A. Morello, A. Laucht, M. Pioro-Ladrière, A. Saraiva, and A. S. Dzurak. Coherent spin control of s-, p-, d- and f-electrons in a silicon quantum dot. *Nature Communications*, 11(1):797, Dec. 2020.
- [156] J. Levy. Universal Quantum Computation with Spin- 1 / 2 Pairs and Heisenberg Exchange. *Physical Review Letters*, 89(14), Sept. 2002.
- [157] H.-O. Li, G. Cao, G.-D. Yu, M. Xiao, G.-C. Guo, H.-W. Jiang, and G.-P. Guo. Conditional rotation of two strongly coupled semiconductor charge qubits. *Nature Communications*, 6(1), Dec. 2015.
- [158] Y.-Y. Liu, L. Orona, S. F. Neyens, E. MacQuarrie, M. Eriksson, and A. Yacoby. Magnetic-Gradient-Free Two-Axis Control of a Valley Spin Qubit in Si x Ge 1 - x. *Physical Review Applied*, 16(2):024029, Aug. 2021.
- [159] D. Loss and D. P. DiVincenzo. Quantum computation with quantum dots. *Physical Review A*, 57(1):120–126, Jan. 1998.
- [160] T. Lundberg, J. Li, L. Hutin, B. Bertrand, D. J. Ibberson, C.-M. Lee, D. J. Niegemann, M. Urdampilleta, N. Stelmashenko, T. Meunier, J. W. A. Robinson, L. Iberson, M. Vinet, Y.-M. Niquet, and M. F. Gonzalez-Zalba. Spin Quintet in a Silicon Double Quantum Dot: Spin Blockade and Relaxation. *Physical Review X*, 10(4):041010, Oct. 2020.
- [161] E. R. MacQuarrie, S. F. Neyens, J. P. Dodson, J. Corrigan, B. Thorgrimsson, N. Holman, M. Palma, L. F. Edge, M. Friesen, S. N. Coppersmith, and M. A. Eriksson. Progress toward a capacitively mediated CNOT between two charge qubits in Si/SiGe. *npj Quantum Information*, 6(1):81, Dec. 2020.
- [162] M. T. Mądzik, S. Asaad, A. Youssry, B. Joecker, K. M. Rudinger, E. Nielsen, K. C. Young, T. J. Proctor, A. D. Baczewski, A. Laucht, V. Schmitt, F. E. Hudson, K. M. Itoh, A. M. Jakob, B. C. Johnson, D. N. Jamieson, A. S. Dzurak, C. Ferrie, R. Blume-Kohout, and A. Morello. Precision tomography of a three-qubit electron-nuclear quantum processor in silicon. *arXiv:2106.03082 [cond-mat, physics:quant-ph]*, July 2021. arXiv: 2106.03082.
- [163] M. T. Mądzik, T. D. Ladd, F. E. Hudson, K. M. Itoh, A. M. Jakob, B. C. Johnson, J. C. McCallum, D. N. Jamieson, A. S. Dzurak, A. Laucht, and A. Morello. Controllable freezing of the nuclear spin bath in a single-atom spin qubit. *Science Advances*, 6(27):eaba3442, July 2020.
- [164] M. T. Mądzik, A. Laucht, F. E. Hudson, A. M. Jakob, B. C. Johnson, D. N. Jamieson, K. M. Itoh, A. S. Dzurak, and A. Morello. Conditional quantum operation of two exchange-coupled single-donor spin qubits in a MOS-compatible silicon device. *Nature Communications*, 12(1):181, Dec. 2021.
- [165] E. Magesan, J. M. Gambetta, and J. Emerson. Characterizing quantum gates via randomized benchmarking. *Physical Review A*, 85(4):042311, Apr. 2012.
- [166] E. Magesan, J. M. Gambetta, B. R. Johnson, C. A. Ryan, J. M. Chow, S. T. Merkel, M. P. da Silva, G. A. Keefe, M. B. Rothwell, T. A. Ohki, M. B. Ketchen, and M. Steffen. Efficient Measurement of Quantum Gate Error by Interleaved Randomized Benchmarking. *Physical Review Letters*, 109(8):080505, Aug. 2012.
- [167] F. K. Malinowski, F. Martins, Ł. Cywiński, M. S. Rudner, P. D. Nissen, S. Fallahi, G. C. Gardner, M. J. Manfra, C. M. Marcus, and F. Kuemmeth. Spectrum of the Nuclear Environment for GaAs Spin Qubits. *Physical Review Letters*, 118(17):177702, Apr. 2017.
- [168] F. K. Malinowski, F. Martins, P. D. Nissen, E. Barnes, Ł. Cywiński, M. S. Rudner, S. Fallahi, G. C. Gardner, M. J. Manfra, C. M. Marcus, and F. Kuemmeth. Notch filtering the nuclear environment of a spin qubit. *Nature Nanotechnology*, 12(1):16–20, Oct. 2016.
- [169] F. K. Malinowski, F. Martins, P. D. Nissen, S. Fallahi, G. C. Gardner, M. J. Manfra, C. M. Marcus, and F. Kuemmeth. Symmetric operation of the resonant exchange qubit. *Physical Review B*, 96(4), July 2017.
- [170] F. K. Malinowski, F. Martins, T. B. Smith, S. D. Bartlett, A. C. Doherty, P. D. Nissen, S. Fallahi, G. C. Gardner, M. J. Manfra, C. M. Marcus, and F. Kuemmeth. Fast spin exchange across a multielectron mediator. *Nature Communications*, 10(1):1196, Dec. 2019.
- [171] F. Martins, F. K. Malinowski, P. D. Nissen, E. Barnes, S. Fallahi, G. C. Gardner, M. J. Manfra, C. M. Marcus, and F. Kuemmeth. Noise Suppression Using Symmetric Exchange Gates in Spin Qubits. *Physical Review Letters*, 116(11), Mar. 2016.
- [172] M. Marx, J. Yoneda, T. Otsuka, K. Takeda, Y. Yamaoka, T. Nakajima, S. Li, A. Noiri, T. Kodera, and S. Tarucha. Spin-orbit assisted spin funnels in DC transport through a physically defined pMOS double quantum dot. *Japanese Journal of Applied Physics*, 58(SB):SBBI07, Apr. 2019.
- [173] B. M. Maune, M. G. Borselli, B. Huang, T. D. Ladd, P. W. Deelman, K. S. Holabird, A. A. Kiselev, I. Alvarado-Rodriguez, R. S. Ross, A. E. Schmitz, M. Sokolich, C. A. Watson, M. F. Gyure, and A. T. Hunter. Coherent singlet-triplet oscillations in a silicon-based double quantum dot. *Nature*, 481(7381):344–347, Jan. 2012.
- [174] R. Maurand, X. Jehl, D. Kotekar-Patil, A. Corna, H. Bohuslavskyi, R. Laviéville, L. Hutin, S. Barraud, M. Vinet, M. Sanquer, and S. De Franceschi. A CMOS silicon spin qubit. *Nature Communications*, 7:13575, Nov. 2016.
- [175] J. Medford, J. Beil, J. M. Taylor, S. D. Bartlett, A. C. Doherty, E. I. Rashba, D. P. DiVincenzo, H. Lu, A. C. Gossard, and C. M. Marcus. Self-consistent measurement and state tomography of an exchange-only spin qubit. *Nature Nanotechnology*, 8(9):654–659, Sept. 2013.
- [176] J. Medford, J. Beil, J. M. Taylor, E. I. Rashba, H. Lu, A. C. Gossard, and C. M. Marcus. Quantum-Dot-Based Resonant Exchange Qubit. *Physical Review Letters*, 111(5), July 2013.
- [177] J. Medford, Ł. Cywiński, C. Barthel, C. M. Marcus, M. P. Hanson, and A. C. Gossard. Scaling of Dynamical Decoupling for Spin Qubits. *Physical Review Letters*, 108(8), Feb. 2012.
- [178] I. A. Merkulov, A. L. Efros, and M. Rosen. Electron spin relaxation by nuclei in semiconductor quantum dots. *Physical Review B*, 65(20), Apr. 2002.
- [179] T. Meunier, K.-J. Tielrooij, I. T. Vink, F. H. L. Koppens, H. P. Tranitz, W. Wegscheider, L. P. Kouwenhoven, and L. M. K. Vandersypen. High fidelity measurement of singlet-triplet state in a quantum dot. *physica status solidi (b)*, 243(15):3855–3858, Dec. 2006.
- [180] T. Meunier, I. T. Vink, L. H. W. van Beveren, K.-J. Tielrooij, R. Hanson, F. H. L. Koppens, H. P. Tranitz, W. Wegscheider, L. P. Kouwenhoven, and L. M. K. Vandersypen. Experimental Signature of Phonon-Mediated Spin Relaxation in a Two-Electron Quantum Dot. *Physical Review Letters*, 98(12), Mar. 2007.
- [181] T. Meunier, I. T. Vink, L. H. Willems van Beveren, F. H. L. Koppens, H. P. Tranitz, W. Wegscheider, L. P. Kouwenhoven, and L. M. K. Vandersypen. Nondestructive measurement of electron spins in a quantum dot. *Physical Review B*, 74(19), Nov. 2006.
- [182] X. Mi, M. Benito, S. Putz, D. M. Zajac, J. M. Taylor, G. Burkard, and J. R. Petta. A coherent spin-photon interface in silicon. *Nature*, 555(7698):599–603, Feb. 2018.
- [183] X. Mi, J. V. Cady, D. M. Zajac, P. W. Deelman, and J. R. Petta.

- Strong coupling of a single electron in silicon to a microwave photon. *Science*, 355(6321):156–158, Jan. 2017.
- [184] X. Mi, J. V. Cady, D. M. Zajac, J. Stehlík, L. F. Edge, and J. R. Petta. Circuit quantum electrodynamics architecture for gate-defined quantum dots in silicon. *Applied Physics Letters*, 110(4):043502, Jan. 2017.
- [185] A. R. Mills, D. M. Zajac, M. J. Gullans, F. J. Schupp, T. M. Hazard, and J. R. Petta. Shuttling a single charge across a one-dimensional array of silicon quantum dots. *Nature Communications*, 10(1), Dec. 2019.
- [186] A. Morello, J. J. Pla, F. A. Zwanenburg, K. W. Chan, K. Y. Tan, H. Huebl, M. Möttönen, C. D. Nugroho, C. Yang, J. A. van Donkelaar, A. D. C. Alves, D. N. Jamieson, C. C. Escott, L. C. L. Hollenberg, R. G. Clark, and A. S. Dzurak. Single-shot readout of an electron spin in silicon. *Nature*, 467(7316):687–691, Oct. 2010.
- [187] P.-A. Mortemousque, E. Chanrion, B. Jadot, H. Flentje, A. Ludwig, A. D. Wieck, M. Urdampilleta, C. Bäuerle, and T. Meunier. Coherent control of individual electron spins in a two-dimensional quantum dot array. *Nature Nanotechnology*, Dec. 2020.
- [188] P.-A. Mortemousque, B. Jadot, E. Chanrion, V. Thiney, C. Bäuerle, A. Ludwig, A. D. Wieck, M. Urdampilleta, and T. Meunier. Enhanced Spin Coherence while Displacing Electron in a Two-Dimensional Array of Quantum Dots. *PRX Quantum*, 2(3):030331, Aug. 2021.
- [189] J. T. Muhonen, J. P. Dehollain, A. Laucht, F. E. Hudson, R. Kalra, T. Sekiguchi, K. M. Itoh, D. N. Jamieson, J. C. McCallum, A. S. Dzurak, and A. Morello. Storing quantum information for 30 seconds in a nanoelectronic device. *Nature Nanotechnology*, 9(12):986–991, Oct. 2014.
- [190] J. T. Muhonen, A. Laucht, S. Simmons, J. P. Dehollain, R. Kalra, F. E. Hudson, S. Freer, K. M. Itoh, D. N. Jamieson, J. C. McCallum, A. S. Dzurak, and A. Morello. Quantifying the quantum gate fidelity of single-atom spin qubits in silicon by randomized benchmarking. *Journal of Physics: Condensed Matter*, 27(15):154205, Apr. 2015.
- [191] U. Mukhopadhyay, J. P. Dehollain, C. Reichl, W. Wegscheider, and L. M. K. Vandersypen. A 2x2 quantum dot array with controllable inter-dot tunnel couplings. *Applied Physics Letters*, 112(18):183505, Apr. 2018. arXiv: 1802.05446.
- [192] S. Nadj-Perge, S. M. Frolov, E. P. A. M. Bakkers, and L. P. Kouwenhoven. Spin-orbit qubit in a semiconductor nanowire. *Nature*, 468(7327):1084–1087, Dec. 2010.
- [193] T. Nakajima, M. R. Delbecq, T. Otsuka, P. Stano, S. Amaha, J. Yoneda, A. Noiri, K. Kawasaki, K. Takeda, G. Allison, A. Ludwig, A. D. Wieck, D. Loss, and S. Tarucha. Robust Single-Shot Spin Measurement with 99.5% Fidelity in a Quantum Dot Array. *Physical Review Letters*, 119(1):017701, July 2017.
- [194] T. Nakajima, A. Noiri, K. Kawasaki, J. Yoneda, P. Stano, S. Amaha, T. Otsuka, K. Takeda, M. R. Delbecq, G. Allison, A. Ludwig, A. D. Wieck, D. Loss, and S. Tarucha. Coherence of a Driven Electron Spin Qubit Actively Decoupled from Quasistatic Noise. *Physical Review X*, 10(1):011060, Mar. 2020.
- [195] T. Nakajima, A. Noiri, J. Yoneda, M. R. Delbecq, P. Stano, T. Otsuka, K. Takeda, S. Amaha, G. Allison, K. Kawasaki, A. Ludwig, A. D. Wieck, D. Loss, and S. Tarucha. Quantum non-demolition measurement of an electron spin qubit. *Nature Nanotechnology*, 14(6):555–560, June 2019.
- [196] J. M. Nichol, L. A. Orona, S. P. Harvey, S. Fallahi, G. C. Gardner, M. J. Manfra, and A. Yacoby. High-fidelity entangling gate for double-quantum-dot spin qubits. *npj Quantum Information*, 3(1), Dec. 2017.
- [197] A. Noiri, T. Nakajima, J. Yoneda, M. R. Delbecq, P. Stano, T. Otsuka, K. Takeda, S. Amaha, G. Allison, K. Kawasaki, Y. Kojima, A. Ludwig, A. D. Wieck, D. Loss, and S. Tarucha. A fast quantum interface between different spin qubit encodings. *Nature Communications*, 9(1):5066, Dec. 2018.
- [198] A. Noiri, T. Takakura, T. Obata, T. Otsuka, T. Nakajima, J. Yoneda, and S. Tarucha. Cotunneling spin blockade observed in a three-terminal triple quantum dot. *Physical Review B*, 96(15):155414, Oct. 2017.
- [199] A. Noiri, K. Takeda, T. Nakajima, T. Kobayashi, A. Sammak, G. Scappucci, and S. Tarucha. Fast universal quantum control above the fault-tolerance threshold in silicon. *arXiv:2108.02626 [cond-mat, physics:quant-ph]*, Aug. 2021. arXiv: 2108.02626.
- [200] A. Noiri, K. Takeda, J. Yoneda, T. Nakajima, T. Kodera, and S. Tarucha. Radio-Frequency-Detected Fast Charge Sensing in Undoped Silicon Quantum Dots. *Nano Letters*, page acs.nanolett.9b03847, Jan. 2020.
- [201] A. Noiri, J. Yoneda, T. Nakajima, T. Otsuka, M. R. Delbecq, K. Takeda, S. Amaha, G. Allison, A. Ludwig, A. D. Wieck, and others. Coherent electron-spin-resonance manipulation of three individual spins in a triple quantum dot. *Applied Physics Letters*, 108(15):153101, Apr. 2016.
- [202] K. C. Nowack, F. H. L. Koppens, Y. V. Nazarov, and L. M. K. Vandersypen. Coherent Control of a Single Electron Spin with Electric Fields. *Science*, 318(5855):1430–1433, Nov. 2007.
- [203] K. C. Nowack, M. Shafiei, M. Laforest, G. E. D. K. Prawiroatmodjo, L. R. Schreiber, C. Reichl, W. Wegscheider, and L. M. K. Vandersypen. Single-Shot Correlations and Two-Qubit Gate of Solid-State Spins. *Science*, 333(6047):1269–1272, Sept. 2011.
- [204] A. Oiwa, T. Fujita, H. Kiyama, G. Allison, A. Ludwig, A. D. Wieck, and S. Tarucha. Conversion from Single Photon to Single Electron Spin Using Electrically Controllable Quantum Dots. *Journal of the Physical Society of Japan*, 86(1):011008, Jan. 2017.
- [205] K. Ono, D. G. Austing, Y. Tokura, and S. Tarucha. Current Rectification by Pauli Exclusion in a Weakly Coupled Double Quantum Dot System. *Science*, 297(5585):1313–1317, Aug. 2002.
- [206] T. OOSTERKAMP, W. VAN DER WIEL, S. DEFANCESCHI, C. Harmans, and L. KOUWENHOVEN. Photon Assisted Tunneling in Quantum Dots. *arXiv: cond-mat*, 9904359, 1999.
- [207] L. A. Orona, J. M. Nichol, S. P. Harvey, C. G. L. Böttcher, S. Fallahi, G. C. Gardner, M. J. Manfra, and A. Yacoby. Readout of singlet-triplet qubits at large magnetic field gradients. *Physical Review B*, 98(12), Sept. 2018.
- [208] T. Otsuka, T. Nakajima, M. R. Delbecq, S. Amaha, J. Yoneda, K. Takeda, G. Allison, T. Ito, R. Sugawara, A. Noiri, A. Ludwig, A. D. Wieck, and S. Tarucha. Single-electron Spin Resonance in a Quadruple Quantum Dot. *Scientific Reports*, 6(1):31820, Oct. 2016.
- [209] P. Pakkiam, A. V. Timofeev, M. G. House, M. R. Hogg, T. Kobayashi, M. Koch, S. Rogge, and M. Y. Simmons. Single-Shot Single-Gate rf Spin Readout in Silicon. *Physical Review X*, 8(4):041032, Nov. 2018.
- [210] Z. V. Penfold-Fitch, F. Sfigakis, and M. R. Buitelaar. Microwave Spectroscopy of a Carbon Nanotube Charge Qubit. *Physical Review Applied*, 7(5):054017, May 2017.
- [211] N. E. Penthorn, J. S. Schoenfield, J. D. Rooney, L. F. Edge, and H. Jiang. Two-axis quantum control of a fast valley qubit in silicon. *npj Quantum Information*, 5(1):94, Dec. 2019.
- [212] K. D. Petersson, L. W. McPaul, M. D. Schroer, M. Jung, J. M.

- Taylor, A. A. Houck, and J. R. Petta. Circuit quantum electrodynamics with a spin qubit. *Nature*, 490(7420):380–383, Oct. 2012.
- [213] K. D. Petersson, J. R. Petta, H. Lu, and A. C. Gossard. Quantum Coherence in a One-Electron Semiconductor Charge Qubit. *Physical Review Letters*, 105(24), Dec. 2010.
- [214] K. D. Petersson, C. G. Smith, D. Anderson, P. Atkinson, G. A. C. Jones, and D. A. Ritchie. Charge and Spin State Readout of a Double Quantum Dot Coupled to a Resonator. *Nano Letters*, 10(8):2789–2793, Aug. 2010.
- [215] L. Petit, J. M. Boter, H. G. J. Eenink, G. Droulers, M. L. V. Tagliaferri, R. Li, D. P. Franke, K. J. Singh, J. S. Clarke, R. N. Schouten, V. V. Dobrovitski, L. M. K. Vandersypen, and M. Veldhorst. Spin Lifetime and Charge Noise in Hot Silicon Quantum Dot Qubits. *Physical Review Letters*, 121(7), Aug. 2018.
- [216] L. Petit, H. G. J. Eenink, M. Russ, W. I. L. Lawrie, N. W. Hendrickx, S. G. J. Philips, J. S. Clarke, L. M. K. Vandersypen, and M. Veldhorst. Universal quantum logic in hot silicon qubits. *Nature*, 580(7803):355–359, Apr. 2020.
- [217] J. R. Petta, A. C. Johnson, C. M. Marcus, M. P. Hanson, and A. C. Gossard. Manipulation of a Single Charge in a Double Quantum Dot. *Physical Review Letters*, 93(18), Oct. 2004.
- [218] J. R. Petta, A. C. Johnson, J. M. Taylor, E. A. Laird, A. Yacoby, M. D. Lukin, C. M. Marcus, M. P. Hanson, and A. C. Gossard. Coherent manipulation of coupled electron spins in semiconductor quantum dots. *Science*, 309(5744):2180–2184, Sept. 2005.
- [219] J. J. Pla, K. Y. Tan, J. P. Dehollain, W. H. Lim, J. J. L. Morton, D. N. Jamieson, A. S. Dzurak, and A. Morello. A single-atom electron spin qubit in silicon. *Nature*, 489(7417):541–545, Sept. 2012.
- [220] J. R. Prance, Z. Shi, C. B. Simmons, D. E. Savage, M. G. Lagally, L. R. Schreiber, L. M. K. Vandersypen, M. Friesen, R. Joynt, S. N. Coppersmith, and M. A. Eriksson. Single-Shot Measurement of Triplet-Singlet Relaxation in a Si / SiGe Double Quantum Dot. *Physical Review Letters*, 108(4), Jan. 2012.
- [221] H. Qiao, Y. P. Kandel, K. Deng, S. Fallahi, G. C. Gardner, M. J. Manfra, E. Barnes, and J. M. Nichol. Coherent Multispin Exchange Coupling in a Quantum-Dot Spin Chain. *Physical Review X*, 10(3):031006, July 2020.
- [222] H. Qiao, Y. P. Kandel, S. Fallahi, G. C. Gardner, M. J. Manfra, X. Hu, and J. M. Nichol. Long-Distance Superexchange between Semiconductor Quantum-Dot Electron Spins. *Physical Review Letters*, 126(1):017701, Jan. 2021.
- [223] H. Qiao, Y. P. Kandel, S. K. Manikandan, A. N. Jordan, S. Fallahi, G. C. Gardner, M. J. Manfra, and J. M. Nichol. Conditional teleportation of quantum-dot spin states. *Nature Communications*, 11(1):3022, Dec. 2020.
- [224] A. G. Redfield. Nuclear Magnetic Resonance Saturation and Rotary Saturation in Solids. *Physical Review*, 98(6):1787–1809, June 1955.
- [225] M. D. Reed, B. M. Maune, R. W. Andrews, M. G. Borselli, K. Eng, M. P. Jura, A. A. Kiselev, T. D. Ladd, S. T. Merkel, I. Milosavljevic, E. J. Pritchett, M. T. Rakher, R. S. Ross, A. E. Schmitz, A. Smith, J. A. Wright, M. F. Gyure, and A. T. Hunter. Reduced Sensitivity to Charge Noise in Semiconductor Spin Qubits via Symmetric Operation. *Physical Review Letters*, 116(11), Mar. 2016.
- [226] D. J. Reilly, C. M. Marcus, M. P. Hanson, and A. C. Gossard. Fast single-charge sensing with a rf quantum point contact. *Applied Physics Letters*, 91(16):162101, Oct. 2007.
- [227] D. J. Reilly, J. M. Taylor, E. A. Laird, J. R. Petta, C. M. Marcus, M. P. Hanson, and A. C. Gossard. Measurement of Temporal Correlations of the Overhauser Field in a Double Quantum Dot. *Physical Review Letters*, 101(23), Dec. 2008.
- [228] D. J. Reilly, J. M. Taylor, J. R. Petta, C. M. Marcus, M. P. Hanson, and A. C. Gossard. Exchange Control of Nuclear Spin Diffusion in a Double Quantum Dot. *Physical Review Letters*, 104(23), June 2010.
- [229] A. Ruffino, T.-Y. Yang, J. Michniewicz, Y. Peng, E. Charbon, and M. F. Gonzalez-Zalba. Integrated multiplexed microwave readout of silicon quantum dots in a cryogenic CMOS chip. *arXiv:2101.08295 [cond-mat, physics:physics, physics:quant-ph]*, Jan. 2021. arXiv: 2101.08295.
- [230] N. Samkharadze, G. Zheng, N. Kalhor, D. Brousse, A. Sammak, U. C. Mendes, A. Blais, G. Scappucci, and L. M. K. Vandersypen. Strong spin-photon coupling in silicon. *Science*, 359(6380):1123–1127, Mar. 2018.
- [231] Y. R. Sanders, J. J. Wallman, and B. C. Sanders. Bounding quantum gate error rate based on reported average fidelity. *New Journal of Physics*, 18(1):012002, Dec. 2015.
- [232] G. Scappucci, C. Kloeffel, F. A. Zwanenburg, D. Loss, M. Myronov, J.-J. Zhang, S. De Franceschi, G. Katsaros, and M. Veldhorst. The germanium quantum information route. *arXiv:2004.08133 [cond-mat, physics:quant-ph]*, Apr. 2020. arXiv: 2004.08133.
- [233] P. Scarlino, E. Kawakami, T. Jullien, D. R. Ward, D. E. Savage, M. G. Lagally, M. Friesen, S. N. Coppersmith, M. A. Eriksson, and L. M. K. Vandersypen. Dressed photon-orbital states in a quantum dot: Intervalley spin resonance. *Physical Review B*, 95(16), Apr. 2017.
- [234] P. Scarlino, E. Kawakami, P. Stano, M. Shafiei, C. Reichl, W. Wegscheider, and L. M. K. Vandersypen. Spin-Relaxation Anisotropy in a GaAs Quantum Dot. *Physical Review Letters*, 113(25):256802, Dec. 2014.
- [235] P. Scarlino, D. J. van Woerkom, U. C. Mendes, J. V. Koski, A. J. Landig, C. K. Andersen, S. Gasparinetti, C. Reichl, W. Wegscheider, K. Ensslin, T. Ihn, A. Blais, and A. Wallraff. Coherent microwave-photon-mediated coupling between a semiconductor and a superconducting qubit. *Nature Communications*, 10(1):3011, Dec. 2019.
- [236] P. Scarlino, D. J. van Woerkom, A. Stockklauser, J. V. Koski, M. C. Collodo, S. Gasparinetti, C. Reichl, W. Wegscheider, T. Ihn, K. Ensslin, and A. Wallraff. All-Microwave Control and Dispersive Readout of Gate-Defined Quantum Dot Qubits in Circuit Quantum Electrodynamics. *Physical Review Letters*, 122(20), May 2019.
- [237] S. Schaal, I. Ahmed, J. A. Haigh, L. Hutin, B. Bertrand, S. Barraud, M. Vinet, C.-M. Lee, N. Stelmashenko, J. W. A. Robinson, J. Y. Qiu, S. Hacohen-Gourgy, I. Siddiqi, M. F. Gonzalez-Zalba, and J. J. L. Morton. Fast Gate-Based Readout of Silicon Quantum Dots Using Josephson Parametric Amplification. *Physical Review Letters*, 124(6):067701, Feb. 2020.
- [238] J. Schliemann, A. Khaetskii, and D. Loss. Electron spin dynamics in quantum dots and related nanostructures due to hyperfine interaction with nuclei. *Journal of Physics: Condensed Matter*, 15(50):R1809–R1833, Dec. 2003.
- [239] L. R. Schreiber and H. Bluhm. Quantum computation: Silicon comes back. *Nature nanotechnology*, 9(12):966, 2014.
- [240] F. J. Schupp, F. Vigneau, Y. Wen, A. Mavalankar, J. Griffiths, G. A. C. Jones, I. Farrer, D. A. Ritchie, C. G. Smith, L. C. Camenzind, L. Yu, D. M. Zumbühl, G. A. D. Briggs, N. Ares, and E. A. Laird. Sensitive radiofrequency readout of quantum dots using an ultra-low-noise SQUID amplifier. *Journal of Applied Physics*, 127(24):244503, June 2020.
- [241] A. E. Seedhouse, T. Tanttu, R. C. Leon, R. Zhao, K. Y. Tan, B. Hensen, F. E. Hudson, K. M. Itoh, J. Yoneda, C. H. Yang,

- A. Morello, A. Laucht, S. N. Coppersmith, A. Saraiva, and A. S. Dzurak. Pauli Blockade in Silicon Quantum Dots with Spin-Orbit Control. *PRX Quantum*, 2(1):010303, Jan. 2021.
- [242] M. Shafiei, K. C. Nowack, C. Reichl, W. Wegscheider, and L. M. K. Vandersypen. Resolving Spin-Orbit- and Hyperfine-Mediated Electric Dipole Spin Resonance in a Quantum Dot. *Physical Review Letters*, 110(10), Mar. 2013.
- [243] Z. Shi, C. B. Simmons, J. R. Prance, J. K. Gamble, T. S. Koh, Y.-P. Shim, X. Hu, D. E. Savage, M. G. Lagally, M. A. Eriksson, M. Friesen, and S. N. Coppersmith. Fast Hybrid Silicon Double-Quantum-Dot Qubit. *Physical Review Letters*, 108(14):140503, Apr. 2012.
- [244] Z. Shi, C. B. Simmons, D. R. Ward, J. R. Prance, R. T. Mohr, T. S. Koh, J. K. Gamble, X. Wu, D. E. Savage, M. G. Lagally, M. Friesen, S. N. Coppersmith, and M. A. Eriksson. Coherent quantum oscillations and echo measurements of a Si charge qubit. *Physical Review B*, 88(7):075416, Aug. 2013.
- [245] Z. Shi, C. B. Simmons, D. R. Ward, J. R. Prance, X. Wu, T. S. Koh, J. K. Gamble, D. E. Savage, M. G. Lagally, M. Friesen, S. N. Coppersmith, and M. A. Eriksson. Fast coherent manipulation of three-electron states in a double quantum dot. *Nature Communications*, 5, Jan. 2014.
- [246] M. D. Shulman, O. E. Dial, S. P. Harvey, H. Bluhm, V. Umansky, and A. Yacoby. Demonstration of Entanglement of Electrostatically Coupled Singlet-Triplet Qubits. *Science*, 336(6078):202–205, Apr. 2012.
- [247] M. D. Shulman, S. P. Harvey, J. M. Nichol, S. D. Bartlett, A. C. Doherty, V. Umansky, and A. Yacoby. Suppressing qubit dephasing using real-time Hamiltonian estimation. *Nature Communications*, 5:5156, Oct. 2014.
- [248] A. Sigillito, J. Loy, D. Zajac, M. Gullans, L. Edge, and J. Petta. Site-Selective Quantum Control in an Isotopically Enriched Si 28 / Si 0.7 Ge 0.3 Quadruple Quantum Dot. *Physical Review Applied*, 11(6), June 2019.
- [249] A. J. Sigillito, M. J. Gullans, L. F. Edge, M. Borselli, and J. R. Petta. Coherent transfer of quantum information in a silicon double quantum dot using resonant SWAP gates. *npj Quantum Information*, 5(1):110, Dec. 2019.
- [250] C. P. Slichter. *Principles of magnetic resonance*. Number 1 in Springer series in solid-state sciences. Springer, Berlin ; New York, 3rd enl. and updated ed edition, 1996.
- [251] C. Spence, B. C. Paz, B. Klemt, E. Chanrion, D. J. Niegemann, B. Jadot, V. Thiney, B. Bertrand, H. Niebojewski, P.-A. Mortemousque, X. Jehl, R. Maurand, S. De Franceschi, M. Vinet, F. Balestro, C. B äuerle, Y.-M. Niquet, T. Meunier, and M. Urdampilleta. Spin-valley coupling anisotropy and noise in CMOS quantum dots. *arXiv:2109.13557 [cond-mat]*, Sept. 2021. arXiv: 2109.13557.
- [252] A. Stockklauser, P. Scarlino, J. V. Koski, S. Gasparinetti, C. K. Andersen, C. Reichl, W. Wegscheider, T. Ihn, K. Ensslin, and A. Wallraff. Strong Coupling Cavity QED with Gate-Defined Double Quantum Dots Enabled by a High Impedance Resonator. *Physical Review X*, 7(1), Mar. 2017.
- [253] T. Struck, A. Hollmann, F. Schauer, O. Fedorets, A. Schmidbauer, K. Sawano, H. Riemann, N. V. Abrosimov, Ł. Cywiński, D. Bougeard, and L. R. Schreiber. Low-frequency spin qubit energy splitting noise in highly purified 28Si/SiGe. *npj Quantum Information*, 6(1):40, Dec. 2020.
- [254] C. Tahan. Democratizing Spin Qubits. *arXiv:2001.08251 [cond-mat, physics:quant-ph]*, Jan. 2020. arXiv: 2001.08251.
- [255] T. Takakura, A. Noiri, T. Obata, T. Otsuka, J. Yoneda, K. Yoshida, and S. Tarucha. Single to quadruple quantum dots with tunable tunnel couplings. *Applied Physics Letters*, 104(11):113109, Mar. 2014.
- [256] K. Takeda, J. Kamioka, T. Otsuka, J. Yoneda, T. Nakajima, M. R. Delbecq, S. Amaha, G. Allison, T. Kodera, S. Oda, and S. Tarucha. A fault-tolerant addressable spin qubit in a natural silicon quantum dot. *Science Advances*, 2(8):e1600694–e1600694, Aug. 2016.
- [257] K. Takeda, A. Noiri, T. Nakajima, J. Yoneda, T. Kobayashi, and S. Tarucha. Quantum tomography of an entangled three-qubit state in silicon. *Nature Nanotechnology*, June 2021.
- [258] K. Takeda, A. Noiri, J. Yoneda, T. Nakajima, and S. Tarucha. Resonantly Driven Singlet-Triplet Spin Qubit in Silicon. *Physical Review Letters*, 124(11):117701, Mar. 2020.
- [259] K. Takeda, J. Yoneda, T. Otsuka, T. Nakajima, M. R. Delbecq, G. Allison, Y. Hoshi, N. Usami, K. M. Itoh, S. Oda, T. Kodera, and S. Tarucha. Optimized electrical control of a Si/SiGe spin qubit in the presence of an induced frequency shift. *npj Quantum Information*, 4(1), Dec. 2018.
- [260] T. Tanttu, B. Hensen, K. W. Chan, C. H. Yang, W. W. Huang, M. Fogarty, F. Hudson, K. Itoh, D. Culcer, A. Laucht, A. Morello, and A. Dzurak. Controlling Spin-Orbit Interactions in Silicon Quantum Dots Using Magnetic Field Direction. *Physical Review X*, 9(2):021028, May 2019.
- [261] S. B. Tenberg, S. Asaad, M. T. Mädzik, M. A. I. Johnson, B. Joecker, A. Laucht, F. E. Hudson, K. M. Itoh, A. M. Jakob, B. C. Johnson, D. N. Jamieson, J. C. McCallum, A. S. Dzurak, R. Joynt, and A. Morello. Electron spin relaxation of single phosphorus donors in metal-oxide-semiconductor nanoscale devices. *Physical Review B*, 99(20):205306, May 2019.
- [262] R. Thalineau, S. Hermelin, A. D. Wieck, C. Bäuerle, L. Saminadayar, and T. Meunier. A few-electron quadruple quantum dot in a closed loop. *Applied Physics Letters*, 101(10):103102, Sept. 2012.
- [263] B. Thorgrimsson, D. Kim, Y.-C. Yang, L. W. Smith, C. B. Simmons, D. R. Ward, R. H. Foote, J. Corrigan, D. E. Savage, M. G. Lagally, M. Friesen, S. N. Coppersmith, and M. A. Eriksson. Extending the coherence of a quantum dot hybrid qubit. *npj Quantum Information*, 3(1):32, Dec. 2017.
- [264] L. A. Tracy, D. R. Luhman, S. M. Carr, N. C. Bishop, G. A. Ten Eyck, T. Pluym, J. R. Wendt, M. P. Lilly, and M. S. Carroll. Single shot spin readout using a cryogenic high-electron-mobility transistor amplifier at sub-Kelvin temperatures. *Applied Physics Letters*, 108(6):063101, Feb. 2016.
- [265] M. Urdampilleta, D. J. Niegemann, E. Chanrion, B. Jadot, C. Spence, P.-A. Mortemousque, C. Bäuerle, L. Hutin, B. Bertrand, S. Barraud, R. Maurand, M. Sanquer, X. Jehl, S. De Franceschi, M. Vinet, and T. Meunier. Gate-based high fidelity spin readout in a CMOS device. *Nature Nanotechnology*, 14(8):737–741, Aug. 2019.
- [266] J. W. G. van den Berg, S. Nadj-Perge, V. S. Pribeag, S. R. Plissard, E. P. A. M. Bakkers, S. M. Frolov, and L. P. Kouwenhoven. Fast Spin-Orbit Qubit in an Indium Antimonide Nanowire. *Physical Review Letters*, 110(6), Feb. 2013.
- [267] W. G. Van der Wiel, S. De Franceschi, J. M. Elzerman, T. Fujisawa, S. Tarucha, and L. P. Kouwenhoven. Electron transport through double quantum dots. *Reviews of Modern Physics*, 75(1):1, 2002.
- [268] C. J. van Diepen, T.-K. Hsiao, U. Mukhopadhyay, C. Reichl, W. Wegscheider, and L. M. K. Vandersypen. Electron cascade for distant spin readout. *Nature Communications*, 12(1):77, Dec. 2021.
- [269] C. J. van Diepen, T.-K. Hsiao, U. Mukhopadhyay, C. Reichl, W. Wegscheider, and L. M. K. Vandersypen. Quantum simulation of antiferromagnetic Heisenberg chain with gate-defined quantum dots. *arXiv:2103.08238 [cond-mat, physics:quant-ph]*, Mar. 2021. arXiv: 2103.08238.

- [270] F. van Riggelen, N. W. Hendrickx, W. I. L. Lawrie, M. Russ, A. Sammak, G. Scappucci, and M. Veldhorst. A two-dimensional array of single-hole quantum dots. *Applied Physics Letters*, 118(4):044002, Jan. 2021.
- [271] I. van Weperen, B. D. Armstrong, E. A. Laird, J. Medford, C. M. Marcus, M. P. Hanson, and A. C. Gossard. Charge-State Conditional Operation of a Spin Qubit. *Physical Review Letters*, 107(3), July 2011.
- [272] D. J. van Woerkom, P. Scarlino, J. H. Ungerer, C. Müller, J. V. Koski, A. J. Landig, C. Reichl, W. Wegscheider, T. Ihn, K. Ensslin, and A. Wallraff. Microwave Photon-Mediated Interactions between Semiconductor Qubits. *Physical Review X*, 8(4):041018, Oct. 2018.
- [273] L. M. K. Vandersypen and M. A. Eriksson. Quantum computing with semiconductor spins. *Physics Today*, 72(8):38–45, Aug. 2019.
- [274] M. Veldhorst, J. C. C. Hwang, C. H. Yang, A. W. Leenstra, B. de Ronde, J. P. Dehollain, J. T. Muñonen, F. E. Hudson, K. M. Itoh, A. Morello, and A. S. Dzurak. An addressable quantum dot qubit with fault-tolerant control-fidelity. *Nature Nanotechnology*, 9(12):981–985, Oct. 2014.
- [275] M. Veldhorst, R. Ruskov, C. H. Yang, J. C. C. Hwang, F. E. Hudson, M. E. Flatté, C. Tahan, K. M. Itoh, A. Morello, and A. S. Dzurak. Spin-orbit coupling and operation of multivalley spin qubits. *Physical Review B*, 92(20), Nov. 2015.
- [276] M. Veldhorst, C. H. Yang, J. C. C. Hwang, W. Huang, J. P. Dehollain, J. T. Muñonen, S. Simmons, A. Laucht, F. E. Hudson, K. M. Itoh, A. Morello, and A. S. Dzurak. A two-qubit logic gate in silicon. *Nature*, 526(7573):410–414, Oct. 2015.
- [277] J. J. Viennot, M. C. Dartailh, A. Cottet, and T. Kontos. Coherent coupling of a single spin to microwave cavity photons. *Science*, 349(6246):408–411, July 2015.
- [278] B. Voisin, R. Maurand, S. Barraud, M. Vinet, X. Jéhl, M. Sanquer, J. Renard, and S. De Franceschi. Electrical Control of  $g$ -Factor in a Few-Hole Silicon Nanowire MOSFET. *Nano Letters*, 16(1):88–92, Jan. 2016.
- [279] C. Volk, A. Chatterjee, F. Ansaloni, C. M. Marcus, and F. Kuemmeth. Fast Charge Sensing of Si/SiGe Quantum Dots via a High-Frequency Accumulation Gate. *Nano Letters*, 19(8):5628–5633, Aug. 2019.
- [280] C. Volk, A. M. J. Zwerver, U. Mukhopadhyay, P. T. Eendebak, C. J. van Diepen, J. P. Dehollain, T. Hengsens, T. Fujita, C. Reichl, W. Wegscheider, and L. M. K. Vandersypen. Loading a quantum-dot based “Qubyte” register. *npj Quantum Information*, 5(1), Dec. 2019.
- [281] L. Vukušić, J. Kukucka, H. Watzinger, J. M. Milem, F. Schäffler, and G. Katsaros. Single-Shot Readout of Hole Spins in Ge. *Nano Letters*, 18(11):7141–7145, Nov. 2018.
- [282] D. Q. Wang, O. Klochan, J.-T. Hung, D. Culcer, I. Farrer, D. A. Ritchie, and A. R. Hamilton. Anisotropic Pauli Spin Blockade of Holes in a GaAs Double Quantum Dot. *Nano Letters*, 16(12):7685–7689, Dec. 2016.
- [283] K. Wang, C. Payette, Y. Dovzhenko, P. W. Deelman, and J. R. Petta. Charge Relaxation in a Single-Electron Si/SiGe Double Quantum Dot. *Physical Review Letters*, 111(4), July 2013.
- [284] K. Wang, G. Xu, F. Gao, H. Liu, R.-L. Ma, X. Zhang, T. Zhang, G. Cao, T. Wang, J.-J. Zhang, X. Hu, H.-W. Jiang, H.-O. Li, G.-C. Guo, and G.-P. Guo. Ultrafast Operations of a Hole Spin Qubit in Ge Quantum Dot. *arXiv:2006.12340 [cond-mat, physics:quant-ph]*, June 2020. arXiv: 2006.12340.
- [285] T. F. Watson, S. G. J. Philips, E. Kawakami, D. R. Ward, P. Scarlino, M. Veldhorst, D. E. Savage, M. G. Lagally, M. Friesen, S. N. Coppersmith, M. A. Eriksson, and L. M. K. Vandersypen. A programmable two-qubit quantum processor in silicon. *Nature*, 555(7698):633–637, Feb. 2018.
- [286] T. F. Watson, B. Weber, Y.-L. Hsueh, L. C. L. Hollenberg, R. Rahman, and M. Y. Simmons. Atomically engineered electron spin lifetimes of 30 s in silicon. *Science Advances*, 3(3):e1602811, Mar. 2017.
- [287] H. Watzinger, C. Kloeffer, L. Vukušić, M. D. Rossell, V. Sessi, J. Kukucka, R. Kirchschlager, E. Lausecker, A. Truhlar, M. Glaser, A. Rastelli, A. Fuhrer, D. Loss, and G. Katsaros. Heavy-Hole States in Germanium Hut Wires. *Nano Letters*, 16(11):6879–6885, Nov. 2016.
- [288] H. Watzinger, J. Kukucka, L. Vukušić, F. Gao, T. Wang, F. Schäffler, J.-J. Zhang, and G. Katsaros. A germanium hole spin qubit. *Nature Communications*, 9(1), Dec. 2018.
- [289] B. Weber, Y.-L. Hsueh, T. F. Watson, R. Li, A. R. Hamilton, L. C. L. Hollenberg, R. Rahman, and M. Y. Simmons. Spin-orbit coupling in silicon for electrons bound to donors. *npj Quantum Information*, 4(1), Dec. 2018.
- [290] A. West, B. Hensen, A. Jouan, T. Tanttu, C.-H. Yang, A. Rossi, M. F. Gonzalez-Zalba, F. Hudson, A. Morello, D. J. Reilly, and A. S. Dzurak. Gate-based single-shot readout of spins in silicon. *Nature Nanotechnology*, Mar. 2019.
- [291] W. K. Wootters. Statistical distance and Hilbert space. *Physical Review D*, 23(2):357–362, Jan. 1981.
- [292] X. Wu, D. R. Ward, J. R. Prance, D. Kim, J. K. Gamble, R. T. Mohr, Z. Shi, D. E. Savage, M. G. Lagally, M. Friesen, S. N. Coppersmith, and M. A. Eriksson. Two-axis control of a singlet-triplet qubit with an integrated micromagnet. *Proceedings of the National Academy of Sciences*, 111(33):11938–11942, Aug. 2014.
- [293] M. Xiao, M. G. House, and H. W. Jiang. Measurement of the Spin Relaxation Time of Single Electrons in a Silicon Metal-Oxide-Semiconductor-Based Quantum Dot. *Physical Review Letters*, 104(9), Mar. 2010.
- [294] X. Xue, B. D’Anjou, T. F. Watson, D. R. Ward, D. E. Savage, M. G. Lagally, M. Friesen, S. N. Coppersmith, M. A. Eriksson, W. A. Coish, and L. M. K. Vandersypen. Repetitive Quantum Nondemolition Measurement and Soft Decoding of a Silicon Spin Qubit. *Physical Review X*, 10(2):021006, Apr. 2020.
- [295] X. Xue, B. Patra, J. P. G. van Dijk, N. Samkharadze, S. Subramanian, A. Corra, B. Paquet Wuetz, C. Jeon, F. Sheikh, E. Juarez-Hernandez, B. P. Esparza, H. Rampurawala, B. Carlton, S. Ravikumar, C. Nieva, S. Kim, H.-J. Lee, A. Sammak, G. Scappucci, M. Veldhorst, F. Sebastian, M. Babaie, S. Pellerano, E. Charbon, and L. M. K. Vandersypen. CMOS-based cryogenic control of silicon quantum circuits. *Nature*, 593(7858):205–210, May 2021.
- [296] X. Xue, M. Russ, N. Samkharadze, B. Undseth, A. Sammak, G. Scappucci, and L. M. K. Vandersypen. Computing with spin qubits at the surface code error threshold. *arXiv:2107.00628 [cond-mat, physics:quant-ph]*, July 2021. arXiv: 2107.00628.
- [297] X. Xue, T. F. Watson, J. Helsen, D. R. Ward, D. E. Savage, M. G. Lagally, S. N. Coppersmith, M. A. Eriksson, S. Wehner, and L. M. K. Vandersypen. Benchmarking Gate Fidelities in a Si / SiGe Two-Qubit Device. *Physical Review X*, 9(2):021011, Apr. 2019.
- [298] Y. Yamamoto. Decoherence, refocusing and dynamical decoupling of spin qubits, 2013.
- [299] C. H. Yang, K. W. Chan, R. Harper, W. Huang, T. Evans, J. C. C. Hwang, B. Hensen, A. Laucht, T. Tanttu, F. E. Hudson, S. T. Flammia, K. M. Itoh, A. Morello, S. D. Bartlett, and A. S. Dzurak. Silicon qubit fidelities approaching incoherent noise limits via pulse engineering. *Nature Electronics*, 2(4):151–158, Apr. 2019. arXiv: 1807.09500.
- [300] C. H. Yang, R. C. C. Leon, J. C. C. Hwang, A. Saraiva,

- T. Tanttu, W. Huang, J. Camirand Lemyre, K. W. Chan, K. Y. Tan, F. E. Hudson, K. M. Itoh, A. Morello, M. Pioro-Ladrière, A. Laucht, and A. S. Dzurak. Operation of a silicon quantum processor unit cell above one kelvin. *Nature*, 580(7803):350–354, Apr. 2020.
- [301] C. H. Yang, A. Rossi, R. Ruskov, N. S. Lai, F. A. Mohiyaddin, S. Lee, C. Tahan, G. Klimeck, A. Morello, and A. S. Dzurak. Spin-valley lifetimes in a silicon quantum dot with tunable valley splitting. *Nature Communications*, 4, June 2013.
- [302] J. Yoneda, T. Otsuka, T. Nakajima, T. Takakura, T. Obata, M. Pioro-Ladrière, H. Lu, C. J. Palmstrøm, A. C. Gossard, and S. Tarucha. Fast Electrical Control of Single Electron Spins in Quantum Dots with Vanishing Influence from Nuclear Spins. *Physical Review Letters*, 113(26), Dec. 2014.
- [303] J. Yoneda, K. Takeda, A. Noiri, T. Nakajima, S. Li, J. Kamioka, T. Kodera, and S. Tarucha. Quantum non-demolition read-out of an electron spin in silicon. *Nature Communications*, 11(1):1144, Dec. 2020.
- [304] J. Yoneda, K. Takeda, T. Otsuka, T. Nakajima, M. R. Delbecq, G. Allison, T. Honda, T. Kodera, S. Oda, Y. Hoshi, N. Usami, K. M. Itoh, and S. Tarucha. A quantum-dot spin qubit with coherence limited by charge noise and fidelity higher than 99.9%. *Nature Nanotechnology*, Dec. 2017.
- [305] D. M. Zajac, T. M. Hazard, X. Mi, E. Nielsen, and J. R. Petta. Scalable Gate Architecture for a One-Dimensional Array of Semiconductor Spin Qubits. *Physical Review Applied*, 6(5), Nov. 2016.
- [306] D. M. Zajac, A. J. Sigillito, M. Russ, F. Borjans, J. M. Taylor, G. Burkard, and J. R. Petta. Resonantly driven CNOT gate for electron spins. *Science*, 359(6374):439–442, Jan. 2018.
- [307] X. Zhang, R.-Z. Hu, H.-O. Li, F.-M. Jing, Y. Zhou, R.-L. Ma, M. Ni, G. Luo, G. Cao, G.-L. Wang, X. Hu, H.-W. Jiang, G.-C. Guo, and G.-P. Guo. Giant Anisotropy of Spin Relaxation and Spin-Valley Mixing in a Silicon Quantum Dot. *Physical Review Letters*, 124(25):257701, June 2020.
- [308] R. Zhao, T. Tanttu, K. Y. Tan, B. Hensen, K. W. Chan, J. C. C. Hwang, R. C. C. Leon, C. H. Yang, W. Gilbert, F. E. Hudson, K. M. Itoh, A. A. Kiselev, T. D. Ladd, A. Morello, A. Laucht, and A. S. Dzurak. Single-spin qubits in isotopically enriched silicon at low magnetic field. *Nature Communications*, 10(1), Dec. 2019.
- [309] G. Zheng, N. Samkharadze, M. L. Noordam, N. Kalhor, D. Brousse, A. Sammak, G. Scappucci, and L. M. K. Vandersypen. Rapid gate-based spin read-out in silicon using an on-chip resonator. *Nature Nanotechnology*, 14(8):742–746, Aug. 2019.
- [310] A. M. J. Zwerver, T. Krähenmann, T. F. Watson, L. Lampert, H. C. George, R. Pillarisetty, S. A. Bojarski, P. Amin, S. V. Amitonov, J. M. Boter, R. Caudillo, D. Corras-Serrano, J. P. Dehollain, G. Droulers, E. M. Henry, R. Kotlyar, M. Lodziari, F. Luthi, D. J. Michalak, B. K. Mueller, S. Neyens, J. Roberts, N. Samkharadze, G. Zheng, O. K. Zietz, G. Scappucci, M. Veldhorst, L. M. K. Vandersypen, and J. S. Clarke. Qubits made by advanced semiconductor manufacturing. *arXiv:2101.12650 [cond-mat, physics:quant-ph]*, Jan. 2021. arXiv: 2101.12650.